DAHLGREN DIVISION
NAVAL SURFACE WARFARE CENTER

Dahlgren, Virginia 22448-5100

THE 1998 VERSION OF THE NSWC AEROPREDICTION CODE: PART I—SUMMARY OF NEW THEORETICAL METHODOLOGY

BY FRANK G. MOORE   ROY M. MCINVILLE   TOM HYMER

WEAPONS SYSTEMS DEPARTMENT

APRIL 1998

DTIC QUALITY INSPECTED 3

19980501 143

REPORT DOCUMENTATION PAGE		Form Approved OMB No. 0704-0188

Public reporting burden for this collection of information is estimated to average 1 hour per response, including the time for reviewing instructions, search existing data sources, gathering and maintaining the data needed, and completing and reviewing the collection of information. Send comments regarding this burden or any other aspect of this collection of information, including suggestions for reducing this burden, to Washington Headquarters Services. Directorate for information Operations and Reports, 1215 Jefferson Davis Highway, Suite 1204, Arlington, VA 22202-4302, and to the Office of Management and Budget, Paperwork Reduction Project (0704-0188), Washington, DC 20503.

1. AGENCY USE ONLY (Leave blank)	2. REPORT DATE April 1998	3. REPORT TYPE AND DATES COVERED

4. TITLE AND SUBTITLE The 1998 Version of the NSWC Aeroprediction Code: Part I—Summary of New Theoretical Methodology	5. FUNDING NUMBERS
6. AUTHOR(s) Frank G. Moore, Roy M. McInville, Tom Hymer	

7. PERFORMING ORGANIZATION NAME(S) AND ADDRESS(ES) Commander Naval Surface Warfare Center Dahlgren Division (Code G04) 17320 Dahlgren Road Dahlgren, VA 22448-5100	8. PERFORMING ORGANIZATION REPORT NUMBER NSWCDD/TR-98/1

9. SPONSORING/MONITORING AGENCY NAME(S) AND ADDRESS(ES)	10. SPONSORING/MONITORING AGENCY REPORT NUMBER

11. SUPPLEMENTARY NOTES

12a. DISTRIBUTION/AVAILABILITY STATEMENT Approved for public release; distribution is unlimited.	12b. DISTRIBUTION CODE

13. ABSTRACT (Maximum 200 words)

The NSWC aeroprediction code has been extended to the roll position of 45 deg (fins in "×" or cross roll orientation) in addition to the roll position of 0 deg (fins in "+" or plus roll orientation). It has also been extended to compute aerodynamics of nonaxisymmetric bodies based on an equivalent axisymmetric body. In addition, the nonlinear aerodynamic loads have been distributed over the body and lifting surfaces to provide a more useful tool for preliminary structural analysis. Finally, new technology was developed to improve the prediction of axial force at angle-of-attack (AOA).

These new technologies have been integrated into the AP95 and will be transitioned to legitimate users as the AP98. To make the AP98 more user friendly, an upgraded pre- and post-processing, personal-computer interface was also developed. Comparisons of the new theory have been made to both experimental data and the AP95. Comparisons of theory and experiment show the AP98 to be at least as good as the AP95 and, in general, maybe slightly better. In general, average accuracy levels of aerodynamics are ±10 percent on axial and normal force and ±4 percent of body length on center of pressure. For nonaxisymmetric body cases, accuracy can be slightly higher than these numbers, although not enough cases have been considered to make a definitive assessment. While these accuracy levels are encouraging for a semiempirical code, they could be improved upon by use of computational fluid dynamics codes or additional experimental data or both to reduce errors due to limited data bases.

14. SUBJECT TERMS aerodynamics, semiempirical method, Aeroprediction Code, Modified Newtonian Theory, freestream, Mach number	15. NUMBER OF PAGES 129
	16. PRICE CODE

17. SECURITY CLASSIFICATION OF REPORTS UNCLASSIFIED	18. SECURITY CLASSIFICATION OF THIS PAGE UNCLASSIFIED	19. SECURITY CLASSIFICATION OF ABSTRACT UNCLASSIFIED	20. LIMITATION OF ABSTRACT UL

NSN 7540-01-280-5500

Standard Form 298 (Rev 2-89)
Prescribed by ANSI std. Z39-18
298-102

<u>Transition Process for the 1998 Version of the Aeroprediction Code (AP98)</u>

The AP98 consists of the AP95 extended in roll to cover the $\Phi = 45°$ roll (fins in "×" or cross orientation) in addition to $\Phi = 0°$ (fins in "+" or plus orientation). It also distributes all the nonlinear aerodynamic loads on the body and lifting surfaces for improved utility by structural engineers. The axial force at angle of attack has been improved upon, along with the wing-tail interference model. Finally, new technology was developed to extend the code to nonaxisymmetric bodies. The interactive pre- and post-processor software for the personal computer has also been redesigned and improved upon.

Transition of the AP98 to U.S. Government agencies, U.S. contractors and universities will be free (like the AP95) to continue to encourage dual-use technology between government and industry and to encourage technology transition. To obtain a copy, please fill out the attached form and mail it to the address listed. <u>Please note the signature line indicating your personal responsibility to not allow the code outside your immediate agency at a given physical site.</u>

Foreign governments can also request copies of the Code by filling out the attached form and sending it to the address at the bottom of the form. A charge for the code will be made. This transition fee, which is established by the IPO and NAVSEA in conjunction with NSWC, has not yet been set. It is expected to be on the order of $20,000.

Pre-approved countries for transition of the Code include NATO member nations plus Australia, Japan, Sweden, Switzerland, South Korea, and Israel. Other countries requesting copies of the Code will be considered on a case by case basis by the sponsoring agency (Office of Naval Technology) and Foreign Military Sales Office.

Since we are sending out a copy of the new code free of charge for most requests, we will not be able to provide the level of consulting that we would like to. However, we do request several things from the users. First, if you find an error in the Code, we would appreciate your bringing it to the attention of either Dr. Frank Moore at (540) 653-3170, Mr. Tom Hymer at (540) 653-4164, or Dr. Roy McInville at (540) 653-8375. Second, if you find areas of success or areas of weakness, we would appreciate hearing from you. We use information such as this to help guide any future modifications. Third, if you find areas where additional code capability would be desirable, again, we would like to hear from you. In all cases, a written letter is preferred, but a phone call is better than no communication at all. Also, if you use the Code for the purpose of comparing the results to other computations within the external literature, we would like you to use the terminology "AP98." If you modify the AP98 to suit your own needs, you could refer to that code as "modified AP98." Finally, we request that you not send any copies of the Code to other agencies or even other activities in your company if at a different location. Please refer other agencies/activities to us so that we can keep track of copies of the Code. This is particularly true for foreign requests since these are now processed through the FMS Office and there is a charge for copies of the Code.

AP98 TRANSITION REQUEST

NAME: _____

COMPANY NAME: _____

ADDRESS: _____

_____

_____

PHONE NUMBER: _____

GOVT CONTRACT NUMBER: _____

MEANS OF TRANSITION: 3.5" Diskettes plus User Guides

We agree that we will not give a copy of the AP98 to any other agency. We will refer other agencies to NSWCDD at the address below for a copy.

Your Signature _____

Supervisor Signature _____

Please send this form completely filled out to:

Commander
Dahlgren Division
Naval Surface Warfare Center
Attn: Dr. Frank Moore (G04)
17320 Dahlgren Road
Dahlgren, VA 22448

We will try to send you a copy of the AP98 along with a user's guide within a month.

If the request is from a foreign country, please send a letter requesting a copy of the Code along with a copy of this form to:

Navy International Programs Office
Attn: IPO-02C (Mr. John Marini)
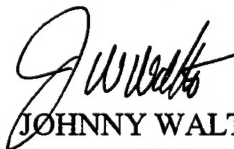1111 Jefferson Davis Highway
Suite 701
Arlington, VA 22202-1111

A charge of $15,000 to $25,000 (the exact fee has not been set but is expected to be in this range) will be required before the Code is transitioned to a foreign country. This cost helps defray the transition costs to send the code to a foreign country.

FOREWORD

The 1995 version of the aeroprediction code (AP95) was limited to zero roll orientation ($\Phi = 0$ deg for fins in plus-fin arrangement) aerodynamic calculations of weapons with axisymmetric bodies. The AP95 had nonlinear total aerodynamic loads computed to angle-of-attack (AOA) of 90 deg, but these loads were not distributed over the wings and body for more effective use by structural analysts. Moreover, the AP95 predictions of axial force at high AOA also needed improvement. As a result of these limitations, new technology was developed over the past 3 years to eliminate these deficiencies. These new technologies were integrated into the AP95 and the new version of the code will be transitioned as the AP98.

The work described in this report was supported through the Office of Naval Research (Mr. Dave Siegel) by the following programs: the Air Launched Weapons Program managed at the Naval Air Warfare Center, China Lake, CA, by Mr. Tom Loftus and Dr. Craig Porter, and the Surface Weapons Systems Technology Program managed at the Naval Surface Warfare Center, Dahlgren Division (NSWCDD) by Mr. Robin Staton and Mr. Gil Graff. Also, some support was provided by the Marine Corps Weaponry Technology Program managed at NSWCDD by Mr. Bob Stiegler. The authors express appreciation for support received in this work.

Approved by:

JOHNNY WALTERS, Deputy Head
Weapons Systems Department

CONTENTS

ILLUSTRATIONS

ILLUSTRATIONS (Continued)

ILLUSTRATIONS (Continued)

ILLUSTRATIONS (Continued)

1.0 INTRODUCTION

1.1 REQUIREMENTS

Estimating missile aerothermodynamics over the flight regime where missiles fly is quite important in all phases of design. These aerodynamics are used by the flight dynamicist to estimate range performance and miss distance; the heating information is used to perform heat transfer analysis; and the aerodynamic and thermodynamic loads are used by the structural engineer to estimate structural integrity of the configuration. Missiles that are launched from a vertical launcher can experience Angles of Attack (AOA) approaching 90 deg if a strong crosswind is present. Missiles that are launched from aircraft undergoing maneuvers can also experience AOA approaching 60 deg. Finally, terminally guided missiles undergoing maneuvers in the endgame can anticipate AOA as high as 40 deg. Hence, it is necessary to have aerodynamics estimates that cover a broad range of flight conditions in terms of Mach number and AOA. In addition to M_∞ and AOA requirements, aerodynamics are generally needed as a function of roll orientation. This is particularly true for a six-degree-of-freedom (6DOF) flight dynamics model. It is also true for a three-degree-of-freedom (3DOF) trim flight dynamics model. A trim model is defined as that AOA where pitching moment is zero. Most of the world's missiles fly in a roll-stable position of $\Phi = 0$ deg (fins in "+" fin arrangement) or $\Phi = 45$ deg (fins in "×" fin arrangement). As AOA increases above about 10 to 20 deg, trim aerodynamics of the missile configurations in these two roll-stabilized positions can be quite different.

In addition to the freestream requirements of AOA, roll, and Mach number, several geometry requirements are also necessary. The first of these is associated with the requirements for axisymmetric bodies. Here, the nose can be sharp, blunt, or truncated with various shaped ogives present. The afterbody is typically cylindrical of various lengths and may or may not have a boattail or flare present. Figure 1 is a sketch of a body-alone axisymmetric case. One or two sets of lifting
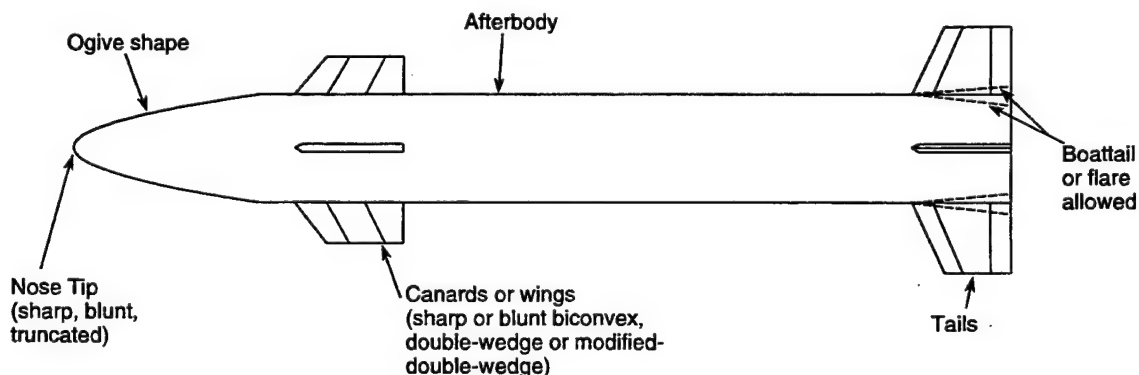
FIGURE 1. TYPICAL AXISYMMETRIC WEAPON CONFIGURATION GEOMETRY
REQUIREMENTS

surfaces can also be present on the configuration as shown in Figure 1. The cross-section of these lifting surfaces is typically symmetric with a sharp or blunt biconvex, double-wedge or modified-double-wedge airfoil section.

The desire to increase weapon range and maneuverability, to design weapons that are more optimum from an aircraft total drag and radar signature standpoint, or to provide optimum loadout of multiple missiles in a ship's vertical launcher has driven weapons designers to consider nonaxisymmetric body shapes. Some typical shapes are shown in Figure 2. While most missiles in the United States and foreign countries in existence today have axisymmetric body configurations, these conceptual design tradeoffs of various configurations other than axisymmetric require
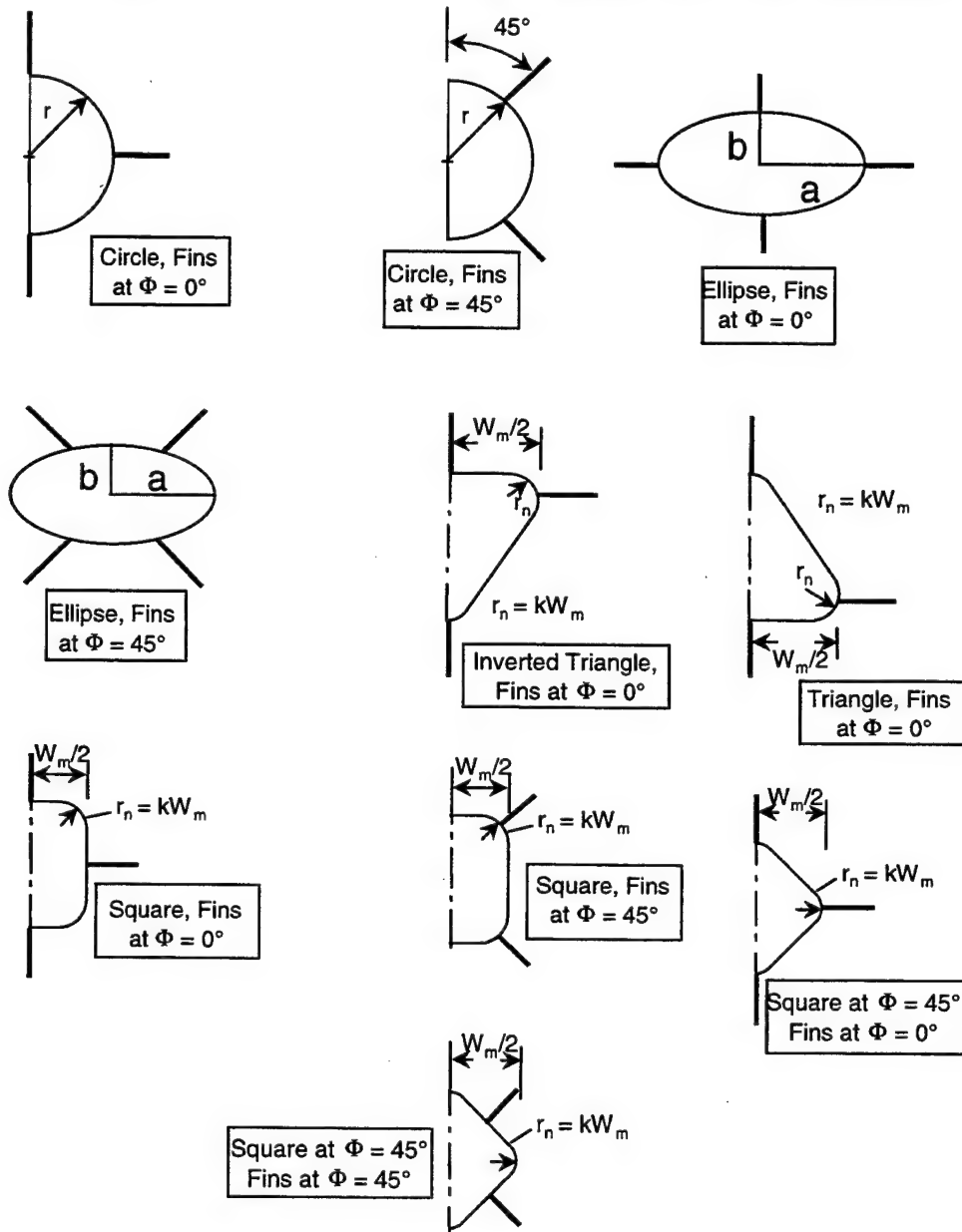
FIGURE 2. NONCIRCULAR CROSS-SECTION, WING-BODY CONFIGURATIONS OF INTEREST FOR THE AEROPREDICTION CODE

engineering estimates of aerodynamics. Current state-of-the-art methods for predicting aerodynamics of nonaxisymmetric body shapes with engineering accuracy are much more limited than for axisymmetric bodies. This is primarily driven by the fact that to get reasonable accuracy of the aerodynamics requires an accurate description of the body geometry. To describe the geometry of a complex body shape accurately can take days or weeks depending on the requirements of the aerodynamics code being used.

1.2   LIMITATIONS OF 1995 VERSION OF THE AEROPREDICTION CODE (AP95)

The latest version of the aeroprediction code, AP95[1], has several limitations when viewed against the overall requirements. First of all, the code is limited to the roll position of $\Phi = 0$ deg aerodynamics. Since the code is a semiempirical model used for preliminary design, it is important that aerodynamics be available in the roll position of $\Phi = 45$ deg as well. This new technology was therefore developed[2] and will be a part of the AP98. Secondly, while the AP95 defined nonlinear aerodynamic loads to AOA 90 deg, it did not distribute all these loads over the body and lifting surfaces to make the code more useful to the structural engineer who might be using the code to perform a beam analysis of a missile structure. This problem was also addressed and documented in Reference 3.

A third problem that existed with the AP95 was the accuracy of the axial force coefficient at high AOA. This problem became more prominent at subsonic Mach numbers, where the axial force could go negative, and at all Mach numbers when a control deflection was of opposite sign to the AOA. New technology was developed[4] to correct this problem and this new technology will also be a part of the AP98. The final weakness of the AP95 compared to the aeroprediction requirements is the limitation of axisymmetric bodies. This was an extremely difficult problem to resolve. However, after a couple of years where several difficult technology shortfalls were overcome, this limitation has also been removed and documentation on the new technology has just been completed.[5]

Figure 3 is a summary that shows the natural evolution of the aeroprediction code from the first version in 1972 to the seventh and most recent version, the AP98. This figure shows how major new technology was developed to meet the tactical weapon's requirements. The remainder of this report will summarize the theoretical methods contained in the aeroprediction code; compare the aerodynamic predictions of the latest version to those of the AP95 and to experimental data; and, finally, summarize and briefly state what new technology is still needed in the realm of approximate aerodynamic codes for future development.

2.0 LOW ANGLE OF ATTACK (AOA) AERODYNAMIC METHODS

Most of the low AOA aerodynamic methods are state-of-the-art and have been used for many years. They are primarily theoretical in nature and based on small perturbation theory or local slope or hypersonic flow methods. They have been well documented in past references. As a result, each

topic will be briefly summarized with appropriate references given for those who want to pursue the methods more thoroughly.

| VERSION | WEAPONS | AERODYNAMICS | FLIGHT CONDITIONS | | | | | COMPUTERS |
			MACH NUMBER	REAL GAS AVAILABLE	AOA RANGE	ROLL	NONLINEAR DISTRIBUTED LOADS AVAILABLE	
1972	AXISYMMETRIC UNGUIDED PROJECTILES	STATIC ONLY	0 - 3	NO	0 - 15°	$\Phi = 0°$	NO	CDC
1974	AXISYMMETRIC MISSILES PROJECTILES ROCKETS	SAME	0 - 3	NO	SAME	SAME	NO	CDC
1977	SAME	STATIC AND DYNAMIC	0 - 3	NO	SAME	SAME	NO	CDC, IBM
1981	SAME	SAME	0 - 8	NO	0 - 15° (LIMITED CONF. AT HIGHER α)	SAME	NO	CDC, IBM, VAX
1993	SAME	SAME	0 - 20	YES	0 - 30°	SAME	NO	CDC, IBM, VAX, SILICON GRAPHICS
1995	SAME	SAME	SAME	YES	0 - 90°	SAME	NO	INTERACTIVE PC
1998	AXISYMMETRIC AND ASYMMETRIC MISSILES, PROJECTILES, AND ROCKETS	SAME	SAME	YES	SAME	$\Phi = 0°, 45°$	YES	IMPROVED INTERACTIVE PC

FIGURE 3. EVOLUTION OF AEROPREDICTION CODE IN TERMS OF MAJOR NEW ADDED CAPABILITY

2.1 BODY ALONE METHODOLOGY

2.1.1 Hybrid Theory of Van Dyke Combined with Modified Newtonian Theory (MNT)[6]

This method was first introduced in Reference 6 and was the key to being able to obtain accurate pressure distributions and axial and normal force coefficients and center of pressure on blunt, truncated or sharp nosed bodies of revolution. Reference 6 was thus the foundation of the first version of the aeroprediction code (AP72) and to the author's knowledge, remains to this day the only accurate way (short of a numerical method to solve the full equations of motion) to obtain static aerodynamics in the Mach number range of 1.2 to 1.8. Reference 6 combined the Hybrid Theory of Van Dyke[7,8] (HTVD) with the MNT.[9] The key to the accurate computation of pressure coefficients all along the surface of a blunt nosed body was the starting solution and match point between the MNT and HTVD.

The HTVD[7] combines a second-order solution to the potential equation with a first-order crossflow solution first espoused by Tsien.[8] The advantage of this method is that it gives second-order accuracy in the axial direction where first-order accuracy is generally unacceptable for drag computations. On the other hand, first-order accuracy in the crossflow plane is typically acceptable for normal force and center of pressure computations. The fundamental reason for this is that perturbations in the flow, due to the presence of a body, have more impact in the axial, as opposed to the normal force direction. Hence, to get axial force accuracy compatible with a goal of ±10 percent requires second-order methods; whereas ±10 percent accuracy on C_N can be obtained with first-order methods, in many cases.

The Hybrid theory comes from the potential equation of fluid mechanics. It is limited to supersonic flow (we have used this method down to $M_\infty = 1.2$) where the assumption of isentropic flow (shock waves are weak) can be made. This typically limits the upper Mach number range to about $M_\infty = 2.0$ to 3.0, depending on the body shape. Also, the slope of the body surface must be less than the Mach angle. The Tsien solution, or crossflow part of the solution, comes from the linearized perturbation equation. On the other hand, the second-order solution to the axial flow is found by obtaining a particular solution to a reduced version of the full potential equation. This is the key to the accuracy improvement afforded by Van Dyke's solution in that some of the nonlinearity inherent in the axial flow problem is brought into the solution by this process. The beauty of the Van Dyke method is that this particular second-order solution is given entirely in terms of the first-order solution. That is, one simply solves the first-order perturbation solution for the axial flow and then solves an algebraic equation for the second-order solution where the boundary condition at the body is satisfied.

Newtonian Impact Theory assumes that, in the limit of high Mach number, the shock lies on the body. This means that the disturbed flow field lies in an infinitely-thin layer between the shock and body. Applying the laws of conservation of mass and momentum across the shock yields the result that density behind the shock approaches infinite values and the ratio of specific heats approaches unity. The pressure coefficient on the surface becomes[9]

$$C_P = 2\sin^2\delta_{eq} \tag{1}$$

where δ_{eq} is the angle between the velocity vector and a tangent to the body at the point in question (see Figures 2 and 3). δ_{eq} is defined by:

$$\sin(\delta_{eq}) = \sin\theta \cos\alpha - \sin\alpha \cos\phi \cos\theta \tag{2}$$

As noted in the earlier discussion, the Hybrid Theory is limited to conditions where the body slope is less than the local Mach angle. This means it is not applicable in the nose region of a blunt missile. On the other hand, MNT gives very acceptable estimates of pressure coefficients in the nose region, even for low supersonic Mach numbers where the assumptions, inherent in the Newtonian Impact Theory, are violated. As already mentioned, the key to the successful combination was in the starting solution. At low supersonic Mach numbers, the pressure overexpands on a blunt nose

tip as it proceeds around the blunt portion from the stagnation point to a given portion of the nose. In order to capture this overexpansion, Reference 6 found that it was necessary to start the HTVD near its maximum acceptable slope and allow the pressure to expand around the surface. Simultaneously, the MNT was started at the stagnation point and allowed to expand until the pressure coefficients of the MNT and the HTVD were equal. This was defined as the match point. Upstream of the match point, MNT was used in the force and moment calculations, whereas downstream, HTVD was used.

2.1.2 Second-Order-Shock-Expansion Theory (SOSET) Combined with MNT

First-order Expansion Theory was first proposed by Eggers et al. for bodies of revolution flying at high supersonic speeds.[10] Basically, the Shock-expansion Theory computes the flow parameters at the leading edge of a two-dimensional (2-D) surface with the oblique shock wave relations and with the solution for a cone at the tip of a three-dimensional (3-D) body. Standard Prandtl-Meyer Expansion (PME) is then applied along the surface behind the leading edge or tip solution to get the complete pressure distribution over the body surface. This theory inherently assumes that the expansion waves created by the change in curvature around the body are entirely absorbed by the shock and do not reflect back to the body surface. Since the theory assumes constant pressure along one of the conical tangent elements of the surface, fairly slender surfaces must be assumed or many points along the surface assumed to obtain a fairly accurate pressure distribution. Another way of stating this is, to minimize the strength of the disturbance created by Mach waves emanating from the expansion corner and intersecting the shock, the degree of turn should be small.

Syvertson et al. extended the generalized Shock-expansion Theory on pointed bodies and sharp airfoils to what he called a second-order theory.[11] He defined the pressure along a conical frustum by

$$p = p_c - (p_c - p_2) e^{-\eta_1} \tag{3}$$

instead of a constant on each segment as was the case in the generalized theory. Here, p_c is the pressure on a cone with the given cone half angle equal to the slope of the conical segment with respect to the axis of symmetry. The term p_2 is the pressure just aft of a conical segment which is calculated from a PME of the flow around a corner.

Also, η_1 is a decay constant that must be positive. If it is negative, it is set to zero and the second-order theory reverts back to the first-order theory.

Jackson et al.[12] combined SOSET with MNT to treat blunt-nosed configurations with or without flares. Jackson et al.[12], like Syvertson and Dennis,[11] assumed that the lifting properties could be predicted by assuming that the original body is made up of several equivalent bodies of revolution represented by the various meridians. They assumed the match point between the MNT and second-order shock pressure prediction to be the angle that corresponds to shock detachment on a wedge with the given freestream Mach number.

DeJarnette et al.[13] made significant improvements to the work of Jackson et al.[12] and Syvertson.[11] These new improvements included the following:

1. An exact (as opposed to an approximate) expression for the pressure gradient downstream of a corner.

2. A new expression for pointed-cone pressures at angle of attack that improves the initial pressure prediction over that of the tangent cone theory.

3. A new technique for calculating pressures of bodies at incidence.

The pressure computations at AOA, showed improvement over the method of Jackson.[12] DeJarnette, et al.[13] derived a new expression for pointed-cone pressure at $\alpha > 0$ by combining Slender Body Theory (SBT), Newtonian Theory, and an approximate expression for $C_{P_{\alpha=0}}$ to give:

$$C_p \ (\alpha, \ \theta, \ \phi, \ M) \ = \ C_{P_{\alpha=0}} \ + \ \Delta C_P \tag{4A}$$

where

$$\Delta C_p \ = \ -\sin2\alpha \ \sin2\theta \ \cos\phi \ + \ \sin^2\alpha \ \cos^2\theta\left[\left(2-\frac{1}{\beta}\right)(1-\tan^2\theta)-\left(2+\frac{2}{\beta}\right)\sin^2\phi\right] \tag{4B}$$

$$C_{P_{\alpha=0}} \ = \ \sin^2\theta_c\left[1 \ + \ \frac{(\gamma \ + \ 1) \ K^2 \ + \ 2}{(\gamma \ - \ 1) \ K^2 \ + \ 2} \ \ell n\left(\frac{\gamma \ + \ 1}{2} \ + \ \frac{1}{K^2}\right)\right] \tag{4C}$$

and

$$K^2 \ = \ (M_\infty^2 \ - \ 1) \ \sin^2\theta_c$$

Note also, that while Equation (4) was strictly defined for pointed cone pressures at angle of attack, it could also be used in a Tangent Cone sense to obtain pressures at any point on a body surface. DeJarnette actually used loading functions to obtain body alone lift properties, however.[13]

Equations (1) through (4) are thus the methods used to calculate pressures between the Mach numbers of about 1.8 and 6.0. Below M_∞ of 1.8, HTVD combined with MNT is used. Above M_∞ of 6.0, a slight improvement of Equation (4B) was found to be

$$\Delta C_P = - (2\alpha) \sin (2\theta) \cos (\phi) + (F\cos^2\theta) \alpha^2 + (4/3 \sin (2\theta) \cos (\phi)) \alpha^3 \qquad (5A)$$

where

$$F = (2 - \frac{1}{\beta}) (1 - \tan^2 \theta_c) - (2 + \frac{2}{\beta}) \sin^2\phi$$

or

$$\Delta C_P = - \frac{(2\alpha) \sin (2\theta) \cos (\phi)}{3} \qquad (5B)$$

Equation (5A) is used for pointed body configurations, as well as for blunt body configurations in the windward plane area 60 deg < ϕ ≤ 180 deg. For the leeward plane area on blunt bodies, Equation (5A) is replaced by Equation (5B).

2.1.3   Skin Friction Drag Methodology

Four options are allowed in the AP98 for skin-friction drag computations. These are: (1) all laminar flow, (2) wind tunnel model with no boundary layer trip, (3) wind tunnel model with boundary-layer trip (all turbulent flow), and (4) typical flight conditions. The code assumes transition from laminar to turbulent flow of 1×10^6 and 0.5×10^6 for the body and fins respectively for a typical flight vehicle that has about normal roughness. For a wind tunnel model with no boundary layer trip, these values of transition Reynolds numbers have been increased to 4×10^6 and 2×10^6 respectively. Also, the values are changed (decreased) as angle-of-attack increases to allow turbulent flow to occur on a larger portion of the vehicle.

For the portion of the vehicle where turbulent flow occurs, the Van Driest II[15] method is used for skin-friction drag computations. Reference 1 gave a method for computing the laminar portion of the skin-friction drag. The reader is referred to References 1, 15, and 16 for more details of the skin-friction drag methodology used in the AP98.

2.1.4   Base Drag

The AP72[6] developed a simplified method to compute base drag on bodies of revolution using an average of several data bases of base pressure coefficient on cylindrical afterbody configurations as a function of freestream Mach number. Turbulent flow ahead of the base was assumed. Boattail effects were accounted for as well as a first approximation to AOA effects in Reference 6. The AP74[17] added fins to the body so as to be able to compute aerodynamics on missiles and rockets as well as unguided projectiles. As a result, a rough approximation to the body

base drag as a result of tail fins was made. Also, the fins themselves, if they had blunt trailing edges, had a base drag of their own. This was based on a two-dimensional base pressure coefficient data base.

Later on, a request was made to the National Aeronautics and Space Administration/Langley Research Center (NASA/LRC) to provide additional base pressure data to allow a more thorough estimate of the effects of AOA, fin thickness and location effects, as well as Mach number. These tests were conducted by NASA/LRC; an improved empirical method for predicting base drag was developed and documentation of the tests and methodology was given in Reference 17.

Figure 4 summarizes the empirical base drag prediction method of Reference 17. The parameters F_1, F_2, and F_3 of Figure 4 are each defined by a set of curves in Reference 17. Once A or B of Figure 4 has been obtained, then power-on or boattail (or both) effects are computed in an additive manner. While the model of Reference 17 has been developed for power-off and power-on effects[18] computed independently, the methodology of combining the two together in an additive manner is an assumption and has never been adequately validated. It is suspected that the Figure 4 methodology could be improved upon with the combined effects of power-on in conjunction with fins and AOA effects, if this type of data were available.

2.1.5   Real Gas and Aeroheating Effects

The main reason the fourth version[19] of the aeroprediction code was limited to Mach number 8 was that, above $M_\infty = 6$, real gas effects start becoming important but can still be neglected at $M_\infty = 8$. However, as Mach number increases substantially above $M_\infty = 6$, the need to include real gas effects into the aeroprediction code increases if one is interested in inviscid surface temperatures. If one is only interested in forces and moments, real gas effects have a slight effect on the pitching moment, but only second-order effects on axial and normal force.[20] However, one of the key issues in high-speed vehicles is aerodynamic heating, material selection, and insulation. Any excess weight can have a strong adverse impact on vehicle performance. Thus, a simple yet accurate method of estimating vehicle surface temperature (inviscid) for use in heat transfer analysis is needed.

To extend the Aeroprediction Code to Real Gases required the SOSET to be extended to include real gas solutions. This required a real gas solution for a cone; a Prandtl Meyer expansion for real gases; a derivation of a pressure derivative (which was part of the η_1 in Equation (3); and a way to compute inviscid temperature, knowing pressure. This was accomplished and documented in Reference 14.

The inviscid surface temperature was not the main interest area in extending the aeroprediction code to real gases. The main interest was in providing better estimates of heat transfer rate; heat transfer coefficients; and recovery or adiabatic wall temperature at each computational point along the vehicle surface. This information could then be used in a heat transfer code as the convective part of the heat transfer. This is typically the most difficult part of the heat transfer to calculate. Standard SOTA methods[21] were used in obtaining the convective portion of heat transfer. These methods are Fay-Riddell[22] on the blunt nose, Beckwith and Gallagher[23] on the blunt leading edge of a wing and the Eckert Reference Enthalpy method[24] on the remaining body and wing points.

A. <u>Body Alone</u>

$$\left(C_{P_B}\right)_{NF, \, \alpha} = \left(C_{P_B}\right)_{NF, \, \alpha=0} \left[1 + 0.01F_1\right]$$

F_1 = Body Alone α Effects

B. <u>Body with Tail Fins</u>

1. Deflection and Thickness Effects

$$\left(C_{P_B}\right)_{\alpha, \, \delta, \, t/c, \, x/c=0} = \left(1 + 0.01F_2\right)\left(C_{P_B}\right)_{NF, \, \alpha=0} + 0.01F_3 \, (t/d)$$

$F_2 = |\alpha + \delta|$ Effects

F_3 = Additional Effects due to Thickness

2. Fin Location Effects when x/c $\neq$ 0

$$\left(C_{P_B}\right)_{\alpha, \, \delta, \, t/c, \, x/c} = \left(C_{P_B}\right)_{NF, \, \alpha} + 0.01 \left(\Delta C_{P_B}\right)_{\alpha, \, \delta, \, t/c, \, x/c}$$

C. <u>Power-On</u>

ΔC_{P_B} due to Power-On by Modified Brazzel[18] Method Added to Above Values of C_{P_B}

D. <u>Boattail</u>

$$C_{A_B} = - \, C_{P_B} \left(d_B/d_{ref}\right)^3$$

E. <u>Flare</u>

$$C_{A_B} = -C_{P_B}(d_B/d_{ref})^2$$

FIGURE 4. EMPIRICAL BASE DRAG PREDICTION MODEL OF AP98

Also, a mass balance technique was used to account for the fact that at high Mach number, the boundary layer swallows the entropy layer. As a result, the entropy at the outer edge of the boundary layer is no longer the value at the surface of the body, but an adjusted value.

2.2   WING ALONE METHODOLOGY

2.2.1   Lifting Surface Theory[25]

Lifting Surface Theory refers to the solution of the flow over a 3-D wing where the distribution of pressure is allowed to vary in both the spanwise and chordwise direction. The fundamental equation is the 3-D perturbation equation, along with boundary conditions that require the flow to be tangent to the wing surface and the velocity on the upper and lower surfaces to be equal at the trailing edge.

The assumptions involved in the Lifting Surface Theory, as applied to most missile configurations, are therefore small perturbations in the flow due to the presence of the wing and the thickness and camber effects are zero or small compared to AOA effects. The current version of the aeroprediction code neglects thickness effects in calculating the lift on the wings. Also, the Prandtl-Glauert rule[26] is used to relate the compressible subsonic normal force and pitching moment of the wing to that calculated at Mach number zero. Using the Prandtl-Glauert rule allows one to solve La Place's equation at Mach number zero and then compute compressible subsonic wing-alone aerodynamics at any Mach number less than about 0.8 to 0.9, where transonic effects become important.

To compute roll and pitch-damping derivatives, the flow tangency boundary condition is changed to relate the local AOA to roll or pitch rate. A more detailed discussion of the wing-alone linear aerodynamics is given in References 27 and 28.

2.2.2   Three-Dimensional Thin Wing Theory (TDTWT)[26]

TDTWT is quite similar to lifting surface theory (LST) in the sense the same perturbation equation is used. The only difference is that TDTWT is normally used to represent the supersonic flow solutions of the perturbation equation, versus LST, representing the subsonic solutions. Since, for supersonic flow, solutions to the perturbation equation are hyperbolic versus elliptic for the subsonic case, they generally are easier to obtain. This is because no upstream influence is felt by a disturbance at a given point on the wing surface. In contrast, the subsonic solutions required a matrix inversion at each wing element to determine the unknown coefficients used to determine the pressure differential from lower to upper surfaces. On the other hand, the assumptions of TDTWT are the same as for LST. They both assume small perturbations in an isentropic flow. The isentropic flow assumption means no shock waves are allowed.

In contrast to the body solutions generated by Van Dyke, adequate wing solutions can be obtained at higher Mach numbers. This is because of the low slopes present on most wing planforms (thickness is generally very small), the wing frontal area is generally less than 10 percent of the body frontal area, and in the region of leading edge bluntness, where perturbation theory is invalid, Modified Newtonian Theory is used for wave drag calculation. While thickness is neglected for normal force and pitching moment calculations, it is not neglected for axial force computations. A similar process to subsonic LST is used to compute the dynamic derivatives of roll and pitch damping where the local AOA is assumed to be a function of either roll or pitching motion.

For transonic flow, which here is considered to be Mach numbers in the range of 0.8 to 1.2, interpolation using the TDTWT and LST methods is done using a process similar to that in the aircraft DATCOM.[29]

2.3   INTERFERENCE AERODYNAMICS

There are two main types of interference dealt with in the low AOA methods. The first has to do with the interference effect the wing has on the body or the body has on the wing. The second has to do with the downwash effect of a tail surface in the wake of a forward lifting surface. Each of these interference effects will be dealt with separately. Wing to wing or shock wave interference will not be discussed at present, but will be alluded to in the discussion on nonlinear aerodynamic methods.

2.3.1   Wing-Body and Body-Wing Interference Effects

To better understand the interference lift components, it is instructive to examine the total normal force of a configuration as defined by Pitts et al.[30] This is given by

$$C_N = C_{N_B} + \left[\left(K_{W(B)} + K_{B(W)}\right) \alpha + \left(k_{W(B)} + k_{B(W)}\right) \delta_W\right] \left(C_{N_\alpha}\right)_W$$

$$+ \left[(K_{T(B)} + K_{B(T)}) \alpha + (k_{T(B)} + k_{B(T)}) \delta_T\right] (C_{N_\alpha})_T + C_{N_{T(V)}} + C_{N_{B(V)}} \tag{6}$$

The first term in Equation (6) is the normal force of the body alone including the linear and nonlinear components; the second term is the contribution of the wing (or canard), including interference effects and control deflection; the third term is the contribution of the tail, including interference effects and control deflection; and the last terms are the negative downwash effect on the tail or body due to wing-shed or body-shed vortices. The K's represent the interference of the configuration with respect to AOA, and the k's represent the interference with respect to control deflection. Each of these interference factors is estimated[28] by slender body or linear theory.[30] As such, they are independent of AOA. Figure 5 plots the SBT values of $K_{W(B)}$, $K_{B(W)}$, $k_{W(B)}$ and $k_{B(W)}$.
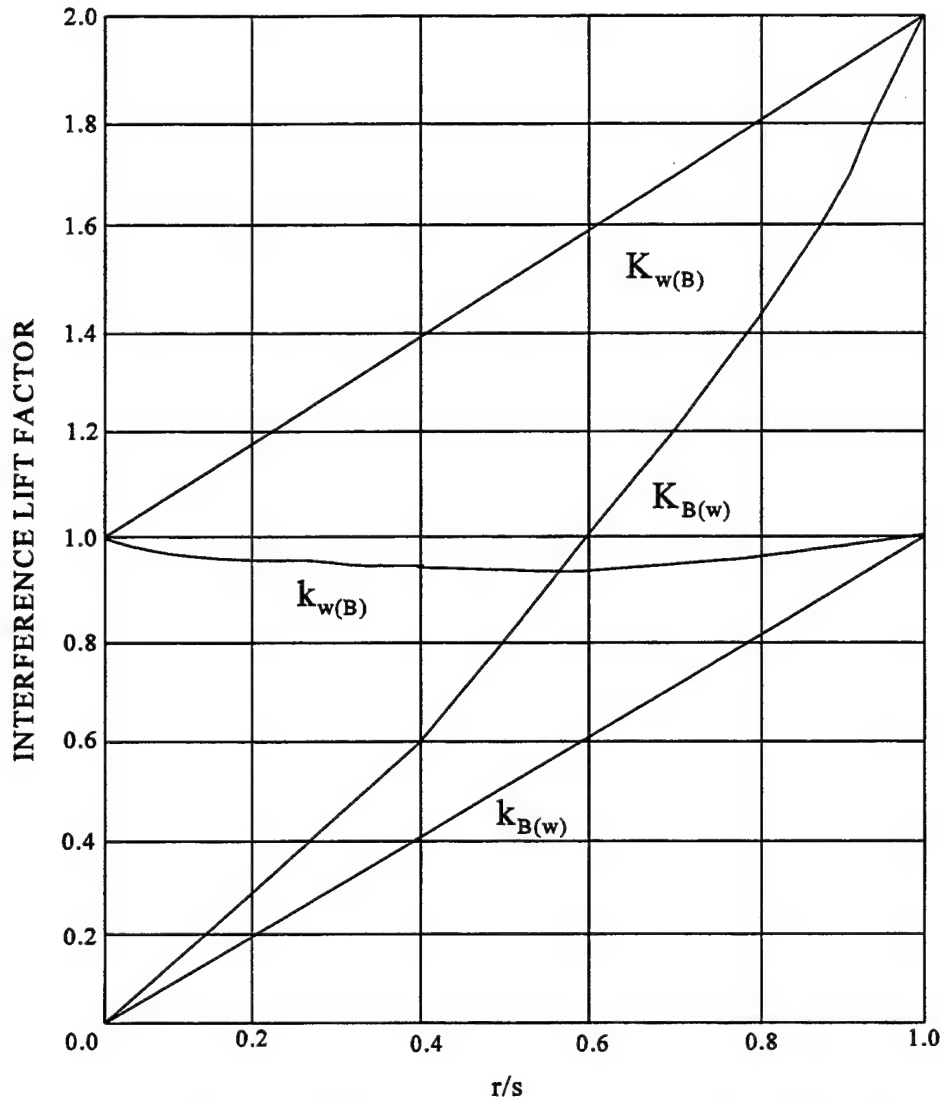
FIGURE 5. SLENDER BODY THEORY INTERFERENCE LIFT FACTORS

As the Mach number increases supersonically, SBT gives values of $K_{B(W)}$ which are too high if the wing is near the missile rear. This is because much of the carryover lift onto the body is actually lost to the wake of the vehicle. Linear theory formulations are available for the infinite and no-afterbody cases to replace Figure 5 if the parameter

$$\beta AR \ (1 \ + \ \lambda) \ [1/ \ (m\beta) \ + \ 1] \ > \ 4 \tag{7}$$

Moore[27] then linearly interpolated between the infinite and no-afterbody cases as a function of the area covered by the Mach lines to obtain $K_{B(W)}$ for the short afterbody case.

Strictly speaking, the methodology discussed here is limited to slender bodies with triangular planforms of low aspect ratio. Experience has shown that if the correct value of wing-alone lift is

13

computed, the interference factors can give very reasonable results for wings which do not have triangular planforms or even have low aspect ratio. Reference 27 showed how an engineering estimate to interference lift could be obtained, even for planforms such as that shown in Figure 6A. The actual SBT configuration is that shown in Figure 6B. Since most of the interference lift occurs near the wing-body juncture, Reference 27 used approximations given by Equation (8),

$$[K_{B(W)}]_{II} = [K_{B(W)}]_I G$$

$$[K_{W(B)}]_{II} = 1 + ([K_{W(B)}]_I - 1)G$$

$$[k_{W(B)}]_{II} = 1 + ([k_{W(B)}]_I - 1)G$$

$$[k_{B(W)}]_{II} = ([K_{W(B)}]_I - [k_{W(B)}]_I)G \tag{8}$$

to estimate the interference factors of the wing in Figure 6A. G in Equation (8) is the ratio of the root chord of the wing for which the interference factor is desired to that of the wing that slender body theory assumes. That is

$$G = \frac{(c_r)_{II}}{(c_r)_I}$$

2.3.2   Wing-Tail Interference Effects

The last two terms of Equation (6) are also interference terms. $C_{N_{T(V)}}$ is the lift on the tail caused by the vortices shed by the wing or canard upstream. $C_{N_{B(V)}}$ is the negative lift on the afterbody due to wing-shed vortices. These terms are also calculated analytically and are given by:

$$C_{N_{T(V)}} = \frac{(C_{N_\alpha})_W (C_{N_\alpha})_T [K_{W(B)}\sin\alpha + k_{W(B)}\sin\delta_W] i (s_T - r_T) A_W}{2\pi (AR)_T (f_w - r_w) A_{ref}} \tag{9}$$

$$C_{N_{B(V)}} = \frac{-4\Gamma}{A_W V_\infty} \left[\frac{f_w^2 - r_w^2}{f_w} - f_T + \frac{r_T^2}{\sqrt{f_T^2 + h_T^2}} \right] \tag{10}$$

14

DESIRE: $\left[K_{W(B)}\right]_{II}$, $\left[K_{B(W)}\right]_{II}$

$\left[k_{W(B)}\right]_{II}$, $\left[k_{B(W)}\right]_{II}$

BODY SURFACE

$(c_r)_{II}$
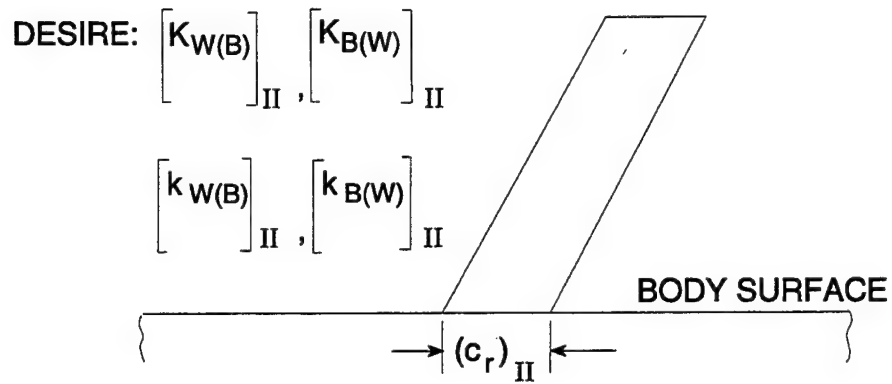
FIGURE 6A. WING FOR WHICH INTERFERENCE LIFT IS DESIRED

KNOWN: $\left[K_{W(B)}\right]_{I}$, $\left[K_{B(W)}\right]_{I}$

$\left[k_{W(B)}\right]_{I}$, $\left[k_{B(W)}\right]_{I}$

BODY SURFACE

$(c_r)_{II}$

$(c_r)_{I}$
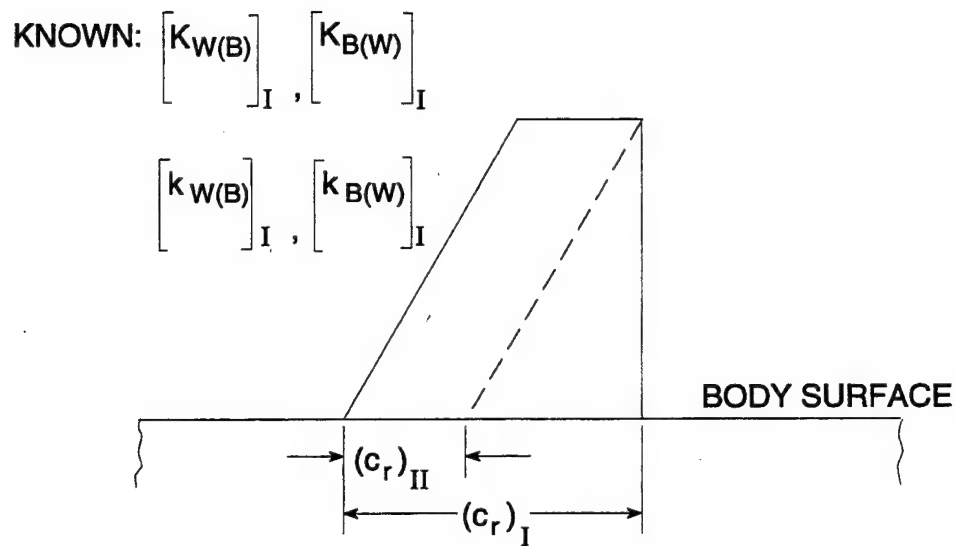
FIGURE 6B. ASSUMED SLENDER BODY REPRESENTATION

Here i is the tail interference factor given by Pitts et al.,[30] and Γ is the strength of the wing-shed vortex.

The AP81[19] and prior versions of the aeroprediction code (APC)[6,27] compute $C_{N_{T(V)}}$ based on Equation (9), but neglect $C_{N_{B(V)}}$ of Equation (10). As a result, some overprediction of normal force occurs, and generally speaking, the vehicle is too stable as well. Later versions of the APC, which include nonlinear effects, inherently account for this term indirectly through the direct use of wind tunnel data bases to estimate wing-tail interference nonlinearities. These nonlinear methods will be discussed later in this report.

2.4   EMPIRICAL METHODS[27,28,19]

It is fair to wonder why approximate linearized aeroprediction codes are defined as semiempirical with all the theoretical methods discussed so far. The truth is that while these methods allow the individual component forces and moments to be calculated fairly rigorously at a given Mach number or AOA, there are still many conditions where the analytical methods presented previously are either not applicable or the difficulty in applying them is not worth the effort. In those cases, empirical methods are generally used. The combination of theoretical and empirical techniques in a code is thus why they are called semiempirical codes. A few examples where empirical methods are used are transonic aerodynamics, body-alone subsonic aerodynamics, rotating band or protuberance aerodynamics, and base drag of the body and lifting surfaces (which was discussed already). There are actually analytical methods available for transonic aerodynamic computations. However, most of the methods are inconsistent from a computational standpoint with the approximate codes. What is done, in many cases, is to use the sophisticated analytical tools[27,28,19] to estimate the transonic aerodynamics, as a function of key geometric parameters, then to include these into an engineering code in a table lookup fashion. Obviously, for a vehicle that spends a large portion of its time in the transonic flow region, $0.8 < M_\infty < 1.2$, it would be justifiable to use a more sophisticated estimation process.

3.0 HIGH AOA AERODYNAMIC METHODS

To calculate aerodynamics at high AOA requires either a sophisticated computational fluid dynamics (CFD) code[31,32] or a semiempirical APC which bases the nonlinear aerodynamics on wind tunnel data bases. Both approaches (CFD and semiempirical) are needed in the design process. The semiempirical methods tend to be less accurate than the CFD methods, but are much less costly and much faster to get answers. As a result, they tend to be used in the conceptual and preliminary design stages of development. On the other hand, the CFD approaches, while being more costly and time consuming, are also more accurate, particularly when a CFD code has been benchmarked against a set of existing experimental data. As a result, CFD codes tend to be used more in the later phases of design, to supplement wind tunnel data, or to answer a technical question as to what is occurring in the overall flow field.

While generic wind tunnel data bases are not necessary for CFD codes, they are essential for semiempirical codes. The general approach of a semiempirical code is to try to back out the nonlinear aerodynamic terms based on wind tunnel data and an estimate of the linear aerodynamics. Secondly, an attempt is made to mathematically model the nonlinearity based on approximations to the experimental nonlinear aerodynamic terms. Thirdly, this model is compared to other data sets and the mathematical model refined.

Much of the nonlinear aerodynamic methodology for the AP98 has been developed recently; hence, a more thorough summary of this methodology will be given in comparison to the low AOA aerodynamic methods discussed in Section 2.0 of this report. Section 3.0 will deal with the new methods for axisymmetric bodies, and Section 4.0 will cover the noncircular body cross-section methodology.

3.1 AXIAL FORCE COEFFICIENT

The new methodology for computing the nonlinear term of axial force is documented in Reference 33. Basically, Reference 33 assumed

$$C_A = C_{A_0} + C_{A_\alpha} \tag{11}$$

where C_{A_0} represents the zero AOA axial force coefficient, and C_{A_α}, the change in axial force as AOA increases or decreases. C_{A_0} is estimated quite well using the low AOA methods discussed in Section 2.0. However, the methodology for treating C_{A_α} in the AP95[1] could be refined considerably, particularly at subsonic Mach numbers where C_A can actually go negative. The other area where C_{A_α} of the AP95 required improvement was when α and δ were of opposite sign.

The new methodology of Reference 33 treated C_{A_α} as a fourth-order equation in AOA. That is

$$C_{A_\alpha} \equiv f(M,\alpha) = A\alpha + B\alpha^2 + C\alpha^3 + D\alpha^4 \tag{12}$$

The constants A, B, C, and D were evaluated using several wind tunnel data bases for body-alone and body-tail configurations. For wing-body-tail cases, the body-tail parameters were adjusted somewhat based on wind tunnel data on wing-body-tail cases in conjunction with the AP95. The constants A, B, C, and D are defined by:

$$A = \quad f'(M,0)$$

$$B = \; -3.509 \; f'(M,0) \quad +11.005 \; f(M,30) \quad -2.757 \; f(M,60) \quad +0.41 \; f(M,90)$$

$$C = \; 3.675 \; f'(M,0) \quad -17.591 \; f(M,30) \quad +7.041 \; f(M,60) \quad -1.179 \; f(M,90)$$

$$D = \; -1.181 \; f'(M,0) \quad +6.771 \; f(M,30) \quad -3.381 \; f(M,60) \quad +0.752 \; f(M,90)$$

(13)

where $f'(M,0)$, $f(M,30)$, $f(M,60)$ and $f(M,90)$ are the values of the function $f(M,\alpha)$ or its derivative at AOA 0, 30, 60 and 90 deg, respectively. These values for body-alone, body-tail, and wing-body-tail cases are shown in Figure 7.

To model the change in axial force with control deflection and AOA, the following equations are utilized:

$$C_{A_{\delta_W}} = (C_{N_{W(B)}} \sin \delta_W) \; f(M,\alpha_W) \tag{14A}$$

$$C_{A_{\delta_T}} = (C_{N_{T(B)}} + C_{N_{T(V)}}) \; \sin \delta_T \; f(M,\alpha_T) \tag{14B}$$

where

$$\alpha_W = \alpha + \delta_W$$

$$\alpha_T = \alpha + \delta_T$$

(15)

It was found that when α and δ were of the same sign, $f(M,\alpha)$ was close to 1.0. However, when α and δ were of opposite signs, the axial force contributions due to control deflection were too high. As a result, empirical expressions were derived for $f(M,\alpha)$ at the two roll positions of $\Phi = 0$ and $\Phi = 45$ deg. These results are given in Figure 8. Figure 8 was derived by use of the AP98 in conjunction with wind tunnel data where the controls were deflected. Note that the only roll dependence of C_{A_α} comes from control deflection. If there are no control surfaces deflected, then C_{A_α} is approximately the same within the present prediction accuracy for $\Phi = 0$ deg and $\Phi = 45$ deg.

3.2   NORMAL FORCE COEFFICIENT

3.2.1   Configuration Aerodynamics

There are basically two approaches, to the author's knowledge, for including configuration nonlinear aerodynamics into the normal force Equation (6), repeated here for convenience.
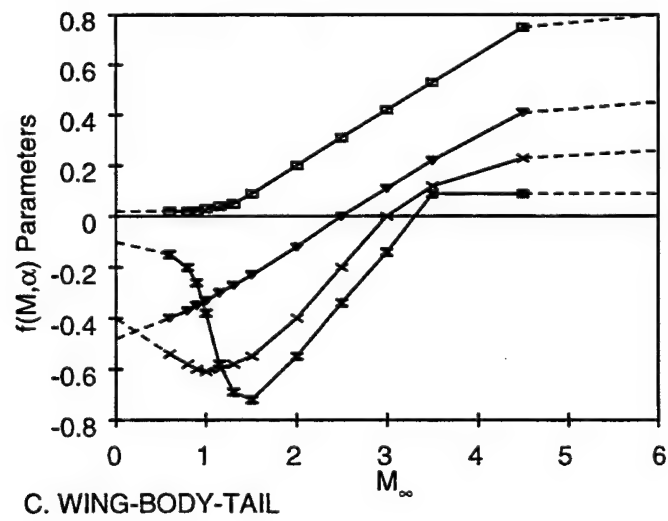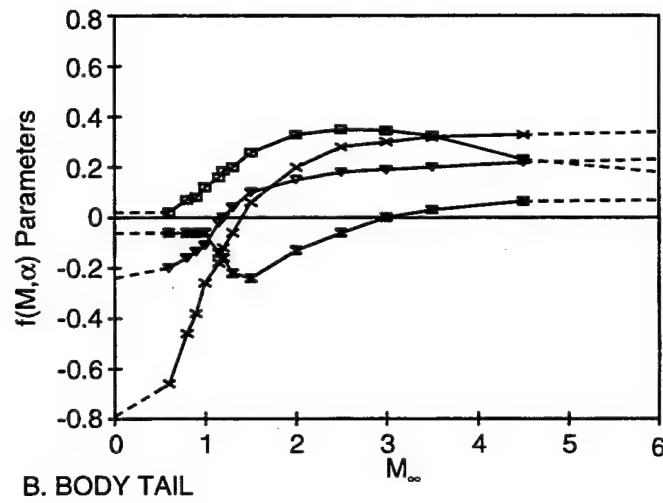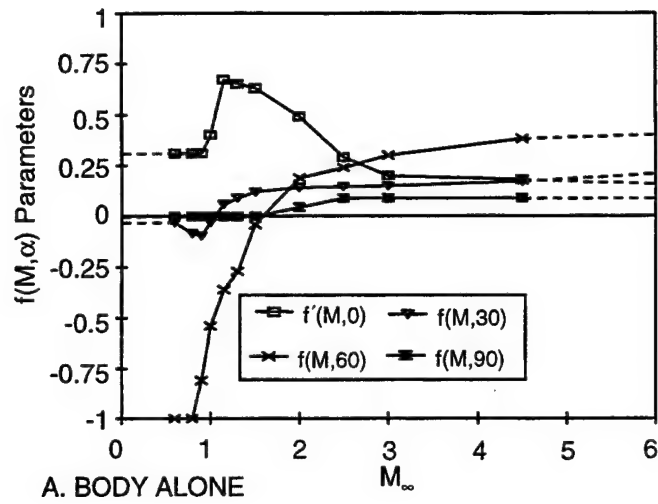
FIGURE 7. AXIAL FORCE AOA VARIATION PARAMETERS
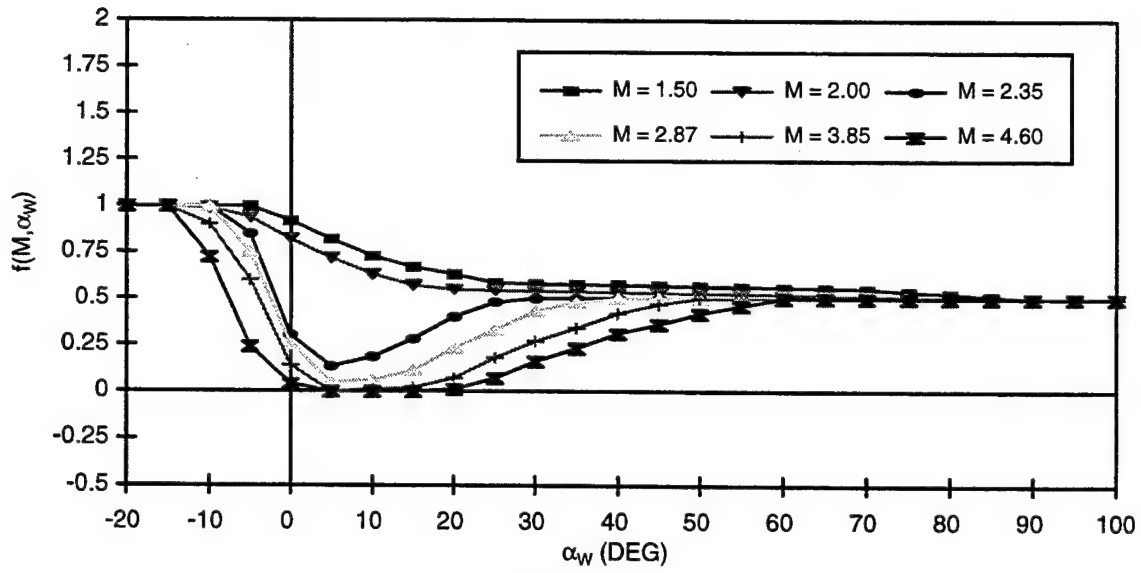
(A) $\Phi = 0$ deg
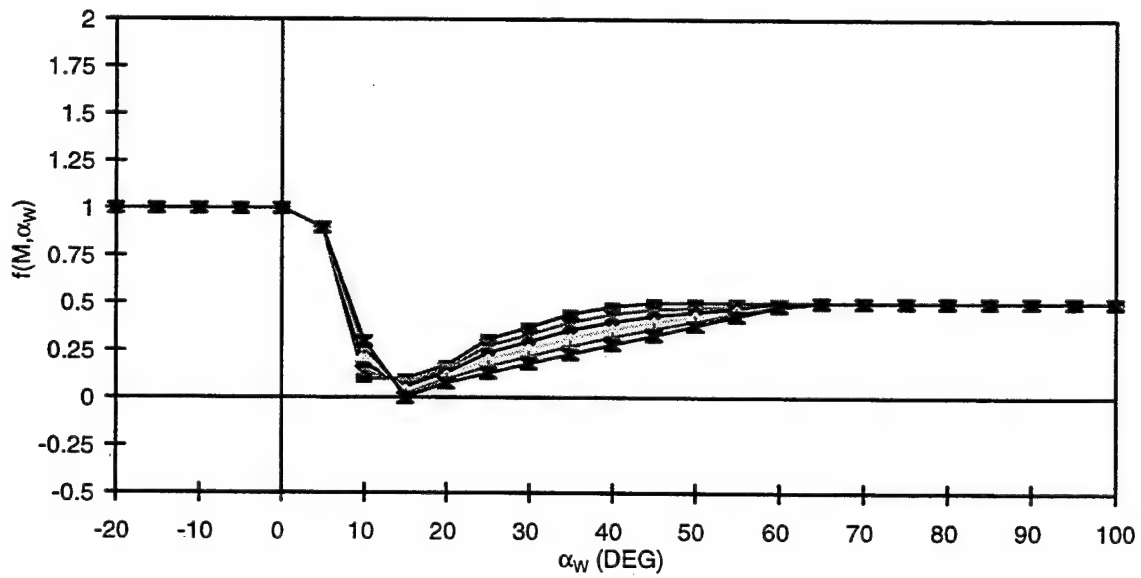
(B) $\Phi = 45$ deg

FIGURE 8. $f(M, \alpha_w)$ VALUES FOR α AND δ OF OPPOSITE SIGNS

$$C_N = C_{N_B} + \left[\left(K_{W(B)} + K_{B(W)}\right)\alpha + \left(k_{W(B)} + k_{B(W)}\right)\delta_W\right]\left(C_{N_\alpha}\right)_W$$

$$+ \left[(K_{T(B)} + K_{B(T)})\alpha + (k_{T(B)} + k_{B(T)})\delta_T\right](C_{N_\alpha})_T + C_{N_{T(V)}} + C_{N_{B(V)}} \tag{6}$$

The first method was the Equivalent AOA (EAOA) method.[34] In basic form, the EAOA method defines an AOA where the wing-alone normal force is twice the single fin value. That is, following Reference 34, the normal force on a single fin at $\Phi = 0$ deg roll and low AOA is

$$C_{N_{F(B)}} = \tfrac{1}{2}\left[K_{W(B)}\alpha + k_{W(B)}\delta + (\Delta\alpha)_W\right]\left(C_{N_\alpha}\right)_W \tag{17}$$

Reference 34 then defined an EAOA as

$$\alpha_{eq} \equiv K_{W(B)}\alpha + k_{W(B)}\delta + (\Delta\alpha)_W \tag{18}$$

The term $(\Delta\alpha)_W$ of Equations (17) and (18) is the average AOA induced on the fins by vortices (either body- or wing-generated). The EAOA was later extended[35,36] to include local Mach number and other configuration effects. The model[34] itself treats $K_{W(B)}$ as a nonlinear term, but assumes $K_{B(W)}$ is based on SBT. The major advantage of this approach is that it allows computation of individual fin aerodynamics at any roll orientation and thus can be used to predict 6DOF aerodynamics. That is, not only C_N, C_A, and X_{CP}, but C_Y, C_n, and C_ℓ as well. It has been shown to be effective in predicting missile aerodynamics with reasonable accuracy for many cases. The major weak points are that the method is still an empirical approximation and the many analytical approximations and assumptions apparently degrade the accuracy in predicting aerodynamics over the direct use of data. Secondly, the concept is confusing to many people. That is, by lumping terms together as in Equation (18), it is hard to follow the physics of each aerodynamic phenomena.

As a result of these two shortcomings, the present author attempted a different approach to incorporating configuration nonlinear aerodynamics into Equation (6), beginning in 1992,[37] and further defined in References 1 and 2. The approach of References 37, 1, and 2 was to take each term of Equation (6) and break it down into a linear component, which is estimated by the theoretical low AOA methods of Section 1, and a nonlinear term, which is estimated directly from several large missile component data bases.[38-40] Since the approach at NSWCDD for estimating 6DOF aerodynamics was either numerical codes[31,32] or wind tunnel data, it was decided to focus on trim aerodynamic models for the APC. These models are used to predict planar aerodynamics of weapons designed to fly in a roll-stabilized mode of either 0 deg or 45 deg. This makes the job of getting accurate aerodynamics much easier than predicting 6DOF aerodynamics. It also ties the physics of the flow much closer to the mathematics since each term of Equation (6) must have a linear and nonlinear estimate. Of course, the disadvantages of the direct approach compared to the EAOA approach are: a) one must derive nonlinear expressions for all aerodynamic terms of Equation (6) versus lumping several together as done by Equation (18); and b) it has not been derived for 6DOF aerodynamics. Using the approach of References 1 and 2, we have been able to obtain average

accuracy levels of ±10 percent on C_A and C_N and ±4 percent of body length on X_{CP}. By "average" is meant enough AOAs or Mach number aeropredictions so as to get a good statistical sample. Usually, the first few degrees AOA are excluded from the sample due to measurement errors.

The way Equation (6) is implemented in the AP93, AP95, and AP98 codes is by computing the nonlinearities of the body-alone term based on AOA only, but all the other nonlinear corrections to the interference factors and wing or tail aerodynamics are based on the total AOA, or $\alpha + \delta$. This was done for ease of implementation into the operational AP81 code. Hence, even though the component nonlinear terms were derived from wind tunnel data bases from AOA data only, they were implemented in a total local AOA sense. The empirical nonlinear corrections were then fine-tuned based on comparisons to other configuration aerodynamics outside the data bases. The center of pressure of individual missile component aerodynamics were treated similarly to the AP81 except shifts in center of pressure based on data were derived. These shifts were implemented in tabular form as a function primarily of AOA and M_∞.

Also, the $C_{N_{B(V)}}$ term of Equation (6), which is the downwash normal force on the body due to the wing-shed vortices, is neglected. This is because it is inherently included in the wind tunnel data bases, and it is believed the errors in trying to analytically estimate the term, subtract it out on one configuration, and then add it back in later on a different configuration, are as large or larger than the errors from incorporating it into the $K_{B(W)}$ term.

Equation (6) can also be rewritten as

$$C_N = C_{N_B} + C_{N_{W(B)}} + C_{N_{B(W)}} + C_{N_{T(B)}} + C_{N_{B(T)}} + C_{N_{T(V)}} \tag{19}$$

where it is understood that $C_{N_{B(T)}}$ encompasses the $C_{N_{B(V)}}$ term. For ease of implementation into an existing code designed primarily for linear aerodynamics, most of the terms in Equation (19) are separated into a linear and nonlinear contribution due to α or δ. For example, the wing-body term is computed in the AP98 code as follows:

$$C_{N_{W(B)}} = \left[\left(C_{N_\alpha} \right)_L + \left(C_{N_\alpha} \right)_{NL} \right]_W \left\{ \left[\left(K_{W(B)} \right)_{SBT} + \left(\Delta K_{W(B)} \right)_{NL} \right] \alpha \right.$$

$$\left. + \left(C_1 \left[k_{W(B)} \right]_{SBT} + C_2 \right) \delta_W \right\} \left(\frac{A_W}{A_{REF}} \right) \tag{20}$$

The linear or small AOA terms of Equation (20) are estimated by linear theory (LT) or SBT (see Section 2). This gives the Aeroprediction Code a good fundamental basis for its aerodynamic estimates. The nonlinear corrections due to higher AOA or control deflection are each estimated directly from component wind tunnel data bases.[38-40] Each of the other terms in Equation (19) is

treated in a similar fashion to Equation (20) in the actual implementation into the Aeroprediction Code.

In the context of Equation (19), we therefore seek the nonlinear definition of each of the terms in Equation (19). It is expected that the body-alone term [first term of Equation (19)] will be independent of ϕ. In reality, this is not necessarily the case for M < 2 and high AOA because of the asymmetric shedding of vortices. The mechanism of this shedding is not clear, but it is suspected that slight imperfections in the flow or body shape, from uniform or axisymmetric, respectively, could contribute to this phenomenon. At present, the Aeroprediction Code does not account for out of plane aerodynamics, and therefore the side force created by the asymmetric shedding of body vortices is not predicted. Also, in the Reference 38 data, normal force varied by about 10 percent as a function of roll in the region of asymmetric vortex shedding. Instead of including this variation, it was averaged out.

Since the AP98 includes aerodynamics at both the $\Phi = 0$ and $\Phi = 45$ deg roll orientations, roll dependence on wing-body aerodynamics were investigated based on slender body and linear theory.[26,41] A detailed summary of these findings is presented in Reference 2. A summary of the key findings in Reference 2 on roll-dependent aerodynamics is repeated here for convenience.

a) For cruciform wings alone or a wing-body combination, the total normal force is independent of roll.

b) For a planar wing-body combination at roll, the loading on the windward plane panel is greater by an equal amount to that on the leeward plane panel. This means that if one were trying to design a code for lateral aerodynamics, roll dependence of each fin planform must be considered. On the other hand, if longitudinal aerodynamics are of primary interest, the total normal force on the entire wing planform can be considered.

c) For a cruciform wing-body-tail configuration at roll, eight vortices are shed in the wing-body region, which adversely affects the tail lift. This is as opposed to four vortices at $\Phi = 0$ deg.

d) The planar theory developed for wing-tail interference can be used to approximate the loss of lift on the tails at $\Phi = 45$ deg.

e) The aerodynamics of a cruciform wing-body-tail combination with zero control deflections are independent of roll position.

These findings for roll dependence from linearized or slender body theory are quite useful in helping plan how to develop a nonlinear APC for both $\Phi = 0$ and $\Phi = 45$ deg. While the conclusions of linear theory roll dependence may not translate to the nonlinear case, we will still use the findings to help guide the nonlinear code development. In particular, the item (a) conclusion implies use of the $\Phi = 0$ deg, wing-alone data for $\Phi = 45$ deg. This is quite important because the available wing-alone data bases are all at $\Phi = 0$ deg. This means that any nonlinear wing-alone roll dependence will be included in the interference factors rather than the wing-alone solution, which is independent of Φ.

The second major result of the key slender body/linear theory roll dependence findings is that for cruciform missiles, we can use the same interference approaches as in the AP95, except the constants need to be changed because of a different roll angle. The combination of these two conclusions are quite important because they basically allow the direct usage of the AP95 code with different constants for the nonlinear interference terms at $\Phi = 45$ deg versus $\Phi = 0$ deg.

The third significant conclusion is that for small AOA, wing-body-tail aerodynamics are independent of roll position. This allows the usage of wing-tail interference methodology designed for planar computations for different roll orientations, so long as the proper number of vortices are considered. Again, different nonlinear corrections are expected for the $\Phi = 45$ deg versus the $\Phi = 0$ deg roll position.

With the approach of how the APC incorporates nonlinear configuration aerodynamics having been discussed, the next few sections will take each of the terms in Equations (6) and (19) and discuss how the nonlinear term is defined. Section 2 of this report has already discussed how the low AOA aerodynamics were calculated.

3.2.2 Body Alone

The nonlinear component of the body-alone normal force is predicted by the Allen-Perkins[42] viscous crossflow theory. In developing this theory, Allen reasoned that the total force on an inclined body of revolution is equal to the potential term discussed in Section 2, plus a crossflow term. This term is based on the drag force experienced by an element of a circular cylinder of the same diameter in a stream moving at the cross component of the stream velocity, $V_\infty \sin \alpha$. This crossflow term is primarily created by the viscous effects of the fluid as it flows around the body, often separating and creating a nonlinear normal force coefficient. In equation form, the so-called viscous crossflow theory is:

$$C_{N_{NL}} = \eta C_{d_c} \left(\frac{A_P}{A_{ref}} \right) \sin^2\alpha \qquad (21)$$

Here, η is the drag proportionality factor or crossflow drag of a cylinder of finite length to one of infinite length. C_{d_c} is the crossflow drag coefficient. C_{d_c} has two possible values in the crossflow Mach number range from about 0.1 to about 0.6 depending on whether the flow is supercritical or subcritical. The criteria for determining if the flow is supercritical is that

$$(R_N)_{eff} > R_{N_C}$$
$$M_N > M_{N_C} \qquad (22)$$

where

$$(R_N)_{eff} = \frac{R_{N_D}}{2} \left\{ \frac{\cos\alpha\cot\alpha}{2} + 2\sin\alpha \right\} \left\{ \frac{1 + [1 + (\frac{1}{2}\cot\alpha)^2]^{\frac{1}{2}}}{[1 + (\frac{1}{2}\cot\alpha)^2]^{\frac{1}{2}}} \right\}$$

$$M_N = M_\infty \sin\alpha$$

The term R_{N_D} in Equation (22) is Reynolds number based on body diameter. The standard values of R_{N_C} and M_C set in the AP98 are 180,000 and 0.1 respectively. However, the user is allowed to change these values if a known value of R_{N_C} and M_C are available from a given wind tunnel test.

The AP98 begins transition from subcritical to supercritical flow when the Equation (22) is satisfied. However, the minimum value of C_{d_c} in Equation (16) is not obtained until

$$R_{N_{eff}} = R_{N_C} + 25,000$$

This way, the flow transitions from subcritical to supercritical flow in a continuous, versus abrupt, way.

The final change to the AP95 methodology is to take into account the fact that bodies with fins present have different physical flow characteristics than bodies alone. Most of the wind tunnel data upon which the characteristics of R_{N_C} and M_{N_C} are determined is based on body-alone data. Since in the vicinity where wings or tails are present, the mechanism of boundary layer reattachment in the leeward plane will be harder to establish, and as a result, the length of the body where the lifting surfaces are present will be taken out of the area for the minimum value of C_{d_c}. This length is assumed to be two root chord lengths. Thus, if $(C_{d_c})_1$ and $(C_{d_c})_2$ are sub- and supercritical values of C_{d_c} respectively, then a modified nonlinear normal force of the body alone for supercritical flow (where wings are present) is:

$$\frac{(C_{N_{NL}})_{MOD}}{C_{N_{NL}}} = 1 - \frac{2c_r}{\ell_{ref}} + \frac{(C_{d_c})_1}{(C_{d_c})_2}\left(\frac{2c_r}{\ell_{ref}} \right) \tag{23}$$

The total normal force of the body alone is then the sum of the linear term from Section 2 and the nonlinear term from Equation (23).

3.2.3 Wing Alone

One of the primary reasons for analyzing the slender body and linear theory implications on component aerodynamics in Reference 2 was to show that the wing-alone methodology developed for the $\Phi = 0$ deg plane could also be applied in the $\Phi = 45$ deg plane. This was at least true in the linear sense. It will also be assumed to be true in the nonlinear sense. Any nonlinearities not accounted for in using the $\Phi = 0$ deg methods for $\Phi = 45$ deg will therefore be included in the interference factors.

As a result of this approach, the methodology of Reference 16 can be used directly. This methodology uses a fourth-order equation in AOA to estimate wing-alone lift, as opposed to the second-order approach of Reference 11. The specific equations are defined by

$$C_{N_w} = a_1 \alpha_w + a_2 \alpha_w^2 + a_3 \alpha_w^3 + a_4 \alpha_w^4 \tag{24}$$

$$a_2 = 34.044 \left(C_N\right)_{\alpha=15°} - 4.824 \left(C_N\right)_{\alpha=35°} + 0.426 \left(C_N\right)_{\alpha=60°} - 6.412 a_1 \tag{25}$$

$$a_3 = -88.240 \left(C_N\right)_{\alpha=15°} + 23.032 \left(C_N\right)_{\alpha=35°} - 2.322 \left(C_N\right)_{\alpha=60°} + 11.464 a_1 \tag{26}$$

$$a_4 = 53.219 \left(C_N\right)_{\alpha=15°} - 17.595 \left(C_N\right)_{\alpha=35°} + 2.661 \left(C_N\right)_{\alpha=60°} - 5.971 a_1 \tag{27}$$

The term a_1 of Equations (24) through (27) is the value of wing-alone lift curve slope at $\alpha = 0$ given by linear theory. The terms $\left(C_N\right)_{\alpha=15°}$, $\left(C_N\right)_{\alpha=35°}$ and $\left(C_N\right)_{\alpha=60°}$ are values of the wing-alone normal force coefficients at $\alpha = 15$, 35, and 60 deg, respectively, defined by the data bases of References 39, 40, and 43. Above α_w of 60 deg, extrapolation of the aerodynamics at α_w of 60 deg is used. For more details of the method, the reader is referred to Reference 44. As shown in Reference 44, the fourth-order method of Equations (24) through (27) improves the wing-alone prediction accuracy below $\alpha_w = 30$ deg over the second-order method used in the AP93, while allowing wing-alone aerodynamic estimation to 180 deg.

The value of C_{N_w} computed by Equation (24) includes the linear and nonlinear term. To include it into a term like Equation (20), requires this term to be separated into a linear and nonlinear component. This is easily done, as the linear term is known; so the nonlinear term is simply the difference between the total wing-alone value and its linear counterpart. The secant slope is then formed for each of these terms by dividing the linear and nonlinear parts by the local AOA, $\alpha + \delta$. This approach was taken for ease of incorporation into an existing, operational, linearized code.

3.2.4 Interference Aerodynamics

Interference aerodynamics treated in a nonlinear sense includes that associated with $K_{W(B)}$, $K_{B(W)}$, $k_{W(B)}$, $k_{B(W)}$ and $C_{N_{T(V)}}$ of Equation (6). The linear form of these interference effects are all estimated based on slender body or linear theory and were discussed in Section 2 earlier. Basically, the first four interference factors are all estimated using the general form

$$K = K_{\underset{LT}{SBT}} + \Delta K (M_\infty; \alpha, AR, \lambda) \tag{28}$$

The nonlinear term ΔK of Equation (28), is defined in terms of five tables that are functions of Mach number, AOA, aspect ratio and taper ratio for both $K_{W(B)}$ and $K_{B(W)}$. The general nonlinear trend of those two interference terms is shown in Figure 9. This general trend is basically the same for both the $\Phi = 0$ and $\Phi = 45$ deg roll orientations. However, the five tables of data are different for $\Phi = 0$ and $\Phi = 45$ deg for both $K_{W(B)}$ and $K_{B(W)}$. As already discussed, for cruciform missiles, SBT gives roll independence for the low AOA values of $K_{W(B)}$ and $K_{B(W)}$. Values of the tables for the five variables in the ΔK nonlinear term for both $K_{W(B)}$ and $K_{B(W)}$ are given in References 1 and 2 and will not be repeated here.

As seen in Figure 9, $K_{W(B)}$ in general can deviate slightly from SBT or LT near AOA 0 deg. It then decreases until it reaches a minimum value and then approaches a value of 1.0 at high AOA. On the other hand, $K_{B(W)}$ can either increase or decrease past AOA 0 deg. Eventually, it also decreases until it reaches some minimum value at high AOA. The physics of what occurs in this nonlinear behavior and the details of the interference factor nonlinearities are given in References 1 and 2.

The general nonlinear model for the wing-body interference due to control deflection is of the form

$$k_{W(B)} = C_1(M) \ [k_{W(B)}]_{SBT} + C_2(|\alpha_W|, M) \tag{29}$$

for both the $\Phi = 0$ and $\Phi = 45$ deg roll orientations. However, the values $C_1(M)$ and $C_2(|\alpha_W|, M)$ are different for the two roll positions. Tables of C_1 and C_2 are given in Reference 2. The nonlinear model for the body-tail interference due to control deflection is of the form

$$k_{B(W)} = [k_{B(W)}]_{SBT} + C(\alpha_W) \tag{30A}$$

for $\Phi = 0$ deg roll and of the form

$$k_{B(W)} = [k_{B(W)}]_{SBT} + C(\delta_W) \tag{30B}$$

for $\Phi = 45$ deg roll. Again, the constants $C(\alpha_W)$ and $C(\delta_W)$ are defined in Reference 2.

Figure 10 presents a qualitative view of how the interference terms $k_{W(B)}$ and $k_{B(W)}$ behave. In examining Figure 10A, it is seen that for low Mach numbers, slender body theory generally underpredicts the value of $k_{W(B)}$ at low AOA. At some value of α_W, which is bout 25 deg, $k_{W(B)}$ starts decreasing rapidly and goes to zero around a value of $\alpha_W = 50$ to 55 deg. This behavior is believed to be the combination of wing stall and air flowing between the wing and body (or blow-by). On the other hand, for high supersonic Mach numbers, just the reverse behavior occurs. At low AOA, SBT overpredicts the value of $k_{W(B)}$. However, as AOA increases, the value of $k_{W(B)}$ increases due to compressibility nonlinearities until a point where the blow-by effects offset the compressibility effects. The additional lift on the wing then goes to zero at around an α_W of 75 deg.

$$K_{W(B)} = [K_{W(B)}]_{SBT} + f([\Delta K_{W(B)}]_{\alpha=0},\ \alpha_C,\ \frac{dK_{W(B)}}{d\alpha},\ \alpha_D,\ \alpha_M)$$
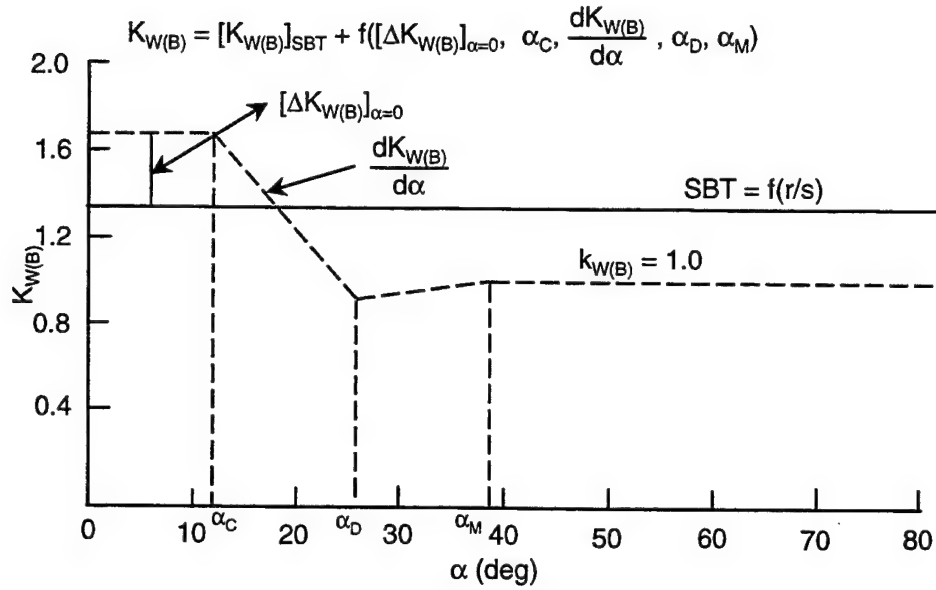
FIGURE 9A. GENERIC REPRESENTATION OF $K_{W(B)}$ WITH AOA
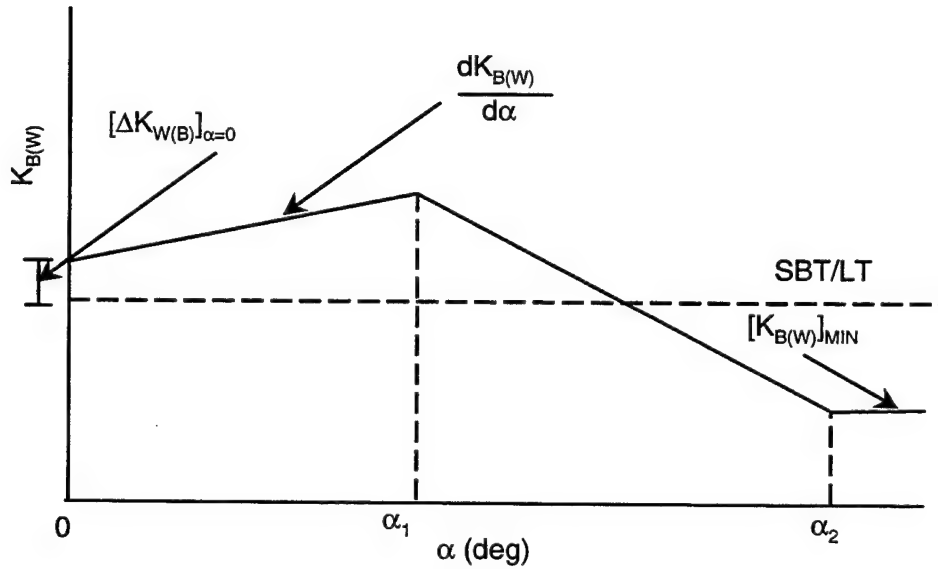
$$K_{B(W)} = [K_{B(W)}]_{\underset{SBT}{LT}} + f([\Delta K_{B(W)}]_{\alpha=0},\ \alpha_1,\ \alpha_2,\ \frac{dK_{B(W)}}{d\alpha},\ [K_{B(W)}]_{MIN})$$

FIGURE 9B. GENERIC REPRESENTATION OF $K_{B(W)}$ WITH AOA

28
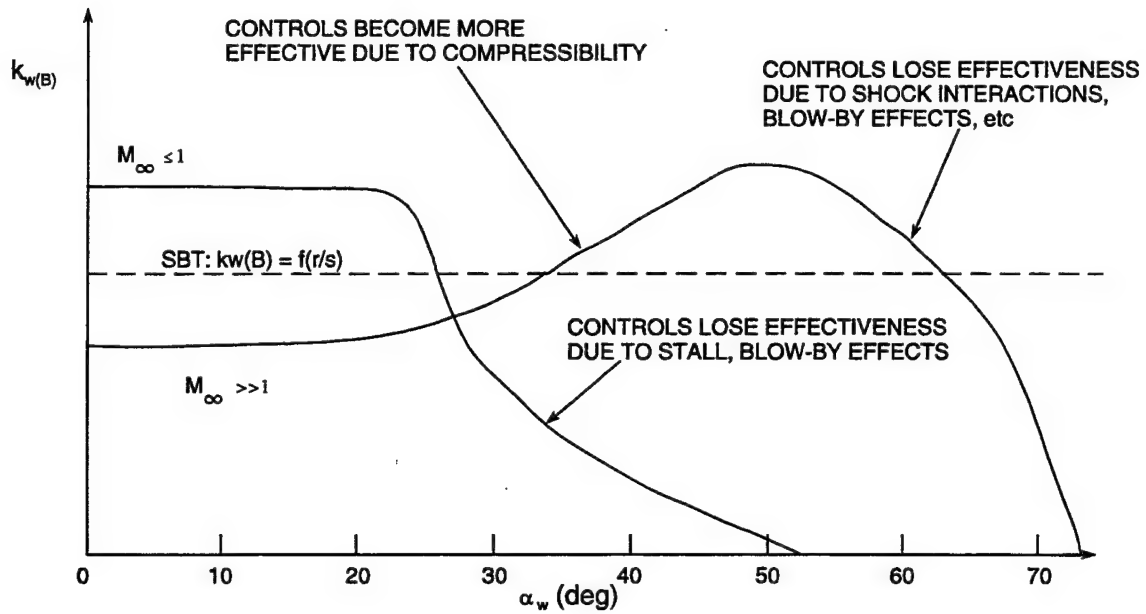
FIGURE 10A. QUALITATIVE TREND OF WING-BODY INTERFERENCE DUE TO CONTROL
DEFLECTION AS A FUNCTION OF M_∞, α_w
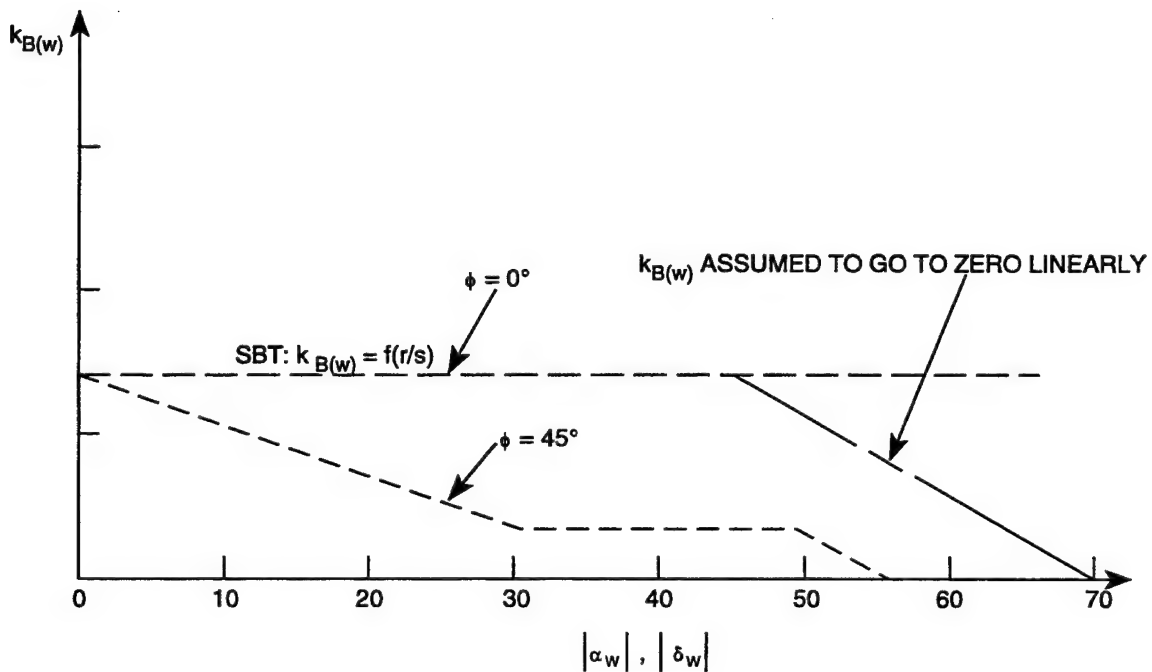
FIGURE 10B. QUALITATIVE TREND OF BODY-WING INTERFERENCE DUE TO CONTROL
DEFLECTION AS A FUNCTION OF α_w, δ_w

29

Figure 10A was derived primarily from total missile configuration data bases as opposed to the missile component data base of Reference 38. The reason for this was the control fins in the Reference 38 data base were too small to get accurate values of the additional lift due to δ. The downside to the approach taken to derive $k_{W(B)}$ is the fact that without missile force and moment components identified, part of the $k_{W(B)}$ term may actually be $k_{B(W)}$. Hence, the model that represents $k_{B(W)}$ of Figure 10B basically represents the remaining load due to control deflection required to match total missile configuration data bases. As seen in Figure 10B, $k_{B(W)}$ starts out with its SBT theory value at $|\alpha_W|$ or $|\delta_W| = 0$ deg (depending on whether roll of 0 or 45 deg is of interest), and then decreases at some value of $|\alpha_W|$ or $|\delta_W|$ in a linear fashion. CFD analysis or additional wind tunnel data with larger control surfaces would allow refinement of Equations (29) and (30).

The last interference term considered is that of the wing-shed vortices on the tail surfaces. It is the next to last term of Equation (6). In general, the nonlinear form of $C_{N_{T(V)}}$ is defined by

$$C_{N_{T(V)}} = \frac{A_W(C_{N_\alpha})_W (C_{N_\alpha})_T \left[K_{W(B)}\alpha + Fk_{W(B)}\delta_W\right]}{2\pi (AR)_T (f_w - r_w) A_{ref}} (s_T - r_T)\left[i_1 \cos\Phi + i_4 \sin\Phi\right] \qquad (31)$$

Equation (31) reverts back to SBT for low AOA. At higher AOA, $(C_{N_\alpha})_W$, $(C_{N_\alpha})_T$, $K_{W(B)}$, $k_{W(B)}$, F, i_1, and i_4 all have nonlinearities. The terms i_1 and i_4 of Equation (31) represent the wing-tail interference factor for the windward and leeward planes respectively. At $\Phi = 0$ deg, only the i_1 factor is of interest, whereas at $\Phi = 45$ deg, both the leeward and windward planes are considered. The nonlinearity is introduced into i_1 and i_4 in the $\Phi = 45$ deg roll by defining loading factors for the windward and leeward plane fins. These factors are:

$$P_W = \left(1.0 + 0.6\frac{\alpha}{65}\right), \quad P_\ell = \left(1.0 - 0.6\frac{\alpha}{65}\right) \; ; \; \alpha \le 65$$

$$P_W = 1.6 \; , \; P_\ell = 0.4 \; ; \; \alpha > 65 \qquad (32)$$

P_W and P_ℓ have the effect of increasing or decreasing the strength of the wing-shed vortex from the windward or leeward plane respectively. These factors are used in the calculation of i_1 and i_4.

The parameter F of Equation (31) is used as a control on the control deflection component of $C_{N_{T(V)}}$ and is determined empirically based on comparisons of theory to experiment. It is defined in the same tables as $k_{W(B)}$ and $k_{B(W)}$ of Reference 2. To put an additional nonlinear control of the first term of $C_{N_{T(V)}}$, Equation (31) was broken down into components due to α and δ. That is,

$$C_{N_{T(V)}} = \left[C_{N_{T(V)}}\right]_\alpha + \left[C_{N_{T(V)}}\right]_\delta \qquad (33)$$

The term due to α, was then defined as

$$\left[C_{N_{T(V)}}\right]_{\alpha} = A + B\alpha + C\alpha^2 + D\alpha^3 \tag{34}$$

for $\Phi = 0$ deg, and as

$$\left[C_{N_{T(V)}}\right]_{\alpha} = G_1 \left[C_{N_{T(V)}}\right]_{SBT} \tag{35}$$

for $\Phi = 45$ deg. A, B, C, D, and G_1 were all constants determined empirically based on data and are also defined in Reference 2. In addition, a maximum value constraint was placed on the overall value of $C_{N_{T(V)}}$ so as not to allow it to exceed the lift on the tail alone.

3.3   CENTER OF PRESSURE

The body-alone center of pressure is computed based on a weighted average of the linear and nonlinear components of normal force. That is

$$X_{CP} = \frac{C_{N_L}(X_{CP})_L + C_{N_{NL}}(X_{CP})_{NL}}{C_{N_L} + C_{N_{NL}}} \tag{36}$$

where the linear center of pressure is defined based on the Section 2 low AOA methods and the nonlinear center of pressure is the centroid of the planform area. Two nonlinear phenomena occur on the body-alone center of pressure that Equation (36) does not fully account for. These are the asymmetric shedding of vortices at AOA greater than about 25 deg and at $M_\infty < 2.0$ and the transonic effects of a shock standing on the body. As a result, a table of center of pressure shifts was defined empirically as a function of AOA and Mach number. This table is given in Reference 1.

The center of pressure of the wing-alone and wing-body normal force is assumed to vary from its linear value at zero AOA to the centroid of the wing planform at 60 deg AOA. If A and B are the centers of pressure of the linear and nonlinear normal force terms (in percent of mean geometric chord), and $\alpha_W = \alpha + \delta$, then the center of pressure of the wing-body or wing-alone lift is

$$\left(X_{CP}\right)_{WB} = \left(X_{CP}\right)_W = A + \frac{1}{36} |\alpha_W| (B-A) + \frac{1}{5400} \alpha_W^2 (A-B) \tag{37}$$

Equation (37) is the methodology used for roll position of 0 deg.

When the fins are rolled to a non-zero roll orientation, the center of pressure Equation (37) will change because of the geometry of the wings and an asymmetric effect on the wing loading. To visualize this effect, imagine a missile rolled to $\Phi = 45$ deg and increasing in AOA. As AOA increases, two things occur. First, the windward plane fins carry more and more of the load

compared to the leeward plane fins. Second, the local Mach number in the windward plane is different, and typically lower, than the leeward plane. This has the effect of shifting the wing-alone center of pressure forward in the windward plane. Since the load and wing centers of pressure are different on the windward and leeward plane fins, this results in a net forward shift in the center of pressure for $\Phi = 45$ deg roll compared to the $\Phi = 0$ deg computation of Equation (37). This shift appears to occur for all Mach numbers, and is largest at moderate AOA, and goes to zero at AOA 0 and 90 deg. At 90 deg AOA, the windward plane fins carry almost all the load compared to the leeward plane fins, but geometrically, the fins are all aligned perpendicular to the AOA plane. This center of pressure shift was derived in Reference 2 and is

$$\left(\Delta X_{CP}\right)_{WB} = - \left[r + \left(\frac{b}{C_r + C_t} \right) \left(\frac{C_r}{2} - \frac{C_t}{3} \right) \right] \cos(\Phi) \ \sin(2\alpha) \left(\frac{0.8\alpha}{65} \right) \ ; \ \alpha \leq 65$$

$$= - \ 0.8 \left[r + \left(\frac{b}{C_r + C_t} \right) \left(\frac{C_r}{2} - \frac{C_t}{3} \right) \right] \cos\Phi \ \sin(2\alpha) \ ; \ \alpha > 65 \quad (38)$$

Equation (38) is added to Equation (37) for the roll orientation of 45 deg.

The center of pressure of the body-wing carryover normal force contribution is at the centroid of the Mach box created by the Mach lines from the leading and trailing edges of the wings as they cross the body planar surface. For $\Phi = 45$ deg roll, the local Mach number, computed by Modified Newtonian Theory, is used to define the Mach box. This has the effect of shifting the center of pressure of this component of normal force slightly forward.

3.4   NONLINEAR AERODYNAMIC LOADS DISTRIBUTION

Section 3.3 discussed how the nonlinear aerodynamic loads were computed for typical missile configurations. This nonlinear aerodynamic load is defined primarily in terms of total force, moment and center of pressure. Some distribution information is provided for the nonlinear component of the body loads, but none is currently available for the lifting surface loads or for their interference effects on the body. This situation is not restrictive in terms of aerodynamic and performance analysis. Structural engineers, however, need to know not only the magnitude of the aerodynamic forces, but also how they are distributed over the surface of a missile if they are to determine the shear and bending moments to which its components will be subjected. For this reason, the AP95 code was modified to allow the prediction of the distribution of the nonlinear, as well as the linear, aerodynamic loads over both the body and control surfaces. All interference effects were included in the analysis in addition to the individual component nonlinear aerodynamics. It is believed that the next version of the Aeroprediction Code (AP98) will be the first code of its kind to offer this capability.

The body-alone load distribution is composed of a linear term that is computed based on integration of the pressures computed along and around the body (see Section 2) and the local component of nonlinear load from the viscous crossflow methodology. That is,

$$C_{n_B} = \left(\frac{-2}{\pi r_r^2}\right) \int_0^\pi C_P(x,\phi)(\cos\phi)rd\phi + \frac{\eta C_{D_C}\sin^2\alpha}{A_{REF}}r(x) \tag{39}$$

Comparison of Equation (39) results to CFD results[3] showed that the predicted load in the nose region was slightly too high at low AOA. As a result, some of the nonlinear load in the nose region was shifted to the afterbody below AOA at 30 deg. The total normal force and pitching moments were held constant before and after the load redistribution. A better match of approximate body loads with CFD was then obtained.

The body-wing and body-tail loads of Equation (6) are represented using the Mach lines from the leading and trailing edges of the wing or tail in conjunction with the total normal force component load. The total normal force component load is used to determine the height of the trapezoidal load created in the vicinity of the root chord by the carryover of the induced wing effects onto the body. If these induced effects fall behind the end of the body, the height of the trapezoid is readjusted to make sure the total local integrated loads equals that of the aerodynamic component.

The load on the wing in conjunction with the body of Equation (6) is treated in the following manner. First, the local linear load and its center of pressure are computed based on Section 2 methods. The local load along any chord of the wing or tail is then:

$$\left[c_n(y)\right]_L = \frac{1}{c(y)} \int_{x_{LE}}^{x_{TE}} \Delta C_P(x,y)dx \tag{40}$$

The chordwise center of pressure of that load is simply the center of gravity of the local chordwise load. The total load on any wing chord is assumed to be of the form

$$\left(c_n(y)\right)_W = \left(\left[c_n(y)\right]_L\right)_W \left(\frac{C_{N_{W(B)}}}{\sum_{SPAN}\left(\left[c_n(y)\right]_L\right)_W}\right) \tag{41}$$

Equation (41) basically assumes the nonlinear load is distributed similarly to the linear load. In validating this assumption against CFD computations, it was found to be quite reasonable.

The wing-tail interference load (next to last term of Equation (6)) is assumed to be distributed in a "$1/r^2$" manner from where the wing-shed vortex hits the tail surface. Also, some of the wing-tail load is distributed onto the body between the tail surfaces. The reader is referred to Reference 3 for the details of this methodology.

When the missile is in the roll position of $\Phi = 45$ deg, the body carryover load shows somewhat of a different behavior than at $\Phi = 0$ deg. At $\Phi = 45$ deg, the high pressure region in the vicinity of the wings is maintained just like at $\Phi = 0$ deg. However, behind the wings, the body carryover can actually go negative. This is modeled by allowing the positive trapezoidal load induced by the Mach lines from the wing leading and trailing edges to go negative behind the root chord. The only constraint is that the total load and pitching moment remain constant at the values determined by the aerodynamic load and pitching moments. Also, the windward plane wing carries more load than the leeward plane wing. This is modeled through the use of Equation (32).

4.0 ASYMMETRIC CONFIGURATION METHODOLOGY

The body-alone nonaxisymmetric body methodology was based on extensions of the method of Jorgensen,[45] and the wing-body interference effects methodology was based on extensions of Nelson[46] and Est and Nelson[47] at low AOA and the method of the present authors[1,2] at high AOA. Several new additions to the state-of-the-art were made in extending the methods of References 45 through 47. Figure 2 shows the noncircular wing-body cases of interest.

Basically, the method of Jorgensen, extended by the Reference 5 methods, defined the axial and normal force and pitching moment coefficients as

$$C_A = C_{A_O} \cos^2\alpha \tag{42}$$

$$C_N = C_{N_L} \left(\frac{C_n}{C_{n_o}}\right)_{SB} + C_{N_{NL}} \left(\frac{C_n}{C_{n_o}}\right)_N NF \tag{43}$$

$$C_M = C_{M_L} \left(\frac{C_n}{C_{n_o}}\right)_{SB} + C_{M_{NL}} \left(\frac{C_n}{C_{n_o}}\right)_N NF \tag{44}$$

The subscripts L and NL represent the linear and nonlinear components of normal force and pitching moment respectively. The factors $(C_n/C_{n_o})_{SB}$ and $(C_n/C_{n_o})_N$ represent the slender-body and Newtonian approximations to the local normal force coefficient per unit length of the desired cross-sectional shape (C_n) to the similar coefficient for the equivalent circular cross-sectional shape (C_{n_o}). The major contribution of Jorgensen was in showing that aerodynamics of a noncircular cross-sectional shape could be computed reasonably accurately to high AOA if the factors C_n/C_{n_o} were defined. He defined these for ellipses.

Jorgensen's theory was more limited than desired to consider all the cases of Figure 2. As a result, Reference 5 provided significant extensions to the Jorgensen methodology. First of all, additional equations were derived for $(C_n/C_{n_0})_N$ for shapes other than ellipses (see Figure 11). Secondly, Newtonian correction factors (NF) were derived for low crossflow Mach numbers where Newtonian theory was inaccurate. Jorgensen had no factor, NF, in his equations. Figures 12 through 14 give these values along with the equations used to compute NF for ellipses, squares, and triangles. Third, a critical Reynolds number was defined for noncircular shapes as a function of the circular value of R_{N_C}. These values are given in Figure 15. Fourth, the AOA axial force was computed using References 1 and 4 for the equivalent axisymmetric body. The only other change in axial force coefficient was in the skin-friction component where

$$\left(C_{A_f}\right)_{NC} = \left(C_{A_f}\right)_C \frac{(Cir)_{NC}}{(Cir)_C} \tag{45}$$

Fifth, wing-body interference factors were derived based on the methods of References 46 and 47 at low AOA (see Figure 16). At high AOA, wing-body interference factors were derived based on the methods of References 1 and 2. Thus, the body cross-sectional shape was allowed to influence the aerodynamics at low and moderate AOA, whereas at AOA greater than about 30 deg, it was not. Finally, slender body theory scaling factors were derived to allow one to compare aerodynamics computed based on an equivalent axisymmetric body or a body of constant width to wind tunnel data taken on a body of constant width or constant cross-sectional area. Figure 17 gives a summary of the slender body theory scaling factors for use in Figure 16B. Figure 16A was based on $\pi d_{eq}^2/4$ and all elliptical wind tunnel data examined by the author was taken that way, so $(SBTSF)_1$ and $(SBTSF)_2$ of Figure 17 are both 1.

The brief summary given here does not go into any of the details of the derivation of Figures 12 through 17 or the equations that accompany them. The interested reader is once again referred to Reference 5 for these details.

One final point needs to be made before leaving the summary on nonaxisymmetric body aerodynamics. That concerns the local loads used by the structural analyst. Reference 3 developed a fairly accurate way of distributing the nonlinear aerodynamic loads over the body and lifting surfaces based on CFD results for an axisymmetric body. What is generated within the aeroprediction code is the aerodynamic load distribution for the equivalent circular body. It is possible that some noncircular cross sections may have loading patterns that are significantly different. Unfortunately, there was not enough data available to determine whether this was the case or to attempt to model these effects if present. To resolve this issue would require either wind tunnel measurements or CFD computations to determine detailed surface pressure maps for an extensive range of cross section shapes. Such an endeavor was beyond the scope of the present work, but should certainly be considered in the future if sufficient time and resources became available.
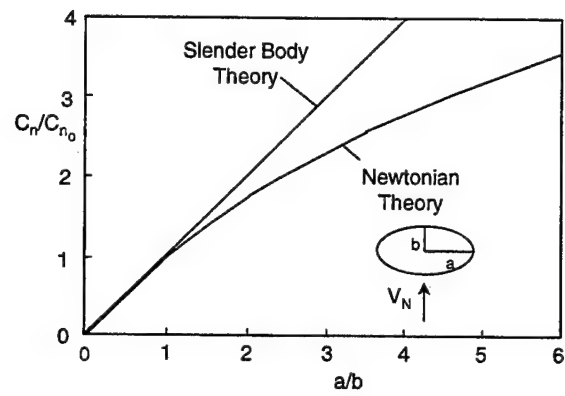
a. Ellipses
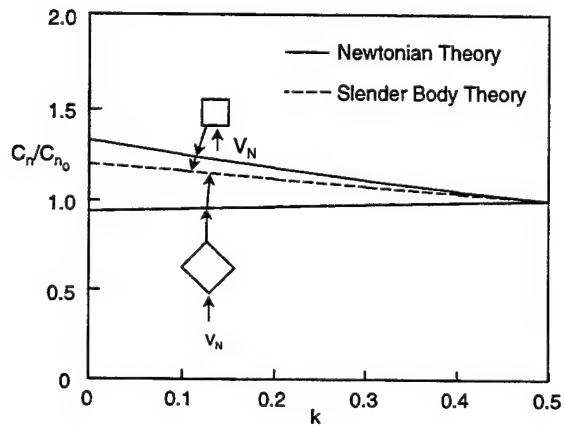
b. Squares
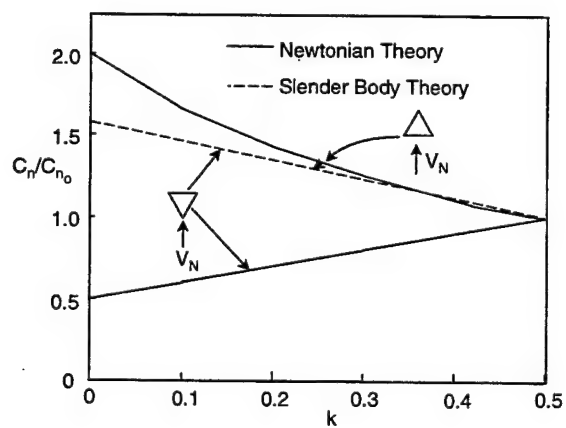
c. Triangles

FIGURE 11. RATIO OF LOCAL NORMAL FORCE COEFFICIENT FOR VARIOUS CROSS SECTIONAL
BODY SHAPES TO THAT FOR THE EQUIVALENT CIRCULAR CROSS SECTION
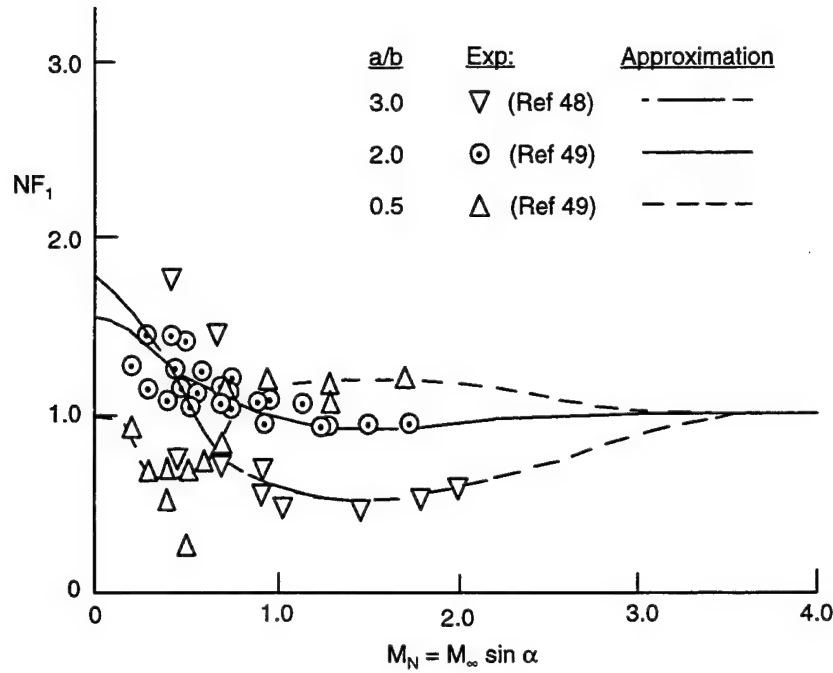
Newtonian Correction Factor for an Elliptical Cross Section ($\alpha \geq 20$ deg)

Low AOA Merging

$$NF = 1 + [(NF)_1 - 1] \frac{\alpha}{20} \quad ; \quad \alpha \leq 20$$

$$NF = (NF)_1 \qquad ; \quad \alpha > 20$$

Values of a/b other than 0.5, 2.0, 3.0

$$NF = (NF)_{a/b=3} \qquad ; \quad a/b > 3.0$$

$$NF = \left\{ (NF)_{a/b=3} - (NF)_{a/b=2} \right\} (a/b - 2) + (NF)_{a/b=2} \quad ; \quad 2 \leq a/b \leq 3.0$$

$$NF = \left\{ (NF)_{a/b=2} - 1 \right\} (a/b - 1) + 1 \qquad ; \quad 1 \leq a/b < 2.0$$

$$NF = \left\{ (NF)_{a/b=0.5} - 1 \right\} 2(1 - a/b) + 1 \qquad ; \quad 0.5 \leq a/b < 1.0$$

$$NF = (NF)_{a/b=0.5} \qquad ; \quad a/b \leq 0.5$$

FIGURE 12. NEWTONIAN CORRECTION FACTOR METHODOLOGY FOR AN ELLIPSE
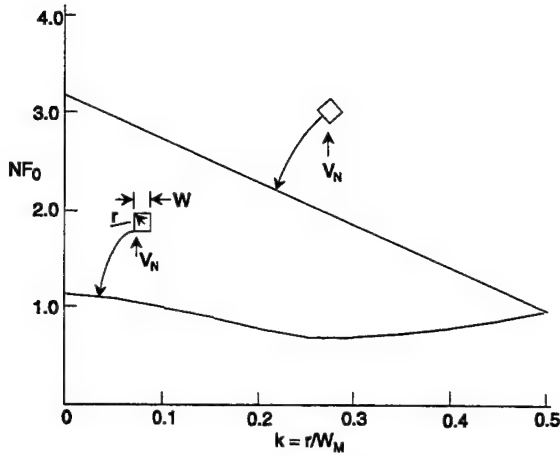
Newtonian Correction Factor for Squares as a Function of Corner Radius at $M_N = 0$
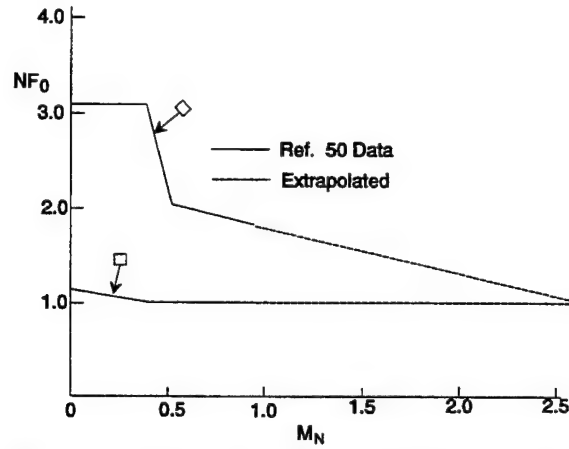
Newtonian Correction Factor for Squares as a Function of Crossflow Mach Number $(k = 0)$

Squares

$$NF = NF_0 \quad ; \quad M_N \leq M_{N_0}$$

$$NF = NF_0 - \left(\frac{M_N - M_{N_0}}{1 - M_{N_0}} \right) (NF_0 - 1) \quad ; \quad M_{N_0} < M_N \leq 1.0$$

$$NF = 1.0 \quad ; \quad M_N > 1.0$$

Diamond

$$NF = NF_0 \quad ; \quad M_N \leq M_{N_0}$$

$$NF = NF_0 - \left(\frac{M_N - M_{N_0}}{0.55 - M_{N_0}} \right) [0.55 (NF_0 - 1)] \quad ; \quad M_{N_0} < M_N \leq 0.55$$

$$NF = (NF)_{M_N=0.55} - \frac{M_N - 0.55}{2.05} \left[(NF)_{M_N=0.55} - 1 \right] \quad ; \quad 0.55 < M_N \leq 2.6$$

$$NF = 1.0 \quad ; \quad M_N > 2.6$$

M_{N_0}

$$M_{N_0} = 0.4 - 2.67k \quad ; \quad k \leq 0.15$$

$$M_{N_0} = 0 \quad ; \quad k > 0.15$$

FIGURE 13. NEWTONIAN CORRECTION FACTOR METHODOLOGY FOR SQUARES
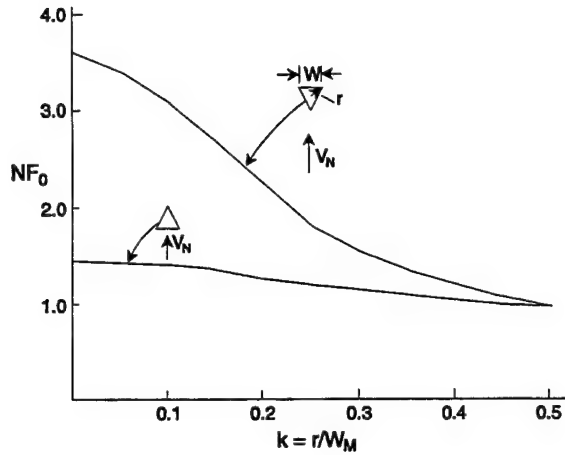
Newtonian Correction Factor for Triangles as a Function of Corner Radius ($M_N = 0$)
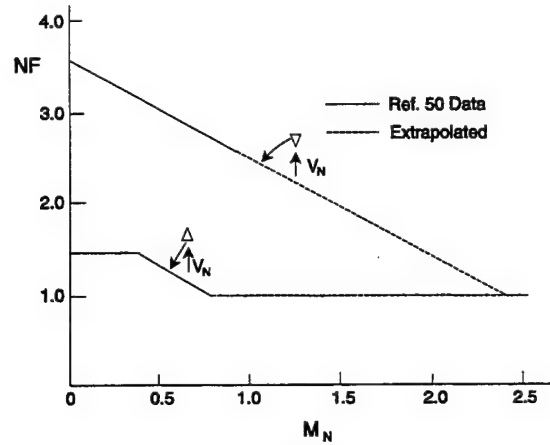
Newtonian Correction Factor for Triangles as a Function of Crossflow Mach Number ($k = 0$)

Triangle

$$NF = NF_0 \quad ; \quad M_N \leq M_{N_0}$$

$$NF = NF_0 - \left(\frac{M_N - M_{N_0}}{0.80 - M_{N_0}} \right) (NF_0 - 1) \quad ; \quad M_{N_0} < M_N \leq 0.80$$

$$NF = 1.0 \quad ; \quad M_N > 0.80$$

Inverted Triangle

$$NF = NF_0 - \left(\frac{M_N - M_{N_0}}{2.4 - M_{N_0}} \right) (NF_0 - 1) \quad ; \quad M_N \leq 2.4$$

$$NF = 1.0 \quad ; \quad M_N > 2.4$$

$\underline{M_{N_0}}$

$$M_{N_0} = 0.4 - 2.67k \quad ; \quad k \leq 0.15$$

$$M_{N_0} = 0 \quad ; \quad k > 0.15$$

FIGURE 14. NEWTONIAN CORRECTION FACTOR METHODOLOGY FOR TRIANGLES
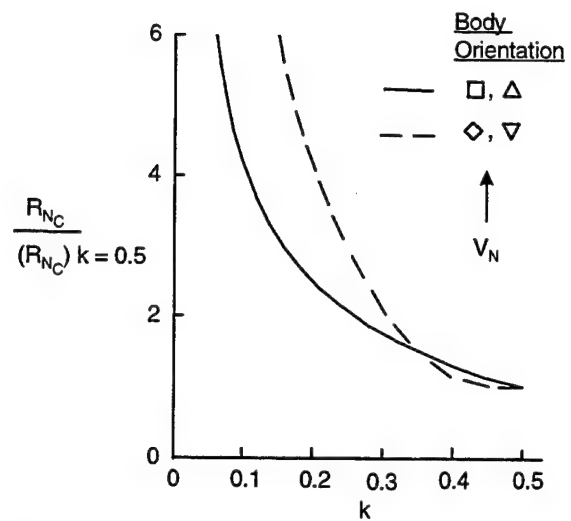
Critical Reynolds Number for Squares and Triangles
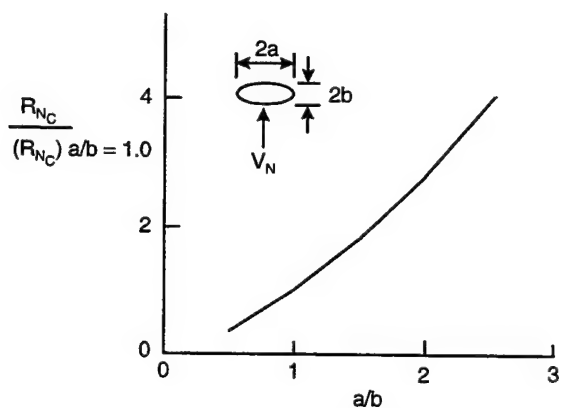
Critical Reynolds Number for Ellipses

where R_{N_C} Defined for a given W/T or Flight Test

R_{N_C} Typically 1×10^5 to 4×10^5

FIGURE 15. CRITICAL REYNOLDS NUMBER FOR NONCIRCULAR SHAPES

Ratio of Wing-body Interference of Elliptical Body to That of Equivalent Circular Body
(Reference 46) (based on $\pi \, d_{eq}^2/4$)
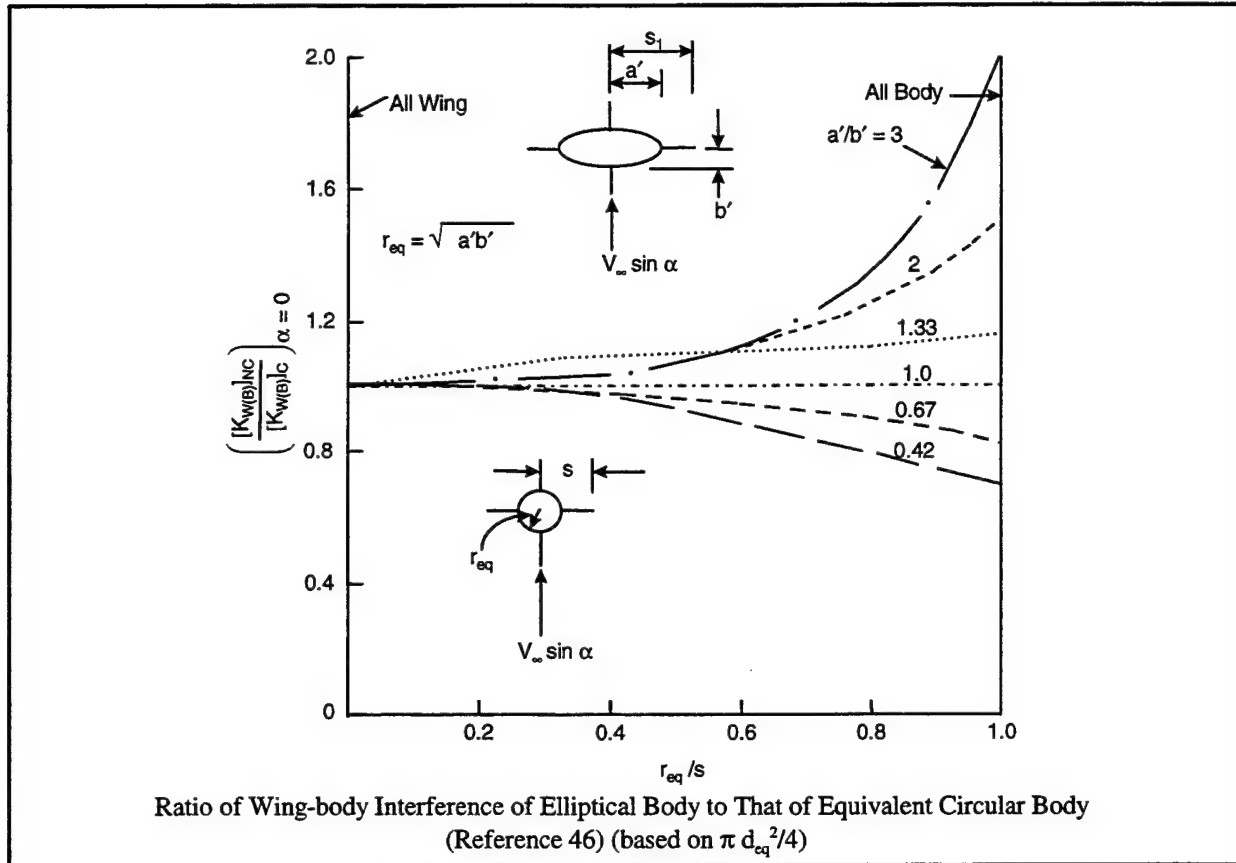
$$F \equiv \frac{\left[K_{W(B)}\right]_{NC, \, \alpha}}{\left[K_{W(B)}\right]_{C, \, \alpha}} \qquad \left[K_{B(W)}\right]_{NC, \, \alpha} = F \left[K_{B(W)}\right]_{C, \, \alpha}$$

$$\left[k_{B(W)}\right]_{NC, \, \alpha} = F \left[k_{B(W)}\right]_{C, \, \alpha} \qquad \left[k_{W(B)}\right]_{NC, \, \alpha} = \left[k_{W(B)}\right]_{C, \, \alpha}$$

Impact of Square and Triangle Body Cross Sections on Low Mach Number Values of $K_{W(B)}$
(Data from References 51 and 52 And Based on $A_{ref} = \pi \, W^2/4$)

$$[K_{W(B)}]_{NC} = \left([K_{W(B)}]_{\substack{NC \\ r/s=1}} - 1\right) r/s + 1$$
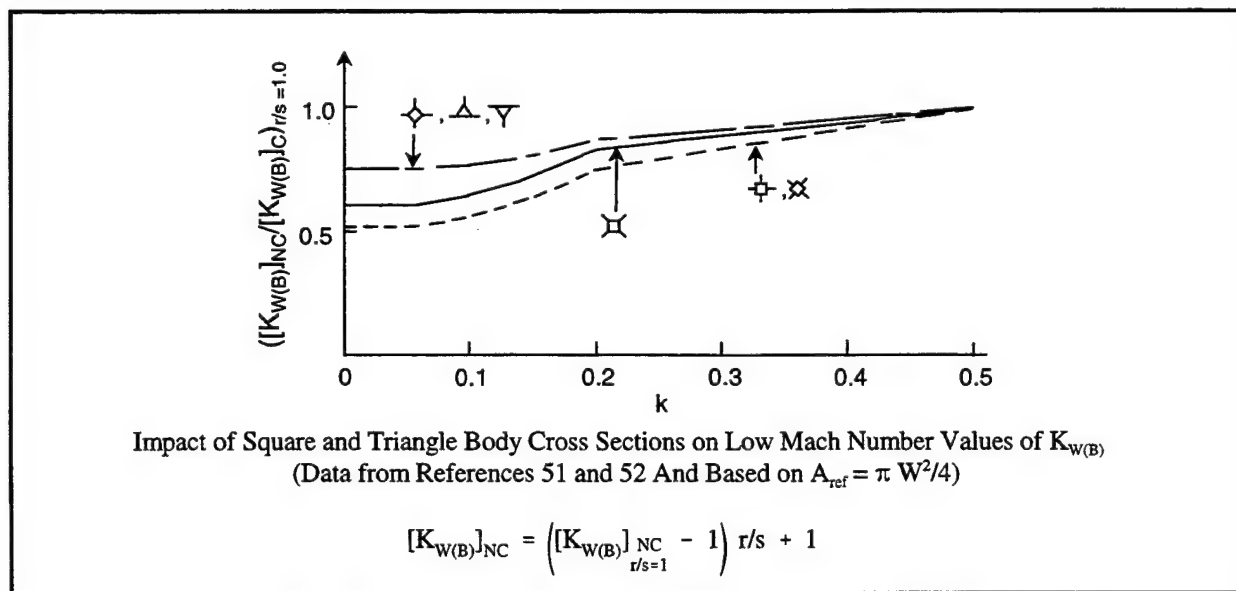
FIGURE 16. WING-BODY INTERFERENCE FACTORS (LOW AOA)

41

$$C_N = C_{N_B}(SBTSF)_1 + \left[C_{N_{W(B)}} + C_{N_{B(W)}}\right](SBTSF)_2 \tag{1}$$

Aero based on $\pi W^2/4$ and W/T data taken that way

$$(SBTSF)_1 = \left(\frac{d_{eq}}{W}\right)^2$$
$$(SBTSF)_2 = 1 \tag{2}$$

Aero based on $\pi d_{eq}^2/4$ and W/T data taken that way

$$(SBTSF)_1 = 1$$

$$(SBTSF)_2 = \frac{\left(\frac{s}{r}\right)_{eq}^2\left[1 - 2\left(\frac{r}{s}\right)_{eq}^2 + \left(\frac{r}{s}\right)_{eq}^4\right]}{\left(\frac{s}{r}\right)_{\ell}^2\left[1 - 2\left(\frac{r}{s}\right)_{\ell}^2 + \left(\frac{r}{s}\right)_{\ell}^4\right]} \tag{3}$$

Aero based on $\pi d_{eq}^2/4$ and W/T data based on $\pi W^2/4$

$$(SBTSF)_1 = \left(\frac{d_{eq}}{W}\right)^2$$

$$(SBTSF)_2 = \frac{\left(\frac{s}{r}\right)_{eq}^2\left[1 - 2\left(\frac{r}{s}\right)_{eq}^2 + \left(\frac{r}{s}\right)_{eq}^4\right]}{\left(\frac{s}{r}\right)_{\ell}^2\left[1 - 2\left(\frac{r}{s}\right)_{\ell}^2 + \left(\frac{r}{s}\right)_{\ell}^4\right]} \tag{4}$$

Note: Equations (1) through (4) apply to triangles and squares of Figure 16B. Ellipses (Figure 16A) derived based on $\pi d_{eq}^2/4$. $(s/r)_{\ell}$ is local value of s/r where wing is located.

FIGURE 17. SBT SCALING

5.0 SUMMARY OF AERODYNAMIC METHODS

A summary of the theoretical and empirical methods used for computing aerodynamics in the AP98 are given in Figures 18 through 20. Figure 18 summarizes the body-alone methods, Figure 19 summarizes the wing and interference aerodynamic methods, and Figure 20 summarizes the dynamic derivative methods. All the methods shown in Figures 18 through 20 were discussed in Sections 2 through 4 of this report. The major new additions to the AP98 are shown in Figures 18 and 19, which include the Improved Axial Force at AOA, $\Phi = 45$ deg aerodynamics, Nonlinear Structural Loads and Nonaxisymmetric Body Aerodynamics. No changes have been made to the dynamic derivative methods of Figure 20, which are still linear with no nonlinear terms included. Also, although not shown in Figures 18 through 20, a significantly more robust pre- and post-processing software package for personal computer usage will be developed for the AP98. Using a personal computer with a 200 megahertz chip, a single case can be executed in much less than a second, even though the computer code listing now exceeds 17,000 lines.

COMPONENT/ MACH NUMBER REGION	SUBSONIC $M_\infty < 0.8$	TRANSONIC $0.8 \leq M_\infty \leq 1.2$	LOW SUPERSONIC $1.2 \leq M_\infty \leq 1.8$	MOD/HIGH SUPERSONIC $1.8 \leq M_\infty \leq 6.0$	HYPERSONIC $M_\infty > 6.0$
NOSE WAVE DRAG	EMPIRICAL (Ref. 6)	SEMIEMPIRICAL BASED ON EULER SOLUTIONS (Ref. 19)	SECOND-ORDER VAN DYKE PLUS MNT (Ref. 6)	SOSET PLUS IMNT (Ref. 13)	SOSET PLUS IMNT MODIFIED FOR REAL GASES (Ref. 14)
BOATTAIL OR FLARE WAVE DRAG	- - -	WU AND AOYOMA (Ref. 6)	SECOND-ORDER VAN DYKE (Ref. 7)	SOSET (Ref. 11)	SOSET FOR REAL GASES (Ref. 14)
SKIN FRICTION DRAG	VAN DRIEST II (Ref. 15)				
BASE DRAG	IMPROVED EMPIRICAL METHOD (Ref. 17)				
AXIAL FORCE AT α	IMPROVED EMPIRICAL METHOD (Ref. 4)				
AEROHEATING INFORMATION	- - -			SOSET PLUS IMNT FOR REAL GASES (Ref. 21)	
INVISCID LIFT AND PITCHING MOMENT	EMPIRICAL (Ref. 6)	SEMIEMPIRICAL BASED ON EULER SOLUTIONS (Ref. 19)	TSIEN FIRST-ORDER CROSSFLOW (Ref. 8)	SOSET (Ref. 11)	SOSET FOR REAL GASES (Ref. 14)
VISCOUS LIFT AND PITCHING MOMENT	IMPROVED ALLEN AND PERKINS CROSSFLOW (Ref. 42)				
NONAXISYMMETRIC BODY AERO ($\Phi = 0, 45°$)	MODIFIED JORGENSEN (Ref. 5)				
NONLINEAR ST. LOADS AVAIL. ($\Phi = 0, 45°$)	NO		YES (Ref. 3)		

FIGURE 18. AP98 METHODS FOR BODY-ALONE AERODYNAMICS

COMPONENT/ MACH NUMBER REGION	SUBSONIC $M_\infty < 0.8$	TRANSONIC $0.8 \leq M_\infty \leq 1.2$	LOW SUPERSONIC $1.2 \leq M_\infty \leq 1.8$	MOD/HIGH SUPERSONIC $1.8 \leq M_\infty \leq 6.0$	HYPERSONIC $M_\infty > 6.0$
WAVE DRAG		EMPIRICAL (Ref. 27)	LINEAR THEORY PLUS MNT (Ref. 27)	SHOCK EXPANSION (SE) PLUS MNT ALONG STRIPS (Ref. 13)	SE PLUS MNT FOR REAL GASES ALONG STRIPS (Ref. 13)
SKIN FRICTION DRAG	VAN DRIEST II (Ref. 15)				
TRAILING EDGE SEPARATION DRAG	EMPIRICAL (Ref. 27)				
BODY BASE PRESSURE CAUSED BY TAIL FINS	IMPROVED EMPIRICAL (Ref. 17)				
INVISCID LIFT AND PITCHING MOMENT • LINEAR	• LIFTING SURFACE THEORY (Ref. 27)	• EMPIRICAL (Ref. 27)	• 3DTWT (Ref. 27)	• 3DTWT OR SE (Ref. 27 or 13)	• 3DTWT OR SE (Ref. 27 or 14)
• NONLINEAR	• EMPIRICAL (Ref. 1, 2)				
WING-BODY, BODY-WING INTERFERENCE ($\Phi = 0, 45°$) • LINEAR	• SLENDER BODY THEORY OR LINEAR THEORY MODIFIED FOR SHORT AFTERBODIES (Ref. 1, 2)				
• NONLINEAR	• EMPIRICAL (Ref. 1, 2)				
WING-BODY, INTERFERENCE DUE TO δ ($\Phi = 0, 45°$) • LINEAR	• SLENDER BODY THEORY (Ref. 2)				
• NONLINEAR	• EMPIRICAL (Ref. 1, 2)				
WING-TAIL INTERFERENCE ($\Phi = 0, 45°$)	LINE VORTEX THEORY WITH MODIFICATIONS FOR $K_{W(B)}$ TERM AND NONLINEARITIES (Ref. 2)				
AEROHEATING	NONE PRESENT			SE PLUS MNT (Ref. 21)	SE PLUS MNT REAL GASES (Ref. 21)
NONAXISYMMETRIC BODY AERO ($\Phi = 0, 45°$)	IMPROVED NELSON ESTIMATE FOR AP98 (Ref. 5, 46, 47)				
NONLINEAR ST. LOADS AVAIL. ($\Phi = 0, 45°$)	NO		YES (Ref. 3)		

FIGURE 19. AP98 METHODS FOR WING-ALONE AND INTERFERENCE AERODYNAMICS

COMPONENT/ MACH NUMBER REGION	SUBSONIC $M_\infty < 0.8$	TRANSONIC $0.8 \le M_\infty \le 1.2$	LOW SUPERSONIC $1.2 \le M_\infty \le 1.8$	MOD/HIGH SUPERSONIC $1.8 \le M_\infty \le 6.0$	HYPERSONIC $M_\infty > 6.0$
BODY ALONE	EMPIRICAL				
WING AND INTERFERENCE ROLL DAMPING MOMENT	LIFTING SURFACE THEORY	EMPIRICAL	LINEAR THIN WING THEORY	LINEAR THIN WING OR STRIP THEORY	
WING MAGNUS MOMENT	ASSUMED ZERO				
WING AND INTERFERENCE PITCH DAMPING MOMENT	LIFTING SURFACE THEORY	EMPIRICAL	LINEAR THIN WING THEORY	LINEAR THIN WING OR STRIP THEORY	

FIGURE 20. AP98 METHODS FOR DYNAMIC DERIVATIVES (REFERENCES 28 AND 16)

6.0 RESULTS AND DISCUSSION

Several cases are considered to try to compare the new AP98 with experimental data, the AP95, and other theoretical methods (if computations are available). In general, it is believed the AP98 comparisons to experimental data are as good as or better than the AP95. However, the AP98 is more robust in terms of roll orientation and configuration cross sectional geometry. Hence, for $\phi = 45$ deg aerodynamics, only AP98 results will be shown. Also, for nonaxisymmetric bodies, only AP98 results will be shown.

6.1 AXISYMMETRIC BODY CONFIGURATION CASES

The first axisymmetric body case considered is a canard-body-tail configuration shown in Figure 21A. This case was tested[53] at $M_\infty = 0.2$ at the Naval Postgraduate School in Monterey. The configuration tested had aspect ratio canards of 1.59 and tails of 0.9. The body was 22.6 calibers in length. Test data were available at 50 deg AOA for both $\Phi = 0$ and 45 deg roll orientation with canards deflected 0 and ±20 deg. Reference 53 pointed out that the sting balance was designed for the large normal forces at high AOA and hence the axial force measurements are not expected to be as accurate. The wind tunnel model with boundary layer trip option was chosen for the aeroprediction computations. Sea level conditions were also assumed. Figures 21B, 21C, and 21D give the axial and normal force and pitching moment coefficients for the roll position of $\Phi = 0$ and control deflections of 0 deg and ±20 deg. Results are given for the experimental data, AP95, AP98 and Missile DATCOM[54] (which was taken from Reference 53). As seen in the figures, the AP95 and AP98 give similar results for normal force and pitching moments and are both in reasonable agreement with data. The AP98 gives some slight improvement over the AP95 in axial force at higher AOA due to the new axial force methodology included. Both the AP95 and AP98 appear to give better results compared to data than the DATCOM results presented in Reference 53.
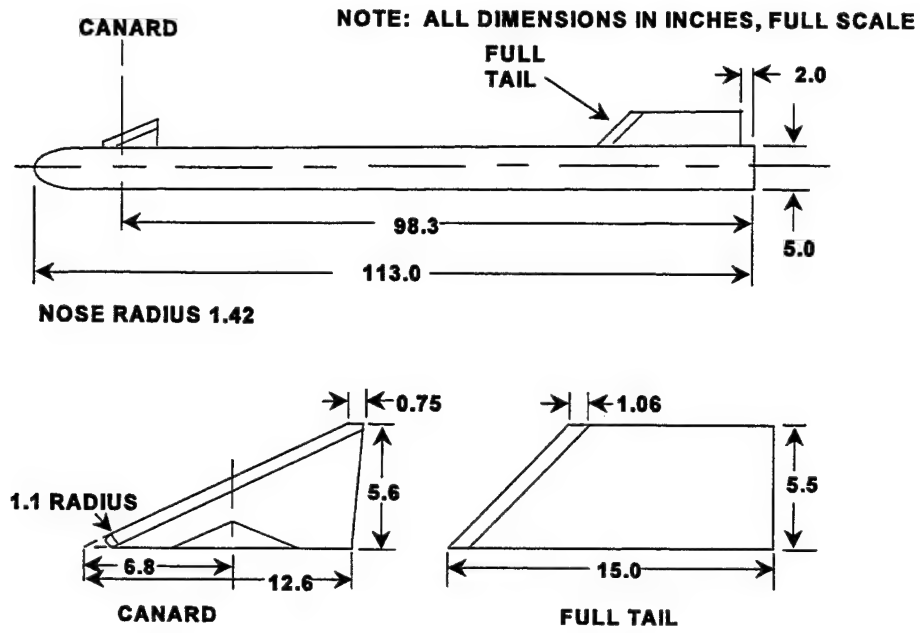
FIGURE 21A. CANARD-CONTROLLED MISSILE CONFIGURATION[53]
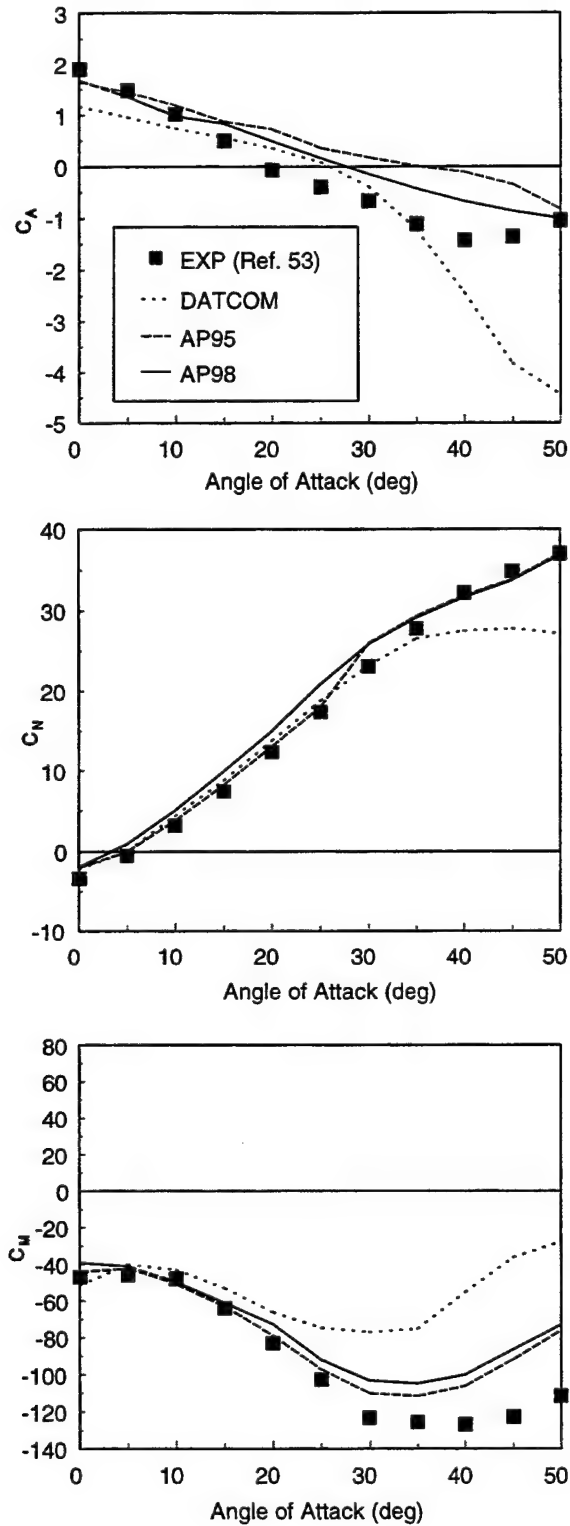
FIGURE 21B. COMPARISON OF STATIC AERODYNAMICS BETWEEN EXPERIMENT AND THEORY FOR FIGURE 21A CONFIGURATION ($\delta = -20$ DEG, $\Phi = 0$ DEG, $M_\infty = 0.2$)
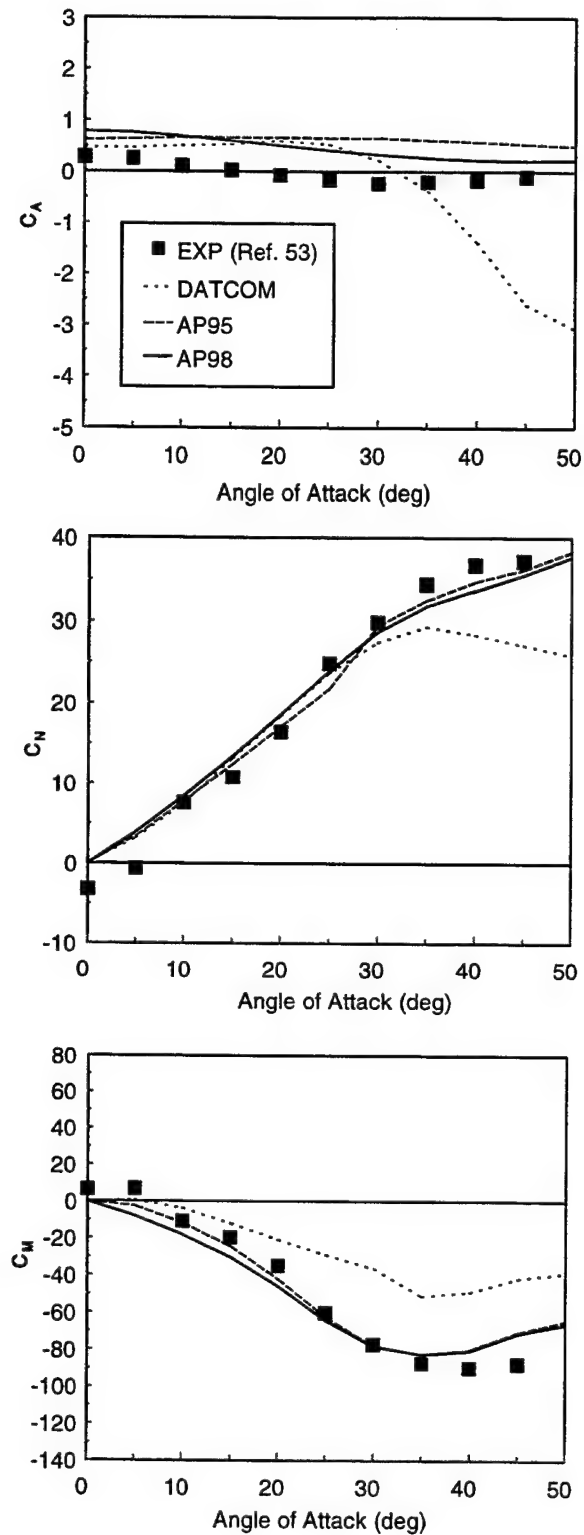
FIGURE 21C. COMPARISON OF STATIC AERODYNAMICS BETWEEN EXPERIMENT AND
THEORY FOR FIGURE 21A CONFIGURATION (δ = 0 DEG, Φ = 0 DEG, M_∞ = 0.2)
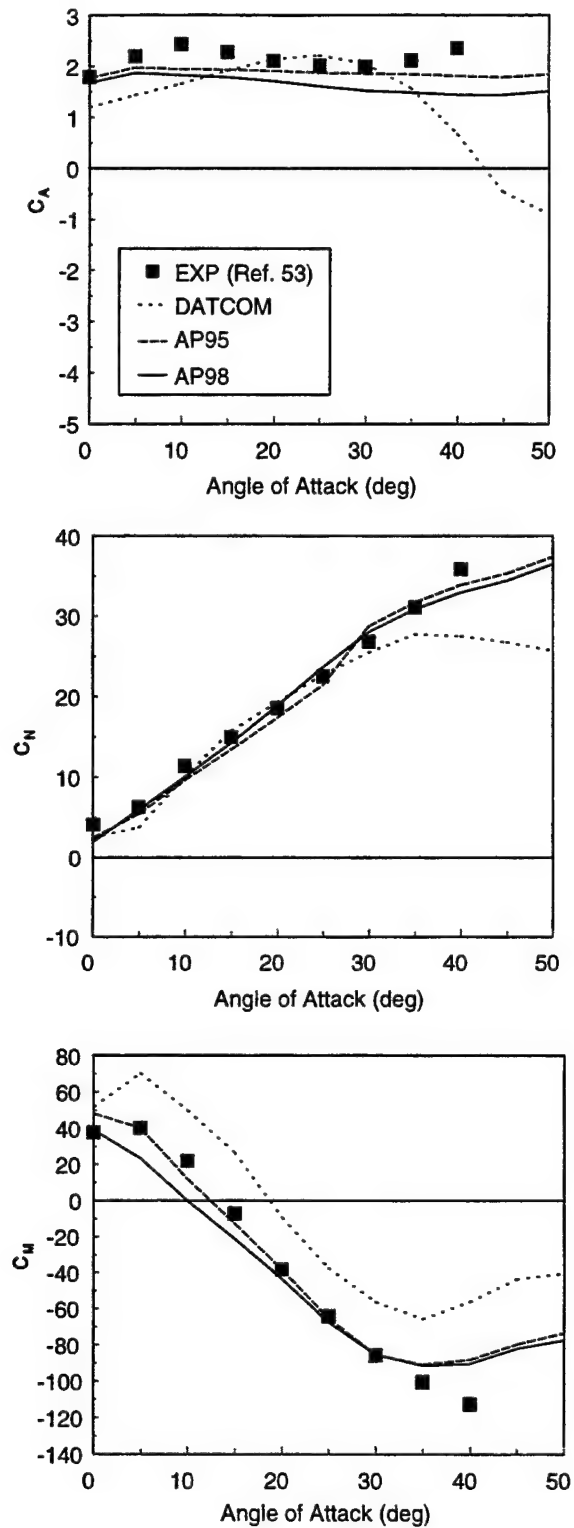
FIGURE 21D. COMPARISON OF STATIC AERODYNAMICS BETWEEN EXPERIMENT AND THEORY FOR FIGURE 21A CONFIGURATION (δ = +20 DEG, Φ = 0 DEG, M_∞ = 0.2)

The second axisymmetric body case is taken from Reference 55. This data set consisted of various length to diameter canard-body-tail configurations tested at $M_\infty = 2.01$ to AOA 25 to 30 deg. Data were taken at a R_N/ft of 3.47×10^6 and with no boundary layer trip present. Figure 22A shows the configurations considered for comparison to data. These cases consist of 19.1, 16.7 and 14.8 caliber canard-body-tail configurations. The tail has about 2 percent of the tip eliminated, but this was not considered in the AP95 and AP98 results. Hence, it should be expected that the theory should be slightly high on normal force and slightly more stable pitching moments compared to data. Figure 22B shows the normal force and pitching moment coefficient comparisons of the AP95 and AP98 to data. Even with the slightly larger tail fins used in the theory, the normal force and center of pressure average errors are well within the ±10 percent and ±4 percent of body length goals respectively. The AP98 normal force predictions are slightly better than the AP95, whereas the opposite is true of the pitching moments.
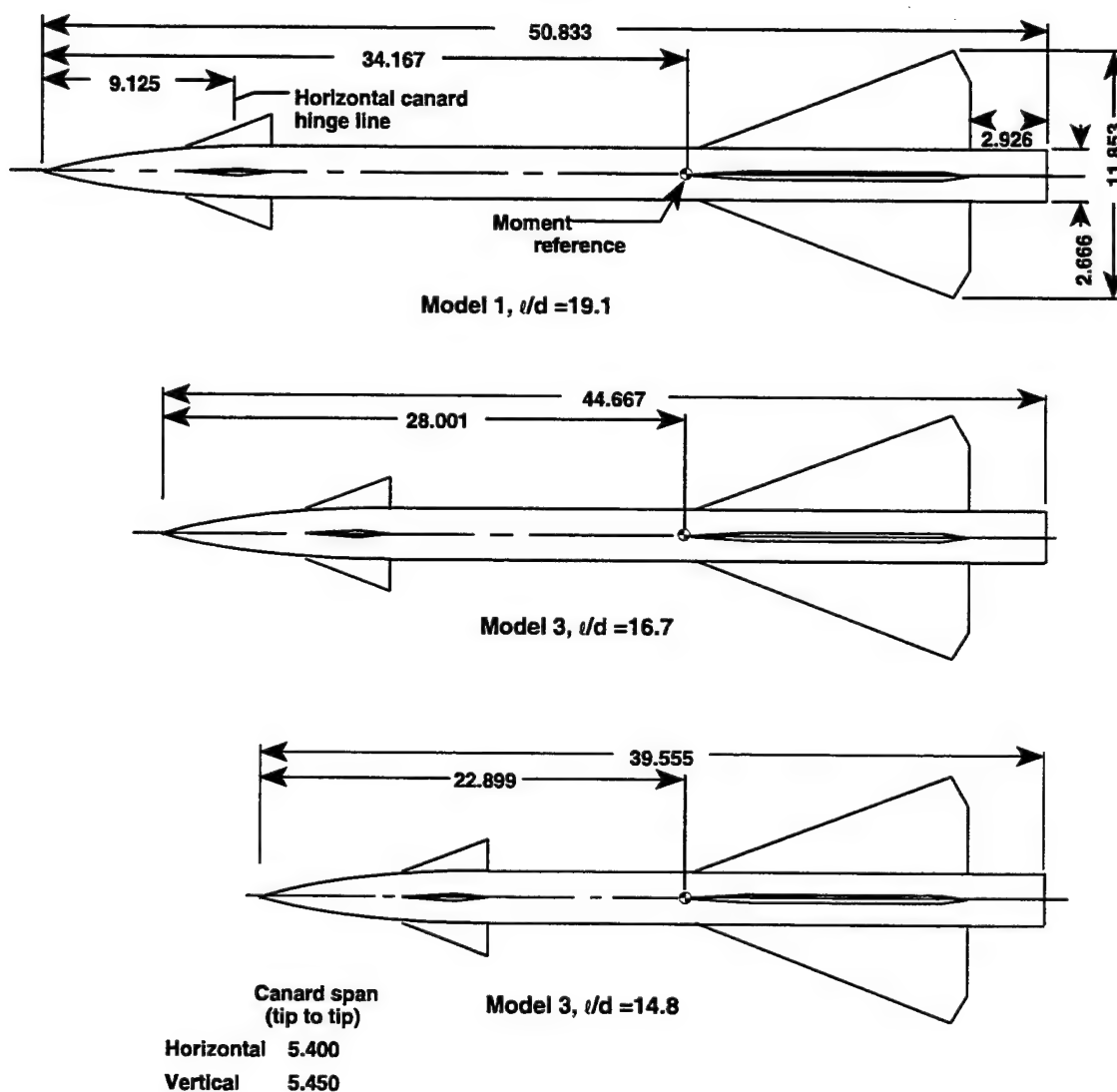
FIGURE 22A. CANARD-BODY-TAIL CONFIGURATIONS OF VARIOUS LENGTH TO DIAMETER RATIOS (REFERENCE 55) (ALL DIMENSIONS IN INCHES)
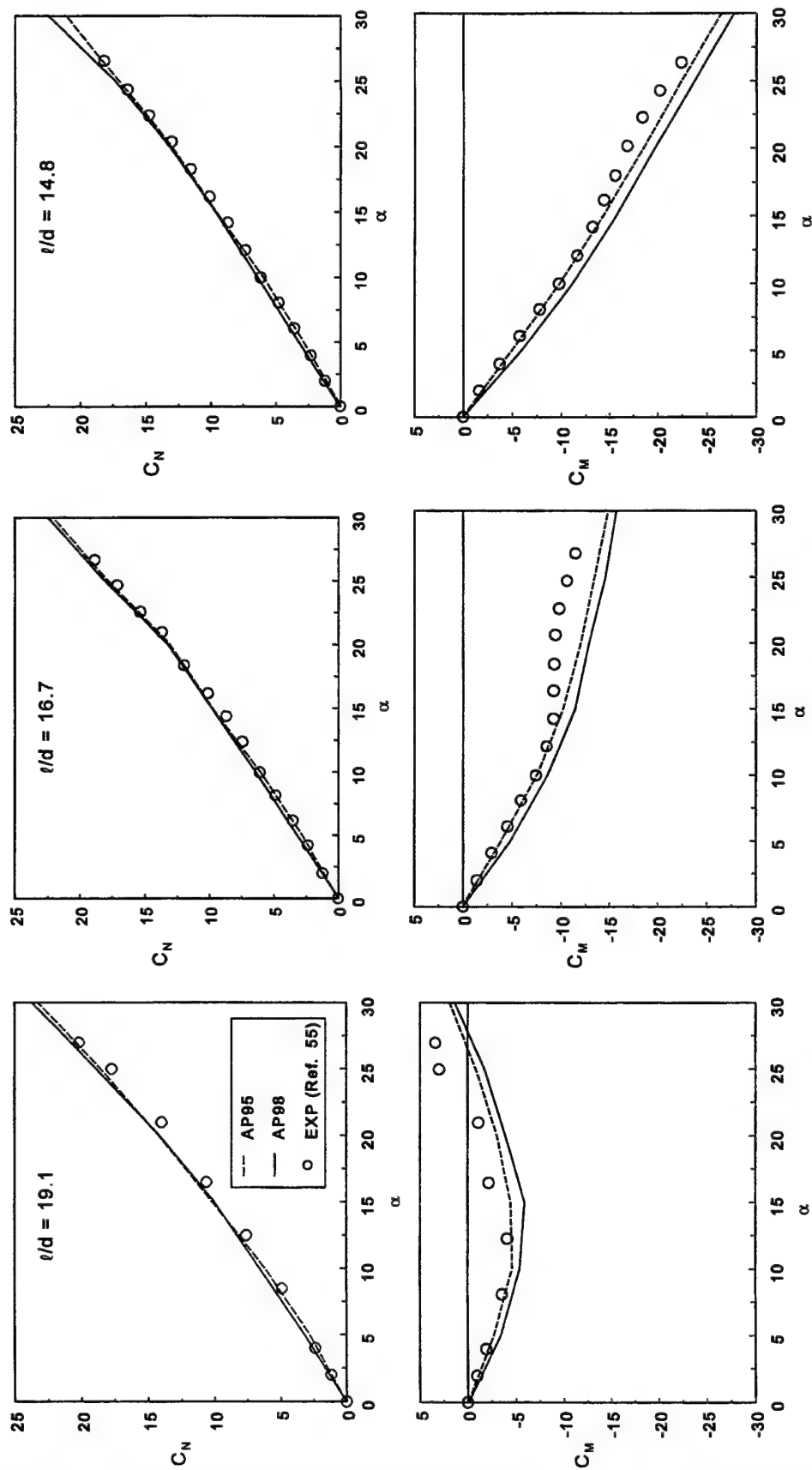
FIGURE 22B. NORMAL FORCE AND PITCHING MOMENT COEFFICIENTS FOR
FIGURE 22A CONFIGURATIONS ($\Phi = 0$ DEG, $\delta = 0$ DEG, $M_\infty = 2.01$)

The third case considered is taken from Reference 56 and is shown in Figure 23. The model was about 22 calibers in length with a sharp nose of 2.25 calibers. The canards had an aspect and taper ratio of 2.0 and 0.3 respectively. Various tail fin spans were considered. This model was tested at Mach numbers 1.6 to 3.5 at AOA to about 18 to 20 deg. It had a boundary layer trip present and was tested at a R_N/ft of 2.0×10^6. Reference 56 gave separate values of base axial force coefficient, which were added to the axial force values given in the reference to compare to the AP98 computations. To compare the experimental data to theory, Mach numbers of 2.5 and 3.5 are selected at roll angle 45 deg. Also, values of the tail-to-canard semispan of 0.47 and 1.25 are considered. Since $\Phi = 45$ deg roll is chosen, no AP95 computations will be shown. Figure 24 presents the comparison of theory to experiment for $b_t/b_c = 0.47$ and $b_t/b_c = 1.25$. Results are shown for C_A, C_N and C_M. As seen in Figure 24, comparison of theory to experiment is quite acceptable and meets the average accuracy goal of ±10 percent on axial and normal force and ±4 percent of body length for center of pressure. The worst case error on pitching moment at $M = 2.5$ and $b_t/b_c = 1.25$ represents an error of less than 3 percent of the body length in terms of center of pressure. Also shown on Figure 24 are M3HAX computations taken from Reference 57 for the $b_t/b_c = 1.25$ case at $M = 2.5$. The C_A results for $\Phi = 0$ deg from Reference 57 were assumed to apply to the $\Phi = 45$ deg case since no control deflections were assumed for this example. As seen in the figure, M3HAX gives reasonable comparison to data at $\Phi = 45$ deg. Reference 57 shows M3HAX giving improved comparisons to data at $\Phi = 0$ deg roll, compared to $\Phi = 45$ deg roll, particularly for normal force and pitching moment coefficients.

The next case considered is a wing-body-tail case with a low aspect ratio wing and tested at the Naval Postgraduate School[58] at $M_\infty = 0.1$. The configuration is shown at the top of Figure 25. Note that the model tested in the wind tunnel at the top of the figure is slightly different than that where calculations were performed with the AP95 and AP98. This is due to the fact the APC cannot handle the detailed dorsal and wing geometry shown at the top of the figure. The configuration shown in the middle of Figure 25 has the same aspect ratio, span, taper ratio, leading edge sweep angle and area of both the dorsal and tail as the actual model at the top of Figure 25. Also, although not shown, the distance to the centroid of the planform areas is also held constant. Of course, the body is also the same between the two cases.

The only results given in Reference 58 were for normal force. Experimental data and Missile DATCOM[54] results were both given in Reference 58 for roll positions of $\Phi = 0$ and 45 deg. These results are compared to the AP95 and AP98 at the bottom of Figure 25 for $\Phi = 0$ deg and to the AP98 only for $\Phi = 45$ deg. Note that comparisons to data are reasonable and quite good except at AOA 40 to 70 deg. It is possible that wind tunnel sting to model interference increased the experimental results in this range somewhat. Previous wind tunnel studies[59,60] have concluded the model sting can increase model normal force loads by 10 to 20 percent in the high AOA range. Both the AP95 and AP98 give slightly better comparisons to data than the Missile DATCOM[54] for this case. It is suspected the low aspect ratio lifting surfaces, which have a great deal of nonlinear lift, is the primary reason for the Missile DATCOM accuracy problems, particularly at $\Phi = 0$ deg.
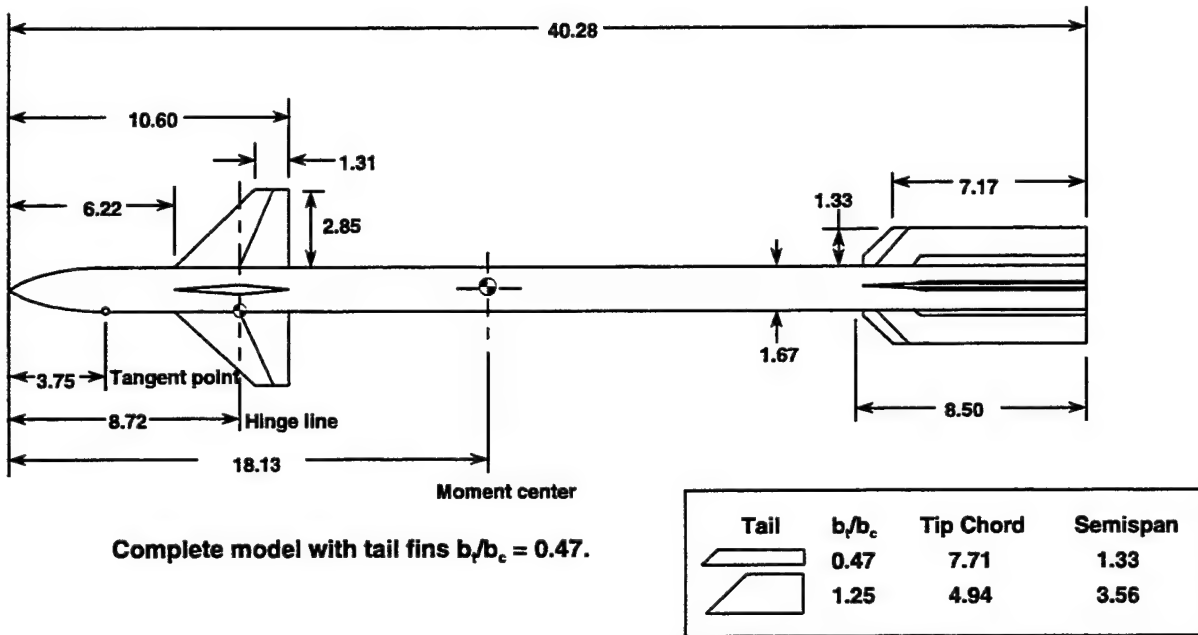
FIGURE 23. CANARD-BODY-TAIL CONFIGURATION WITH VARYING TAIL SPAN
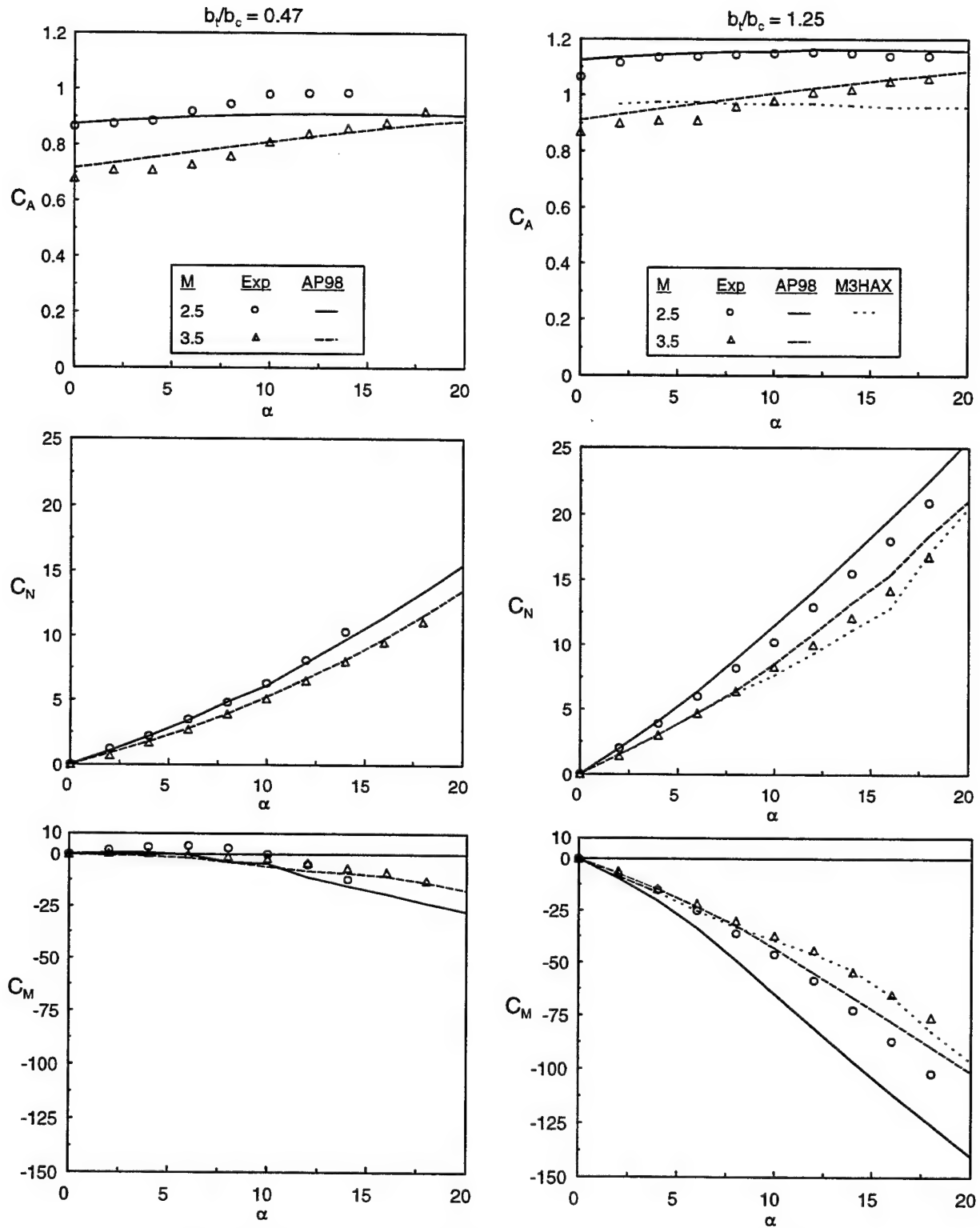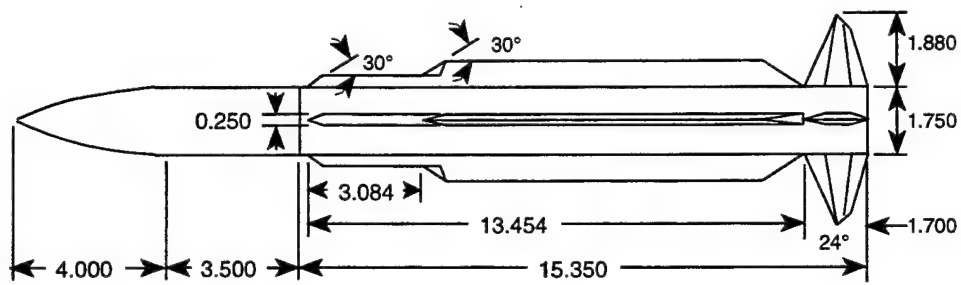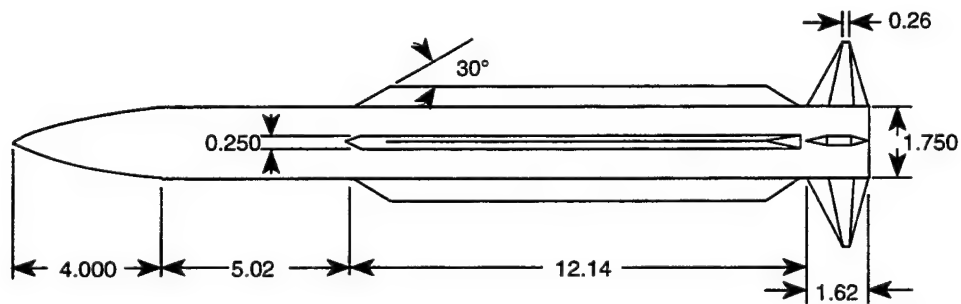(ALL DIMENSIONS IN INCHES)

FIGURE 24. COMPARISON OF THEORY AND EXPERIMENT[56] FOR
CONFIGURATIONS OF FIGURE 23 (Φ = 45 DEG)

54

CONFIGURATION TESTED IN WIND TUNNEL (From Ref. 58)
(ALL DIMENSIONS IN INCHES)

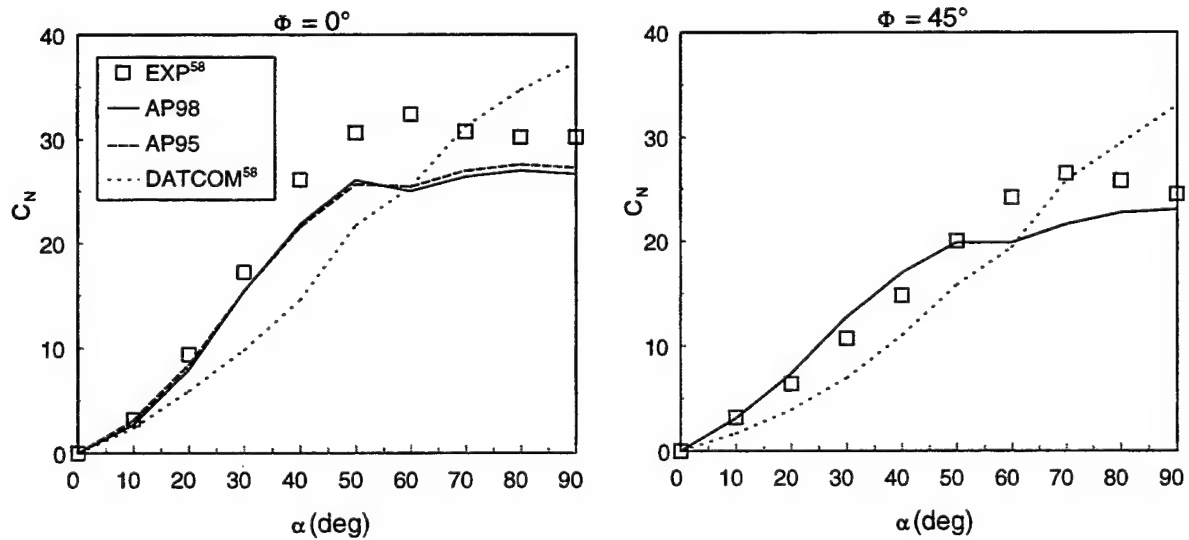MODIFIED CONFIGURATION USED IN AEROPREDICTICTION COMPUTATIONS

FIGURE 25. NORMAL FORCE COEFFICIENT COMPARISONS OF BODY-DORSAL-TAIL ($M_\infty = 0.1$)

The next axisymmetric-body missile configuration chosen is a wing-body-tail case shown in Figure 26, where the wings are used for control. Experimental results for this case were taken from Reference 61. This configuration has a length of about 18 calibers with a tangent ogive nose 2.25 calibers in length. It has wings and tails of fairly high aspect ratios of 2.8 and 2.6 respectively. Data were taken at Mach numbers 1.5 to 4.63, for AOAs to 45 deg and control deflections of 0 and 10 deg at M of 1.5 and 2.0 and 0 to 20 deg at M of 2.35 to 4.63. The data were taken at a Reynolds number of 2.5×10^6/ft and boundary layer trips were also used. The model had a hollow chamber, and chamber axial force measurements were given separately in Reference 20. These results were added to the forebody axial force measurements to compare with the AP95 and new AOA axial force prediction method presented in this report.

Figure 27 shows the comparisons of the AP98 and AP95 to the data of Reference 61 for $\Phi = 0$ deg and $\Phi = 45$ deg. Figure 27A and 27B give C_A, C_N and C_M for M = 1.5 at $\delta = 0$ and $\delta_W = 10$ deg at $\Phi = 0$ deg. In general, both the AP95 and AP98 give acceptable comparisons to data, with the AP98 giving slightly better results on axial force at AOA than the AP95. On the other hand, the pitching moments of the AP95 are slightly better than those of the AP98. Figure 27C and 27D give similar results for M = 2.87, and Figure 27E and 27F, for M = 4.6. Overall, for this configuration, at $\Phi = 0$ deg roll, the AP95 and AP98 are about equal in overall accuracy comparisons. The worst case errors are for center of pressure at higher Mach number and AOA, where the bow shock intersects the wing shocks. This nonlinear phenomena is not modeled in the $\Phi = 0$ deg roll orientation at all. For the $\Phi = 45$ deg roll, the center of pressure shift, Equation (38), partially accounts for this phenomena, but not entirely. Center of pressure errors approach a full caliber or 5 percent of the body length at M = 4.6 and $\alpha = 40$ deg.

Figure 27G and 27H present M = 1.5 results for $\Phi = 45$ deg roll. Since the AP95 is not applicable to 45 deg roll, only the AP98 and experimental data are available. Figure 27G and 27H give C_A, C_N and C_M for M = 1.5 and $\delta = 0$ and 10 deg. Figure 27I and 27J give similar results for M = 2.87 and $\delta = 0$ and 20 deg, and Figure 27K and 27L give results for M = 4.6 and $\delta = 0$ and 20 deg. Note that good agreement is obtained between experimental data and the AP98 for all static aerodynamics at all three Mach numbers and for all control deflections. Here, the worst case center of pressure error is less than 3 percent of the body length.

Figure 28 presents results for the Figure 26 configuration where the tail, versus the wing is used for control. Here, only the $\delta_T = -10$ deg and -20 deg results are shown as the $\delta_T = 0$ deg control is basically the same as that in Figure 27 for $\delta_W = 0$ deg. Both the AP95 and AP98 give acceptable results for the $\Phi = 0$ deg roll for C_N and C_M. However, the AP98 is clearly superior to the AP95 for axial force at high AOA and Mach number. Figures 28B, D and F give the tail control, $\Phi = 45$ deg roll results. Again, only the AP98 and experimental results are given. Note the good agreement of the AP98 with the data. Again, the worst case error on pitching moment results is a center of pressure error of less than 3 percent of the body length.

In viewing the comparison of theory to experiment in Figures 27 and 28 for both the wing and tail control alternatives of the Figure 26 configuration, several conclusions can be drawn. In terms of accuracy, both the AP95 and AP98 give acceptable predictions for C_A, C_N and C_M for $\Phi = 0$ deg roll when α and δ are of the same sign. The AP98 gives superior results to the AP95 for C_A when α and δ are of opposite signs. The AP98 gives equally good results for $\Phi = 45$ deg roll as

for $\Phi = 0$ deg roll, whereas the AP95 is only applicable for $\Phi = 0$ deg roll. The AP98 gives slightly better center of pressure predictions than the AP95, primarily due to Equation 38.
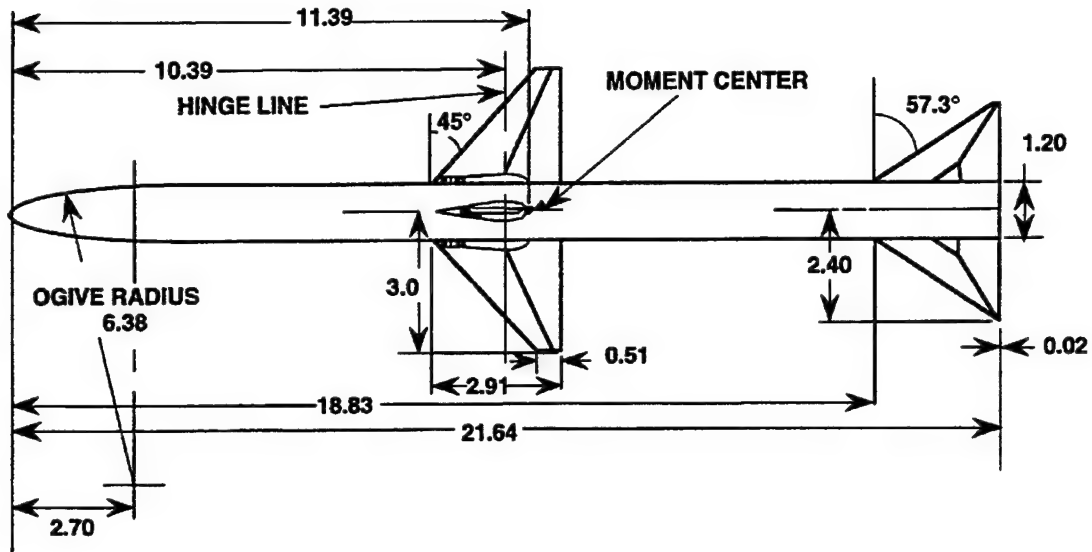
FIGURE 26. WING-BODY-TAIL CONFIGURATION USED IN VALIDATION PROCESS[61]
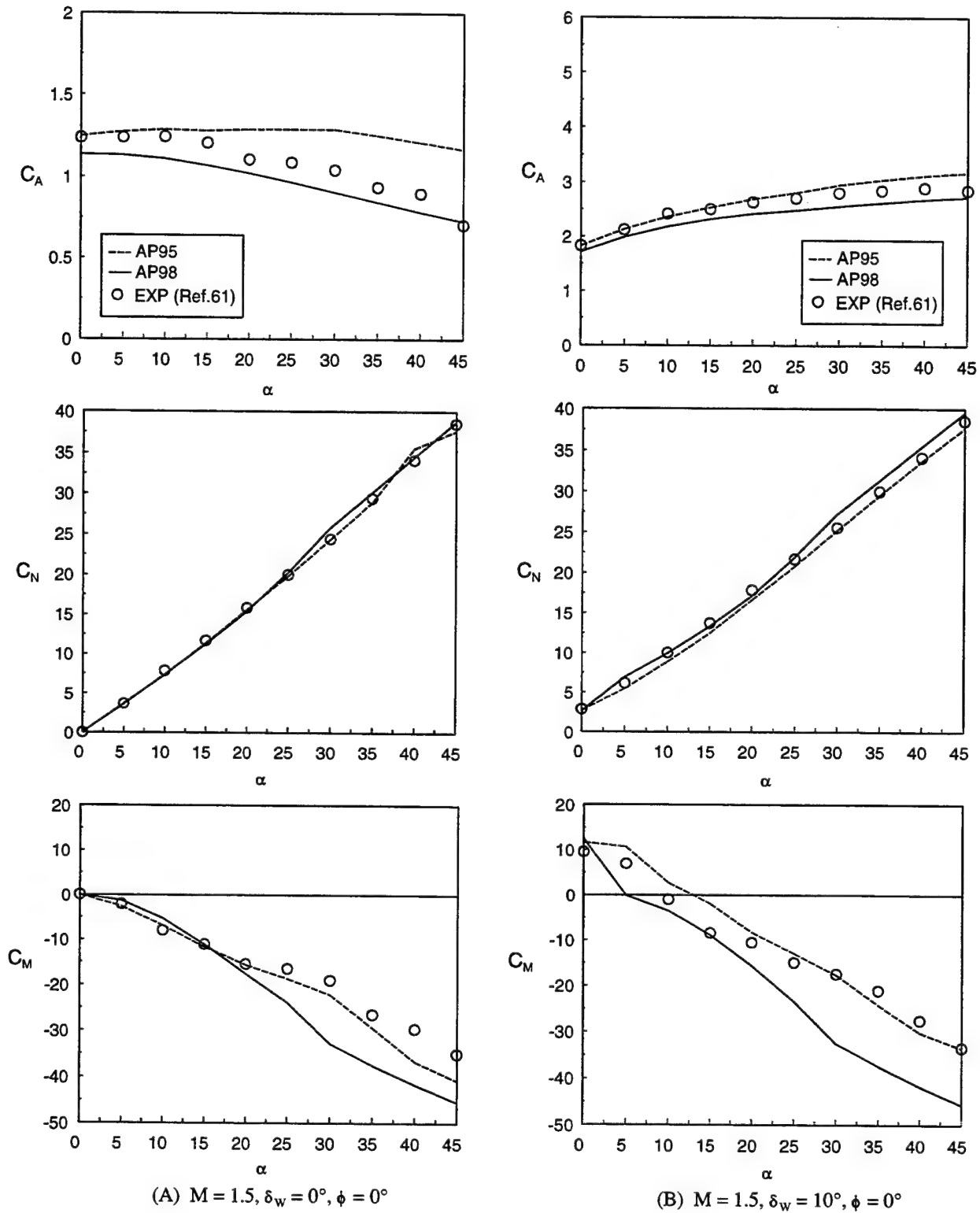
(A) M = 1.5, $\delta_W = 0°$, $\phi = 0°$

(B) M = 1.5, $\delta_W = 10°$, $\phi = 0°$

FIGURE 27. COMPARISON OF EXPERIMENT AND THEORY FOR C_A, C_N AND C_M
FOR FIGURE 26 WING CONTROL CASE

(C) M = 2.87, δ_W = 0°, ϕ = 0°   (D) M = 2.87, δ_W = 20°, ϕ = 0°

FIGURE 27. COMPARISON OF EXPERIMENT AND THEORY FOR C_A, C_N AND C_M
FOR FIGURE 26 WING CONTROL CASE (Continued)

(E) $M = 4.6, \delta_W = 0°, \phi = 0°$ (F) $M = 4.6, \delta_W = 20°, \phi = 0°$

FIGURE 27. COMPARISON OF EXPERIMENT AND THEORY FOR C_A, C_N AND C_M
FOR FIGURE 26 WING CONTROL CASE (Continued)

(G) $M = 1.5, \delta_W = 0°, \phi = 45°$

(H) $M = 1.5, \delta_W = 10°, \phi = 45°$

FIGURE 27. COMPARISON OF EXPERIMENT AND THEORY FOR C_A, C_N AND C_M
FOR FIGURE 26 WING CONTROL CASE (Continued)

(I) $M = 2.87, \delta_w = 0°, \phi = 45°$

(J) $M = 2.87, \delta_w = 20°, \phi = 45°$
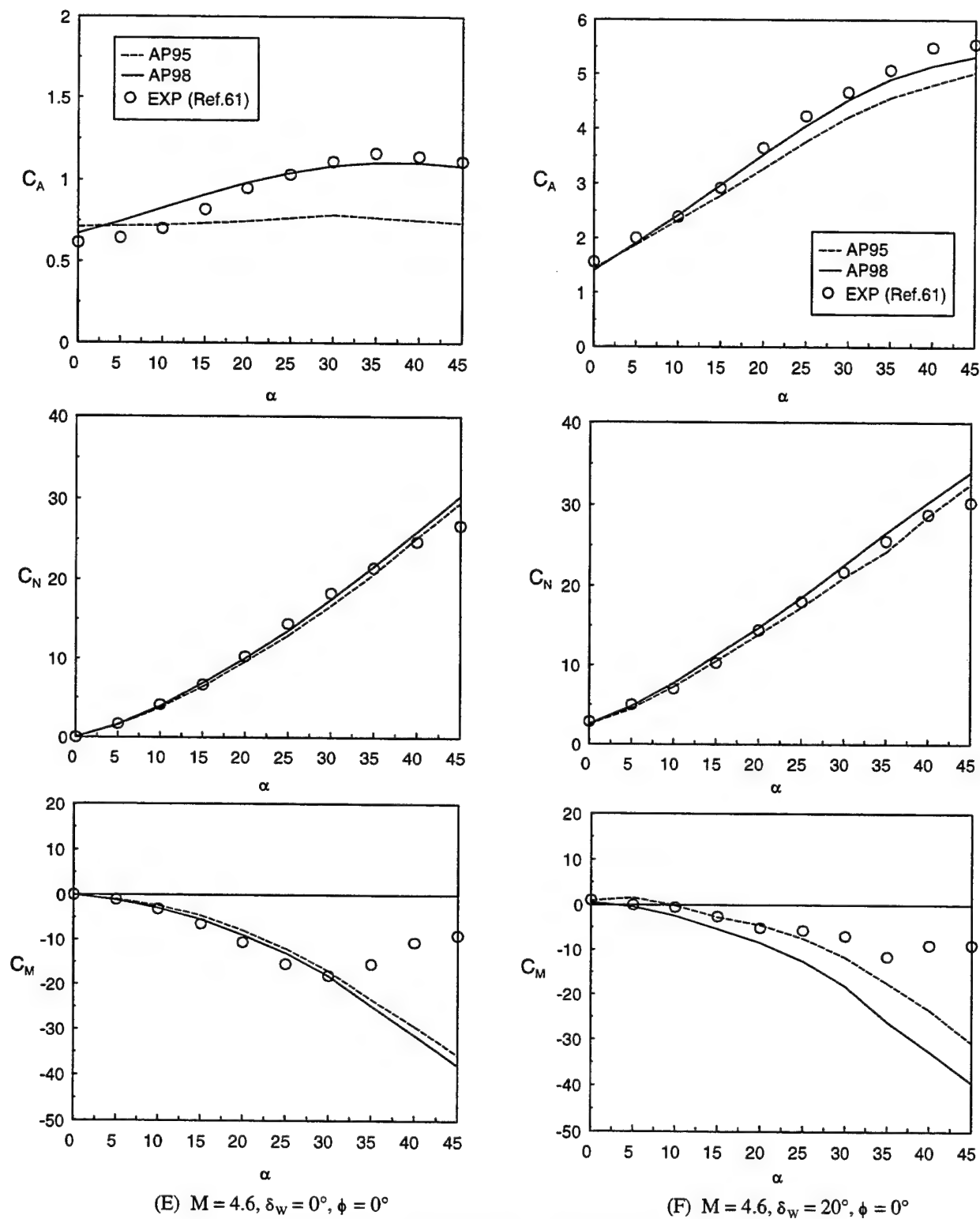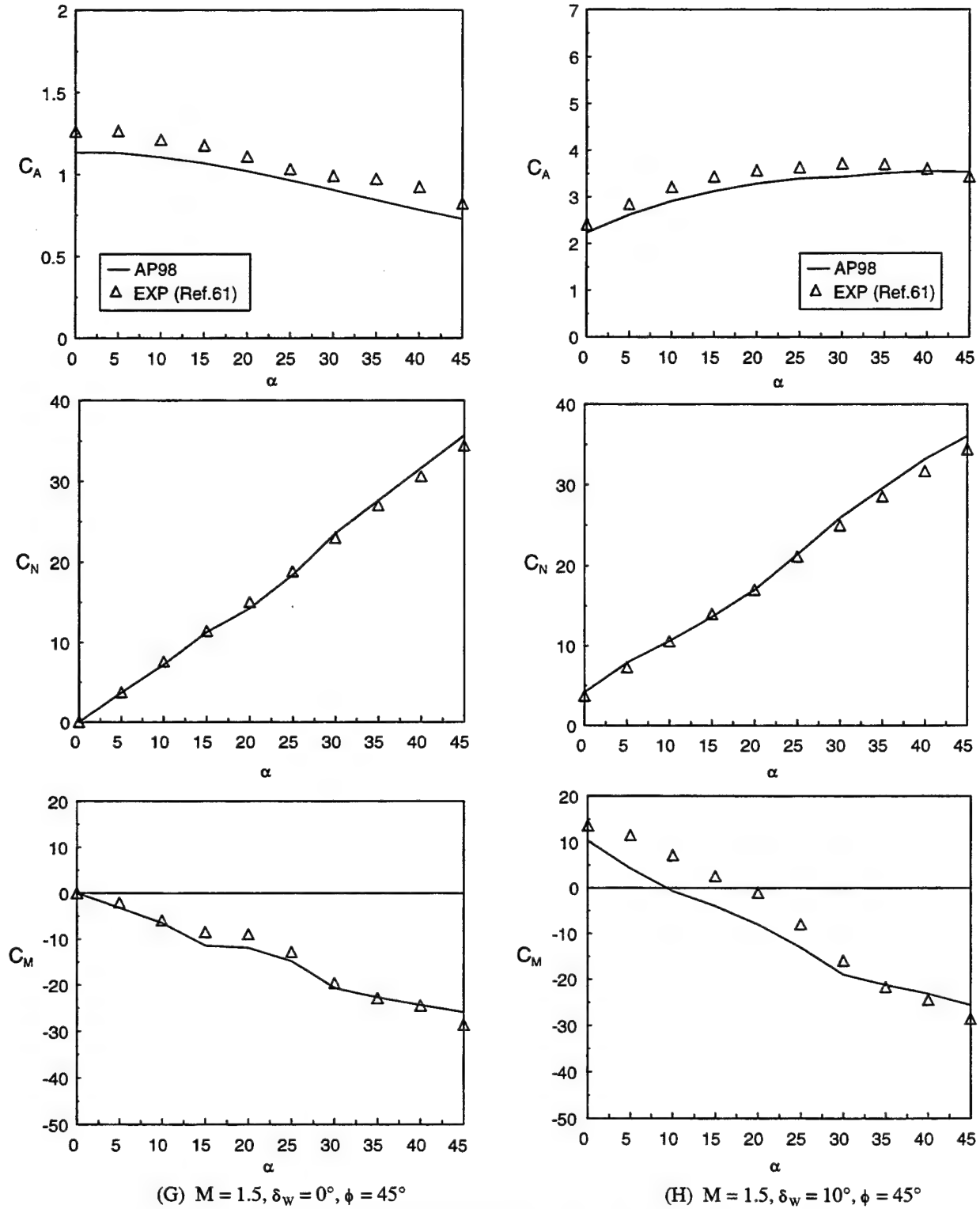
FIGURE 27. COMPARISON OF EXPERIMENT AND THEORY FOR C_A, C_N AND C_M
FOR FIGURE 26 WING CONTROL CASE (Continued)
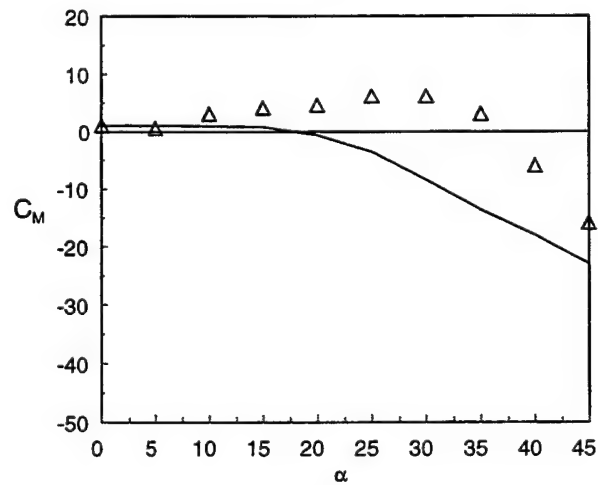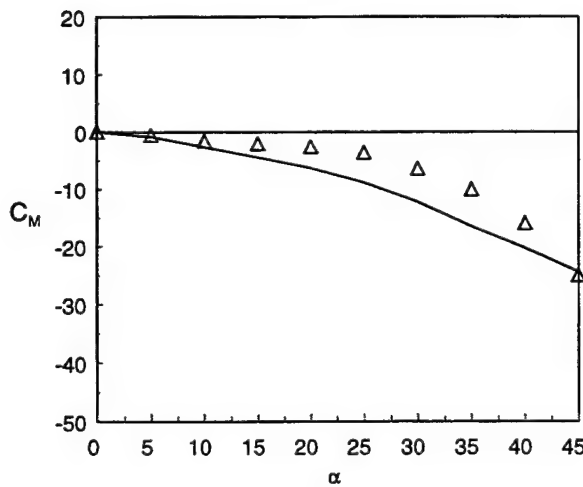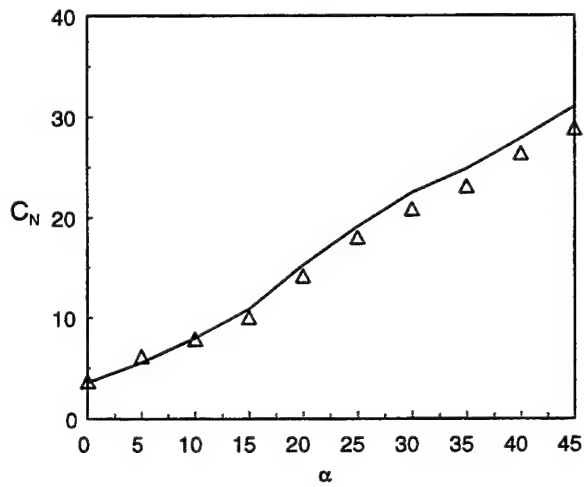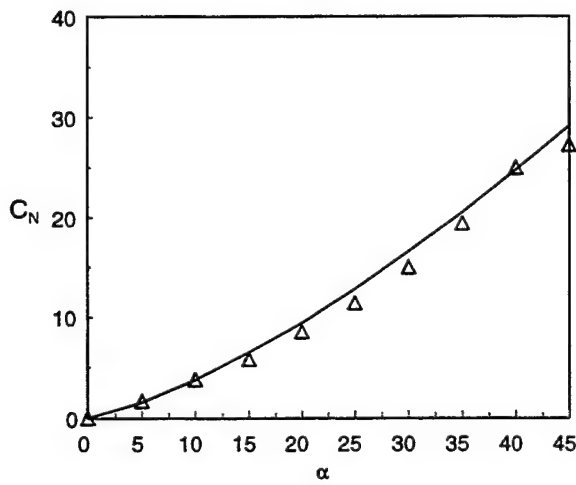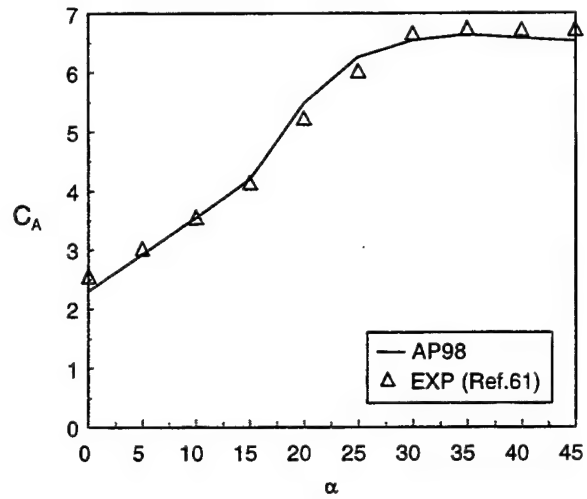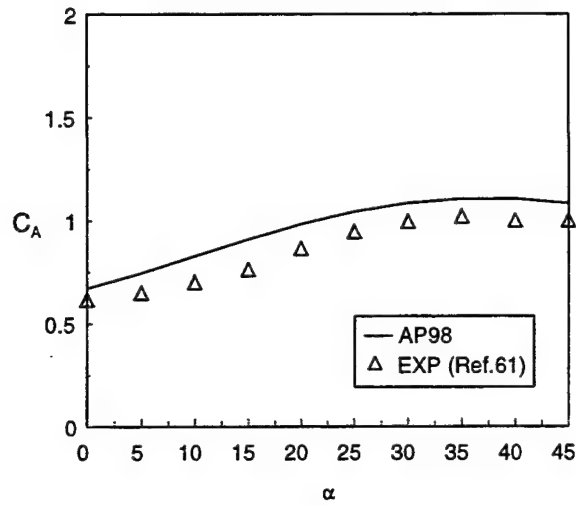
(K) M = 4.6, $\delta_W = 0°$, $\phi = 45°$

(L) M = 4.6, $\delta_W = 20°$, $\phi = 45°$

FIGURE 27.   COMPARISON OF EXPERIMENT AND THEORY FOR C_A, C_N AND C_M
FOR FIGURE 26 WING CONTROL CASE (Continued)

(A) M = 1.5, $\delta_T = -10°$, $\phi = 0°$

(B) M = 1.5, $\delta_T = -10°$, $\phi = 45°$
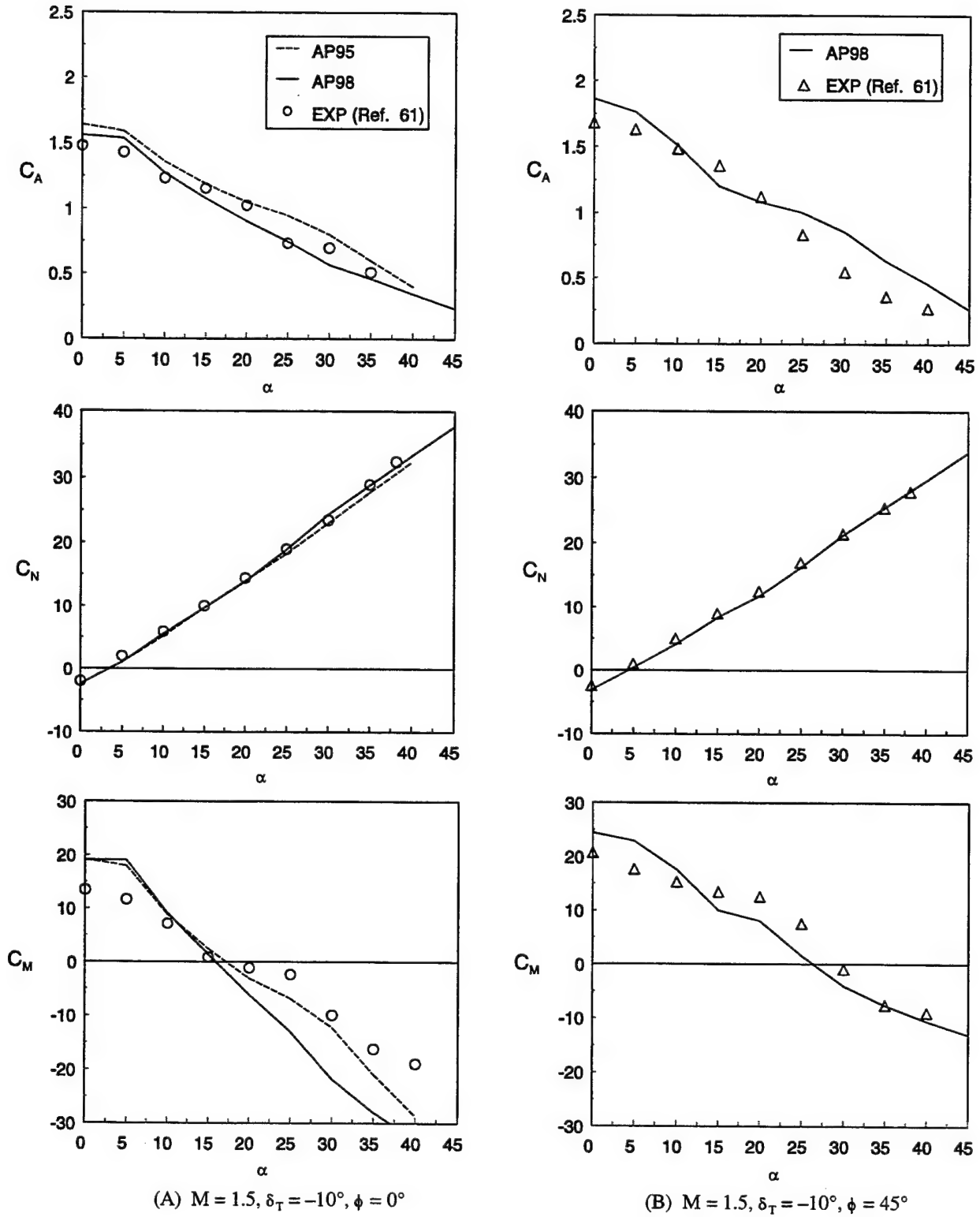
FIGURE 28. COMPARISON OF EXPERIMENT AND THEORY FOR C_A, C_N AND C_M
FOR FIGURE 26 TAIL CONTROL CASE
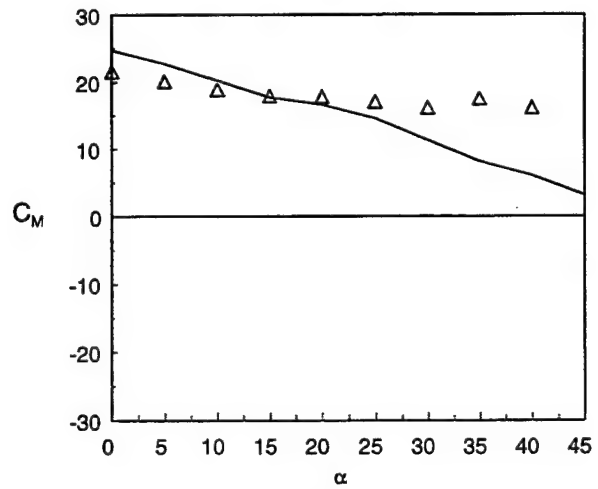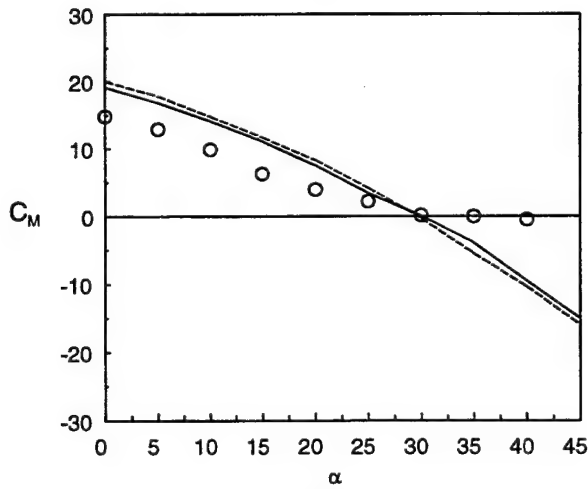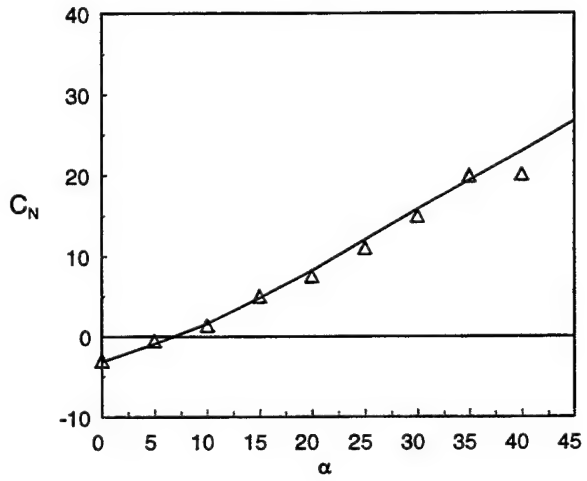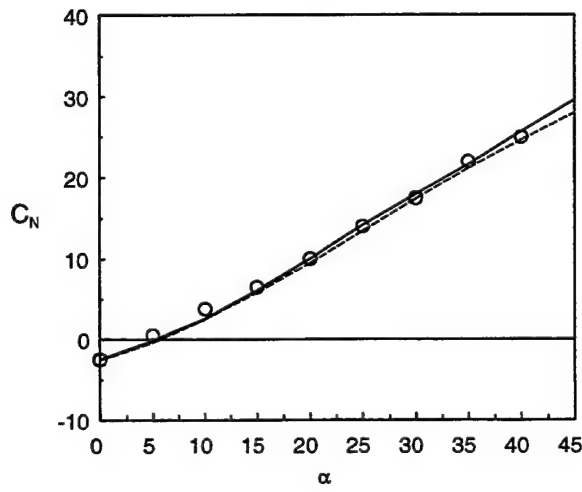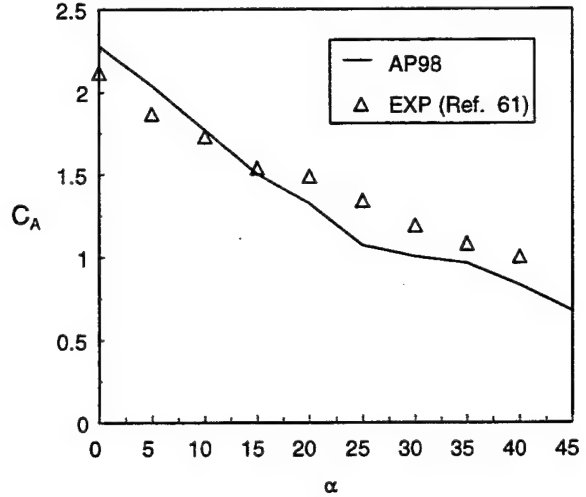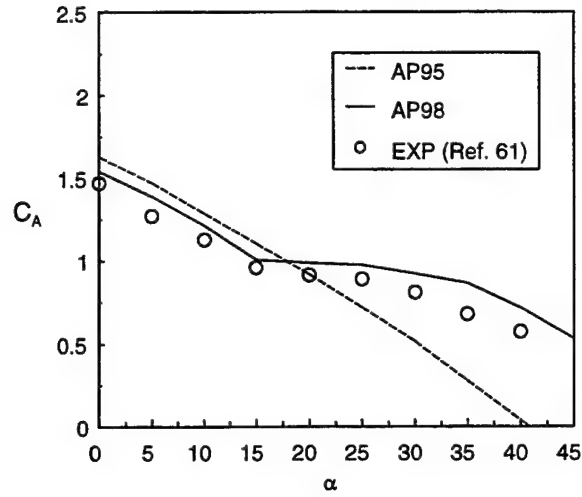
(C) $M = 2.87, \delta_T = -20°, \phi = 0°$

(D) $M = 2.87, \delta_T = -20°, \phi = 45°$

FIGURE 28. COMPARISON OF EXPERIMENT AND THEORY FOR C_A, C_N AND C_M
FOR FIGURE 26 TAIL CONTROL CASE (Continued)

(E) M = 4.6, $\delta_T = -20°$, $\phi = 0°$

(F) M = 4.6, $\delta_T = -20°$, $\phi = 45°$
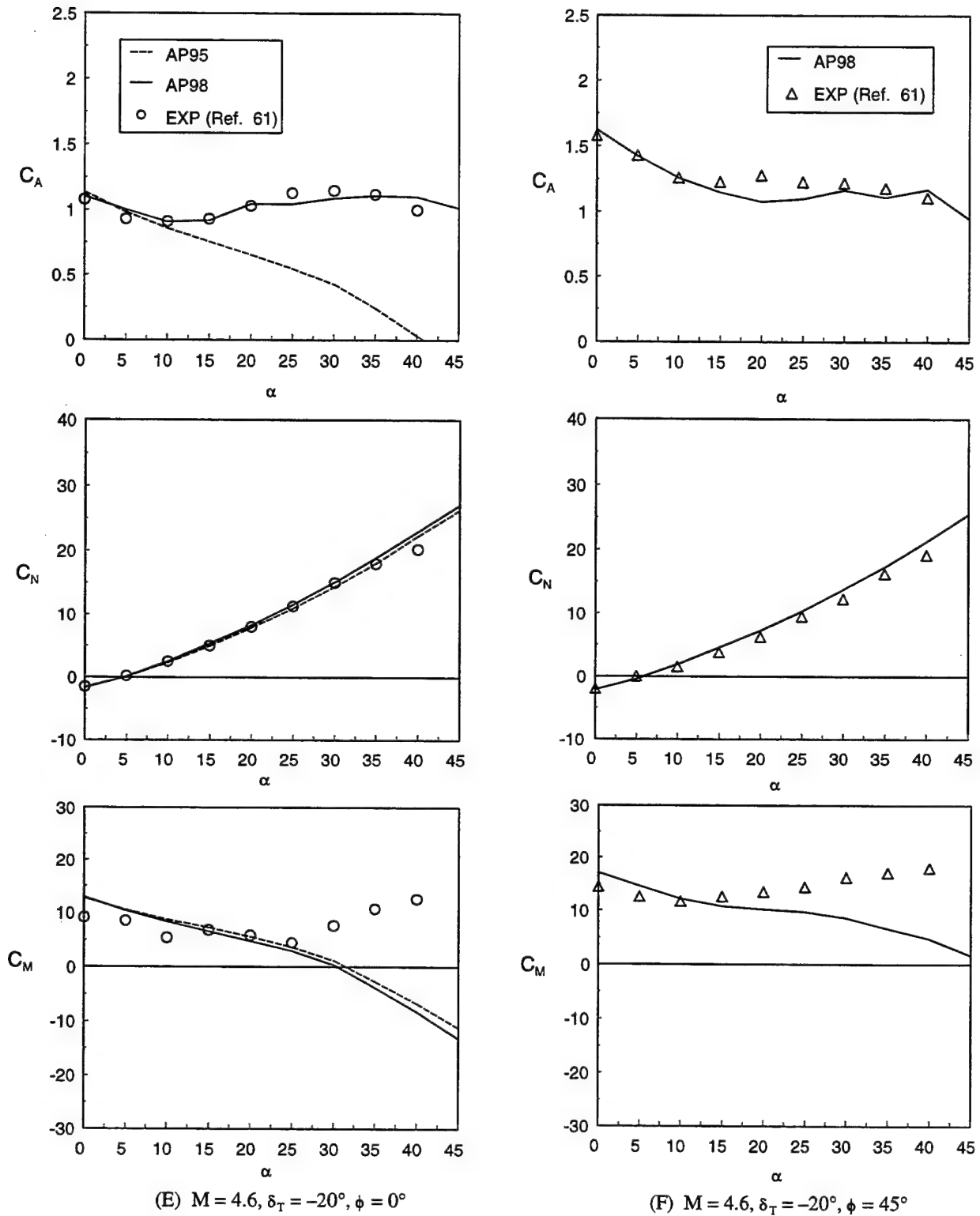
FIGURE 28. COMPARISON OF EXPERIMENT AND THEORY FOR C_A, C_N AND C_M
FOR FIGURE 26 TAIL CONTROL CASE (Continued)

The next case considered in the validation process is shown in Figure 29. This configuration was tested[62] with a body alone, body with flare and with fins. The options chosen here for comparison are the body alone and body with a 10 deg flare and body with 15 deg fins. The basic body of Figure 29 consists of a 5-caliber ogive forebody with a 20 percent blunt nose. The fins were flat plates having rounding leading edges and blunt trailing edges. Tests were conducted at $M = 2.01$ and R_N/ft of 2×10^6. Base axial force measurements were subtracted out of the experimental data so the axial force will not include the base drag term. No boundary layer trip was mentioned in Reference 62 so the "smooth model with no boundary layer trip" option was used in both the AP95 and AP98 computations. Data were given to AOA 24 deg to 28 deg.

Figure 30 presents the AP95 and AP98 computations of $C_A - C_{A_B}$, C_N and C_M compared to the data of Reference 62. Comparison of the theory to data is acceptable. However, the $C_A - C_{A_B}$ comparisons are not as good as desired. It is suspected that the process of subtracting out the base pressure from experiment and theory is the primary source of the disagreement. To get accurate base pressure measurements from experimental data generally requires at least a three to one ratio of base to sting diameter plus several base pressure taps. Also the values of wave plus skin friction drag given by the experiment for the body alone case of 0.065 to 0.085 appear low. If the base pressure component were too high by 0.02 to 0.04, this could account for the error between experiment and theory for the axial force coefficient on Figure 30A. Figure 30B gives the same static aerodynamic results for the 10 deg flare case of Figure 29; and Figure 30C, the results for the 15 deg fin case of Figure 29. Comparison of the AP98 and AP95 to experiment is excellent, with the exception of the base pressure issue discussed previously.

The next set of wind tunnel data considered for comparison purposes is taken from Reference 63. Body alone, body-tail and wing-body-tail configurations were all a part of this test series. Figure 31A shows one of the configurations tested and considered here for validation of the AP98 results. The model is 13.5 calibers in length with a 1.5 caliber tangent ogive nose. The wing surfaces are fairly large with thickness of $t/c_r = 0.0178$ and wedge angles on the leading and trailing edges of 15 deg. The tail surfaces have thickness of $t/c_r = 0.05$ and wedge angles of 20 deg. The tests were conducted at Mach numbers 0.7 to 3.08 with Reynolds number varying from about 2×10^6 to 4.6×10^6 per foot. The smooth model without boundary layer trip option was used for the AP98 calculations. AOA to 25 deg were considered in the wind tunnel test. For comparison purposes, normal force and pitching moments are compared to data at $M = 1.42$ and 3.08 for the $\Phi = 0$ deg roll orientation. Figure 31B presents these results. As seen in the figure, both the AP95 and AP98 give quite acceptable comparisons to data, with the AP98 giving slightly better comparisons for pitching moment. The AP95 gives slightly better normal force coefficient comparisons to data at the $M = 3.08$ case for $\alpha > 18$ deg. Both versions of the APC give aerodynamics well within the accuracy goals. Reference 63 also gave axial force information where the base pressure had been subtracted out. Unfortunately, only a side chamber tap was used so the AOA information was not believed to be accurate. Hence, no axial force comparisons with AOA are shown.
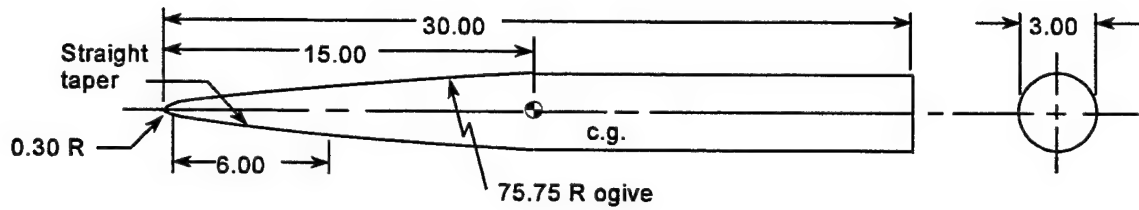
(A) Basic Body
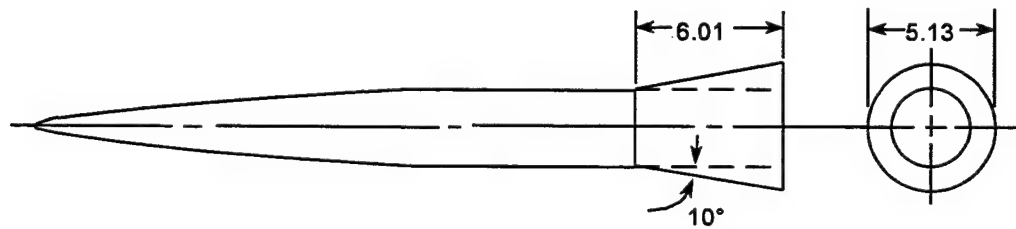
(B) Body with 10 deg flare.
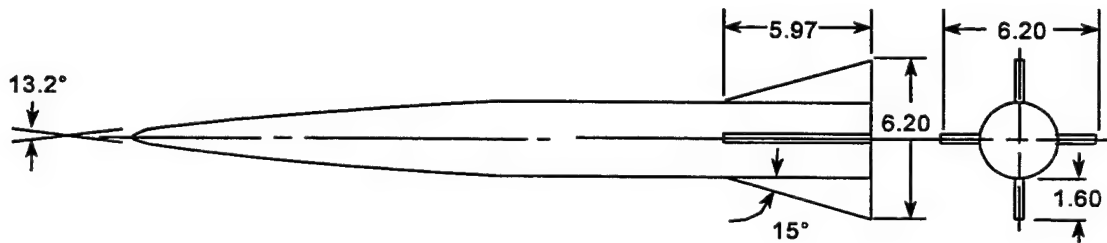
(C) Body with 15° fins.

FIGURE 29. SOME CONFIGURATIONS TESTED AT M = 2.01 (REFERENCE 62)
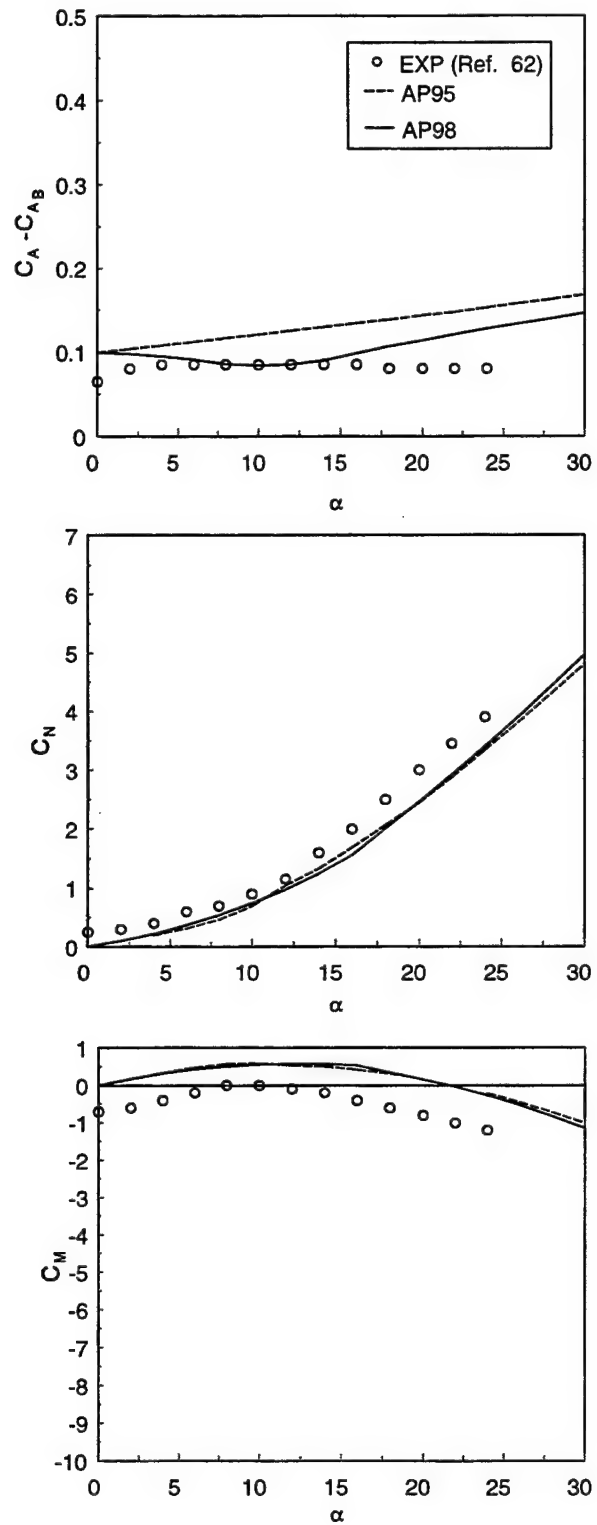
FIGURE 30A. STATIC AERODYNAMICS FOR BODY ALONE CASE OF FIGURE 29
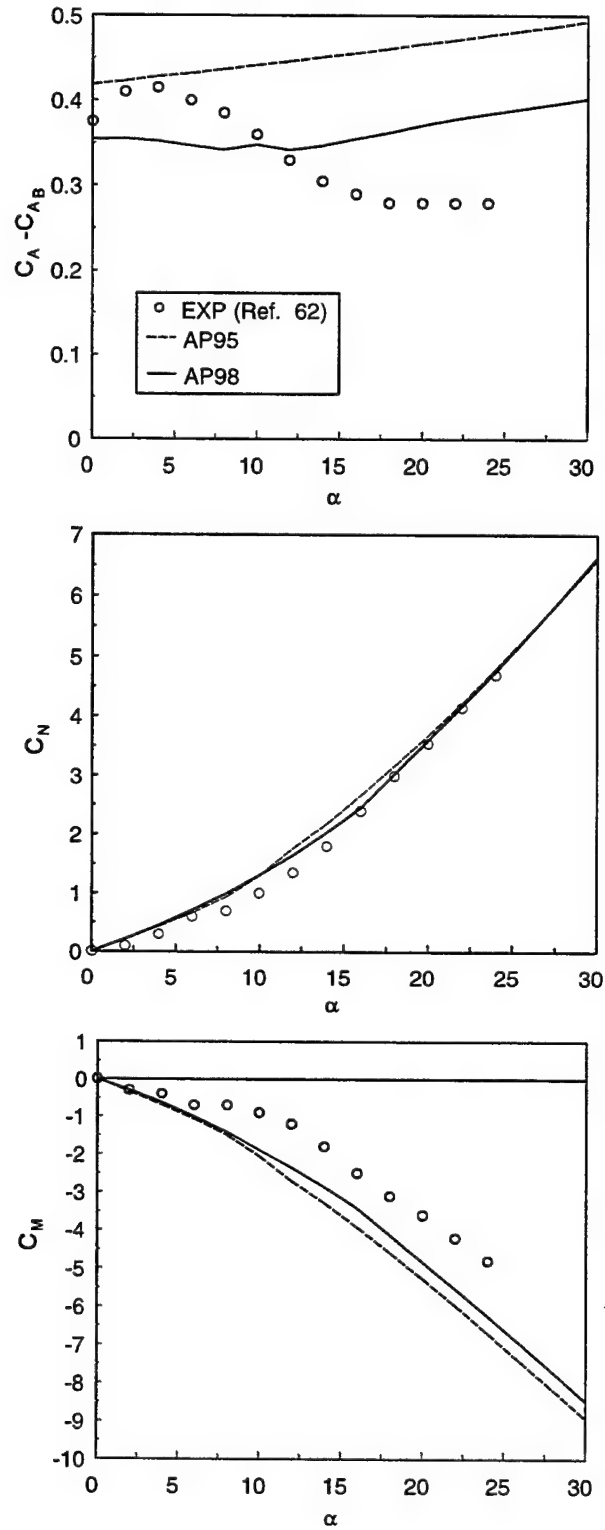
FIGURE 30B. STATIC AERODYNAMICS FOR 10 DEG FLARE CASE OF FIGURE 29
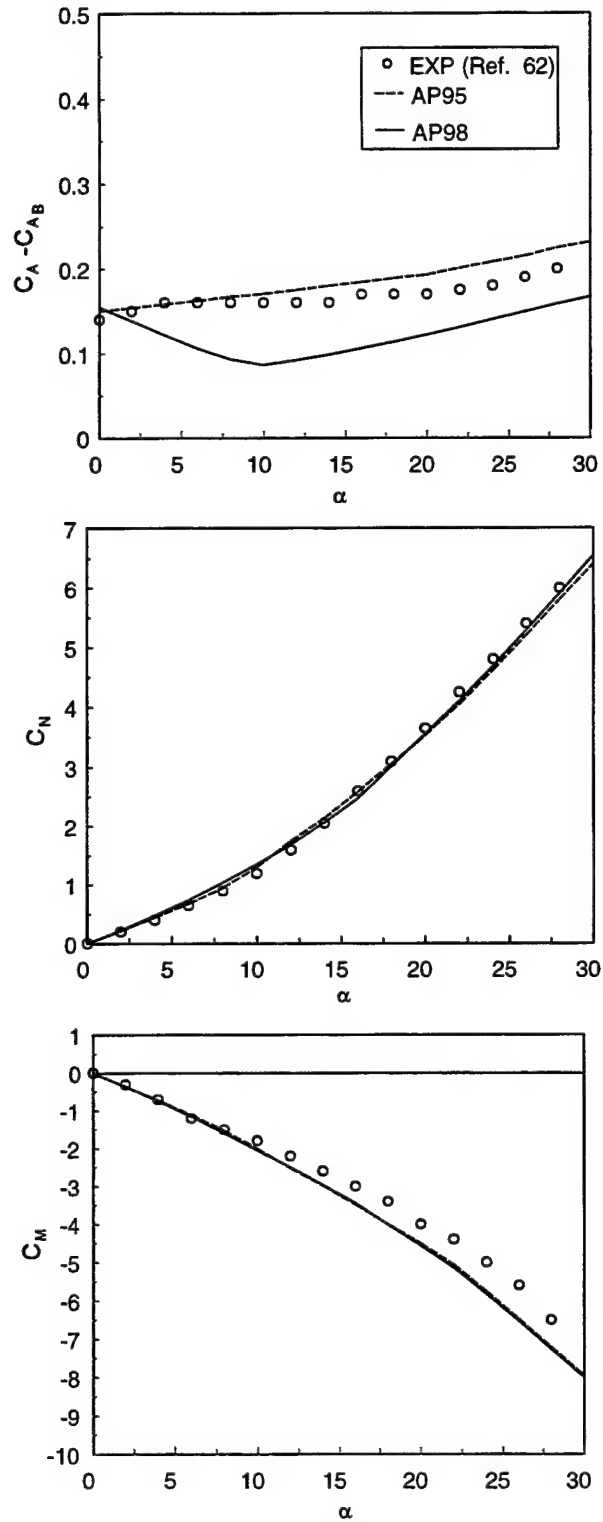
FIGURE 30C. STATIC AERODYNAMICS FOR 15 DEG FIN CASE OF FIGURE 29
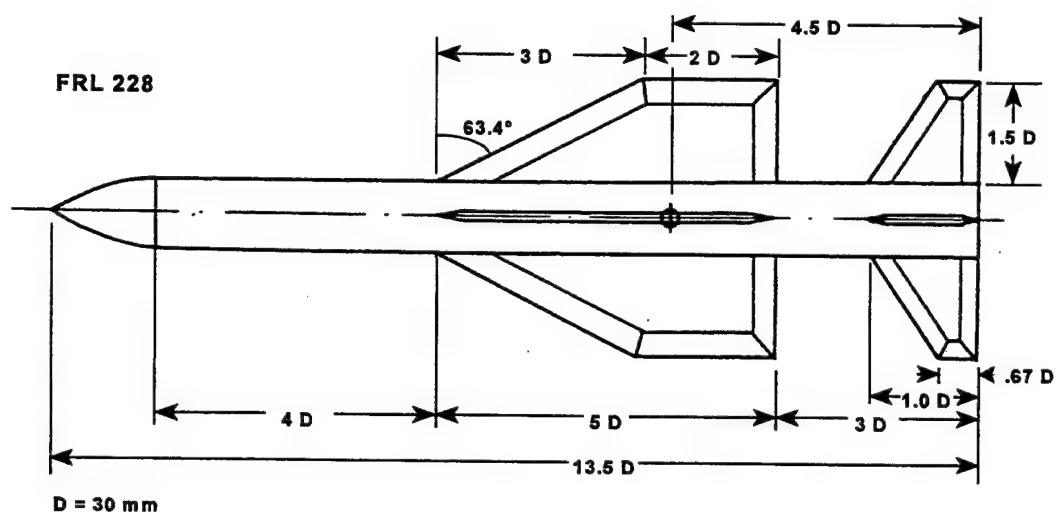
FIGURE 31A. WING-BODY-TAIL CONFIGURATION CONSIDERED FOR
VALIDATION WITH AP98 AND AP95 (REFERENCE 63)
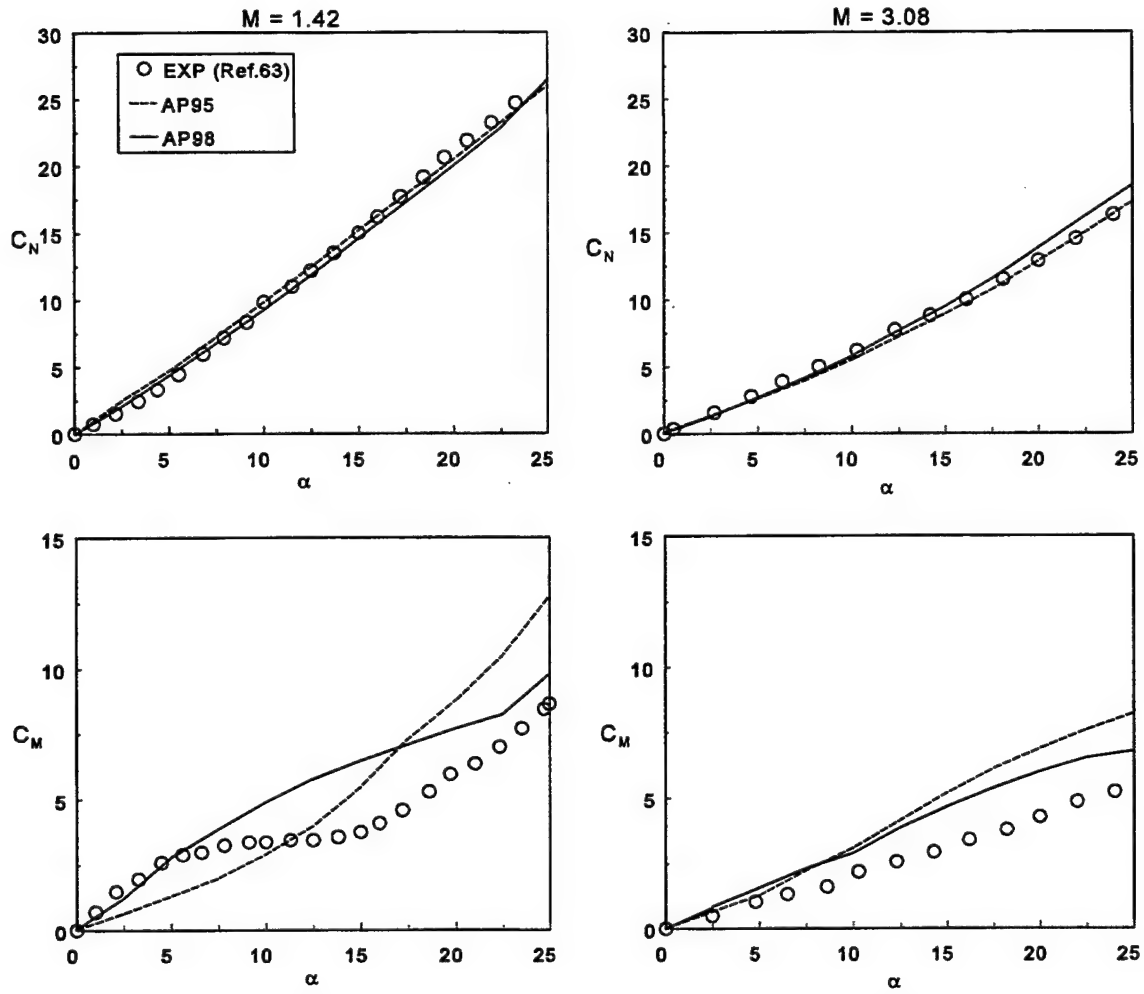
FIGURE 31B. NORMAL FORCE AND PITCHING MOMENT COMPARISONS OF THEORY
AND EXPERIMENT FOR FIGURE 31A CONFIGURATION (Φ = 0 DEG)

The next axisymmetric body configuration considered is a 22.2 caliber long canard-body-tail configuration with a 100 percent nose bluntness (hemisphere nose). The tail surfaces are fairly large, with aspect ratio 0.87, and fairly thick with truncated trailing edges. The canards are aspect ratio of 1.73. The configuration is shown in Figure 32A. The hangars which are on the wind tunnel model were not modeled by the aeroprediction code. Tests were conducted for $M_\infty = 0.2$ to 4.63, AOA 0 to 20 deg, control deflections 0 to 20 deg, roll of 0 to 45 deg, R_N/ft of 2×10^6 for a model with boundary layer trips. Base pressure values as a function of M_∞ and AOA were given in Reference 64, and these values were added to the axial force information so total axial force values could be shown.

Figure 32B gives the comparison of theory and experiment for $\Phi = 0$ deg roll for both 0 and 20 deg control deflections. Results are shown in terms of C_A, C_N and C_M versus Mach number for $\alpha = 0$ deg and 20 deg. Both C_N and C_M are zero for $\alpha = 0$ deg so only the 20 deg control deflection case is shown. Viewing Figure 32B, it is seen that the AP95 and AP98 both give good agreement to data and are both fairly comparable in terms of average accuracy. The worst errors are the $M = 0.2$ pitching moments where theory gives a too stable configuration by 1.6 calibers or 7.2 percent of the body length. This is outside the range of the average accuracy criteria of ±4 percent of body length for center of pressure. However, if all Mach number values for center of pressure are averaged, the theory is well within the ±10 percent criteria for axial and normal force and ±4 percent for center of pressure.

The roll 45 deg results are shown in Figure 32C. Here, only experiment and AP98 results are given. Very good comparisons are given for the AP98 compared to data at both control deflections and both AOAs as a function of Mach number.

Two six-fin projectile configurations are next considered to show how the AP98 and AP95 can be applied to cases like this, even though the code only has two and four fin options at present. The first of these configurations is shown in Figure 33A and is taken from Reference 65. It consists of a cone-cylinder body with six tail fins for stability. The fins have 100 percent blunt leading and trailing edges. Ballistic range data was available, and it was assumed the model was smooth. Hence, the "wind tunnel model with no boundary layer trip" option was chosen in both the AP95 and AP98 for viscous calculations. Reynolds number was computed based on sea level conditions at the given Mach number for a model 35.2 mm in diameter. Reference 65 gave both ballistic range and CFD results.

Figure 33B shows the comparison of the AP95 and AP98 to the ballistic range and CFD results of Reference 65. Excellent agreement of the AP98 and data is shown. However, the AP95 deviates from experiment significantly below $M = 3.25$. The reason for this large deviation is an error in the AP95 code for cases which have large leading edge bluntness. This error was corrected and is the reason the AP98 gives excellent agreement with data over the Mach number range that data was available. To obtain the C_A values from the AP95 and AP98, the four fin case was executed with the APC. Then the values in the tables of data for axial force of four fins was multiplied by 1.5. These values were then added to the body alone listed in the tables of the APC. Hence, even though the APC is limited to four fins, six-fin computations can be obtained by using the APC and performing some hand calculations using the output tables from the APC.
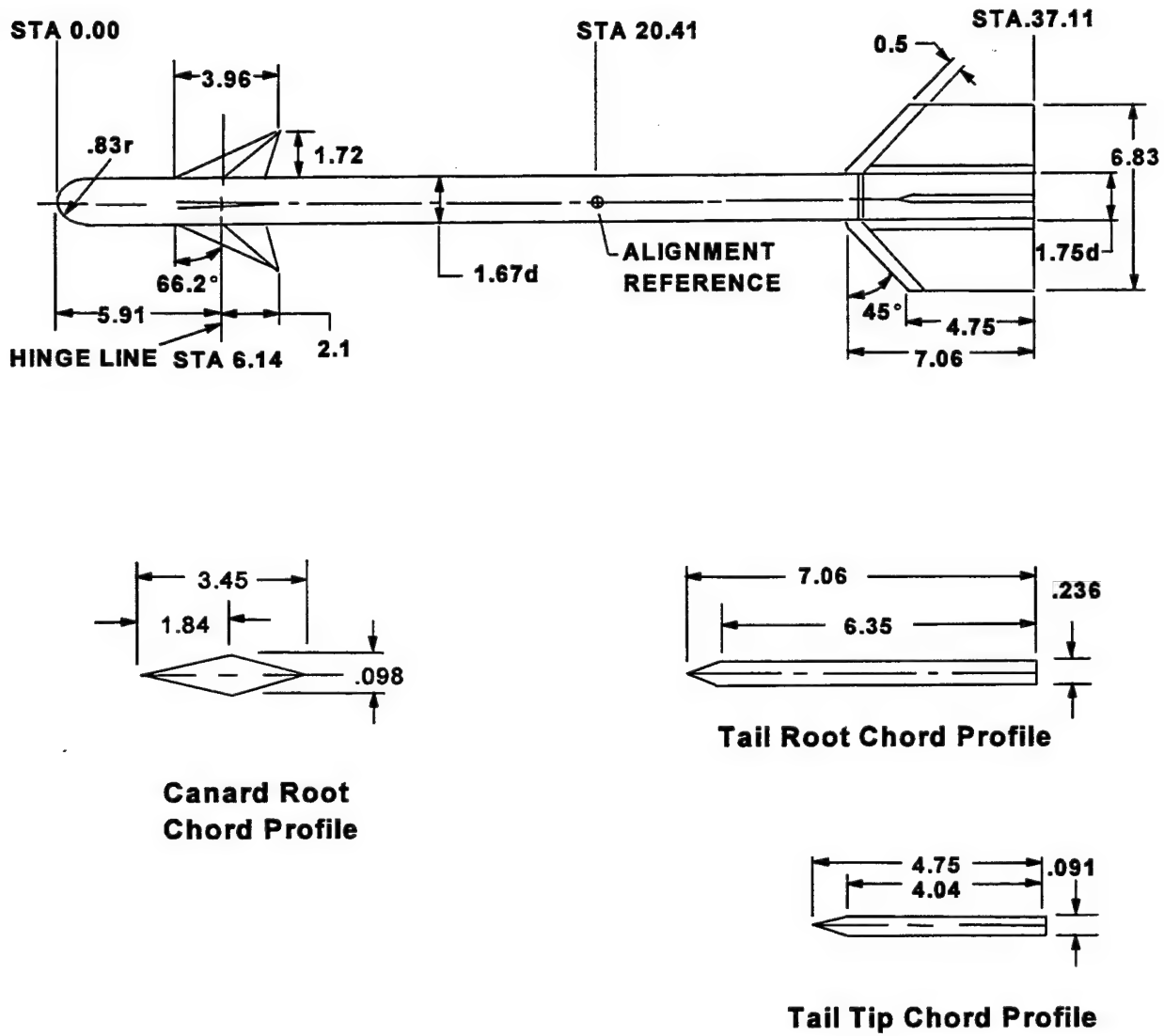
FIGURE 32A. CANARD-BODY-TAIL CONFIGURATION WITH HEMISPHERICAL NOSE[64]
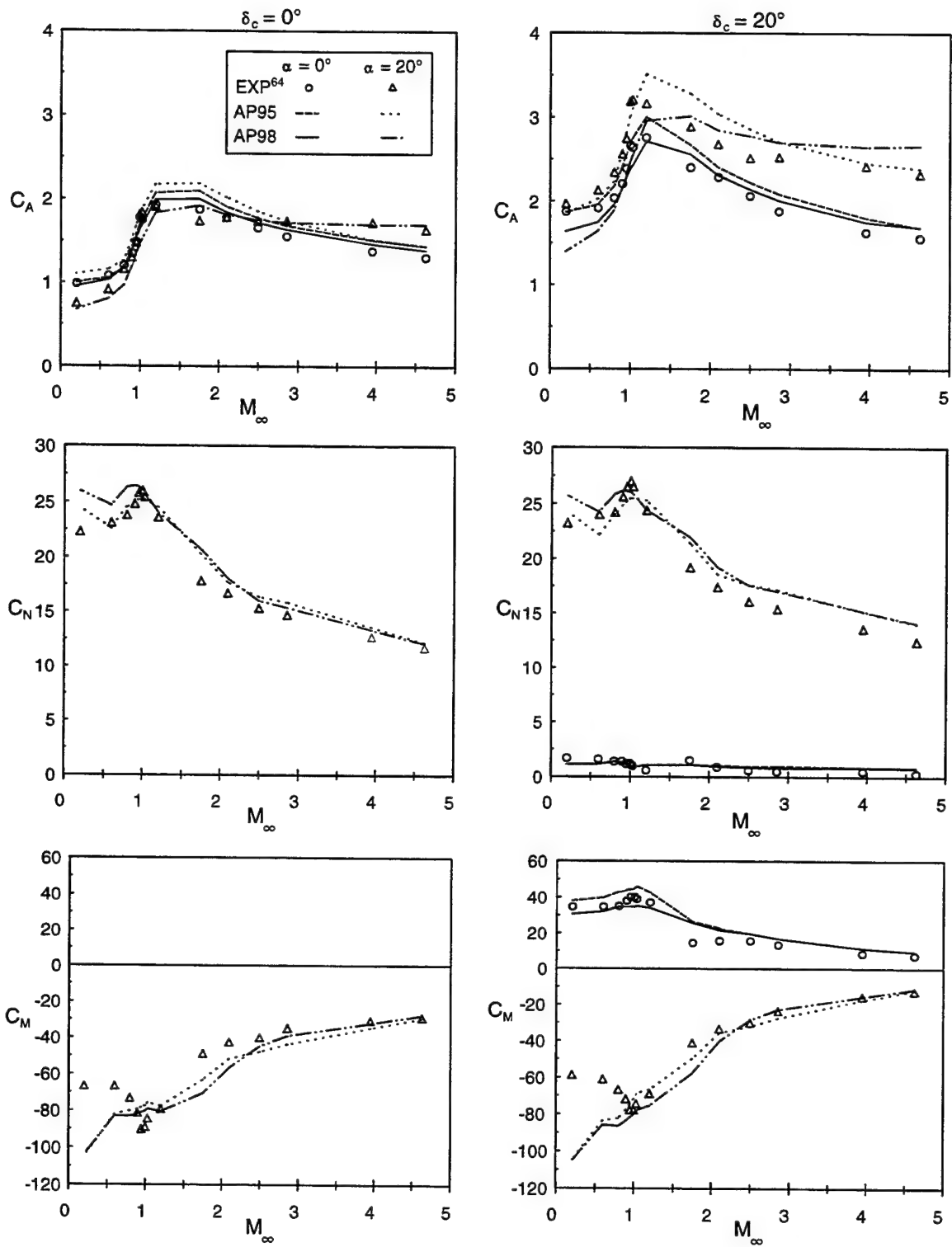
FIGURE 32B. C_A, C_N AND C_M VERSUS MACH NUMBER FOR CONFIGURATION
OF FIGURE 32A ($\Phi = 0$ DEG)
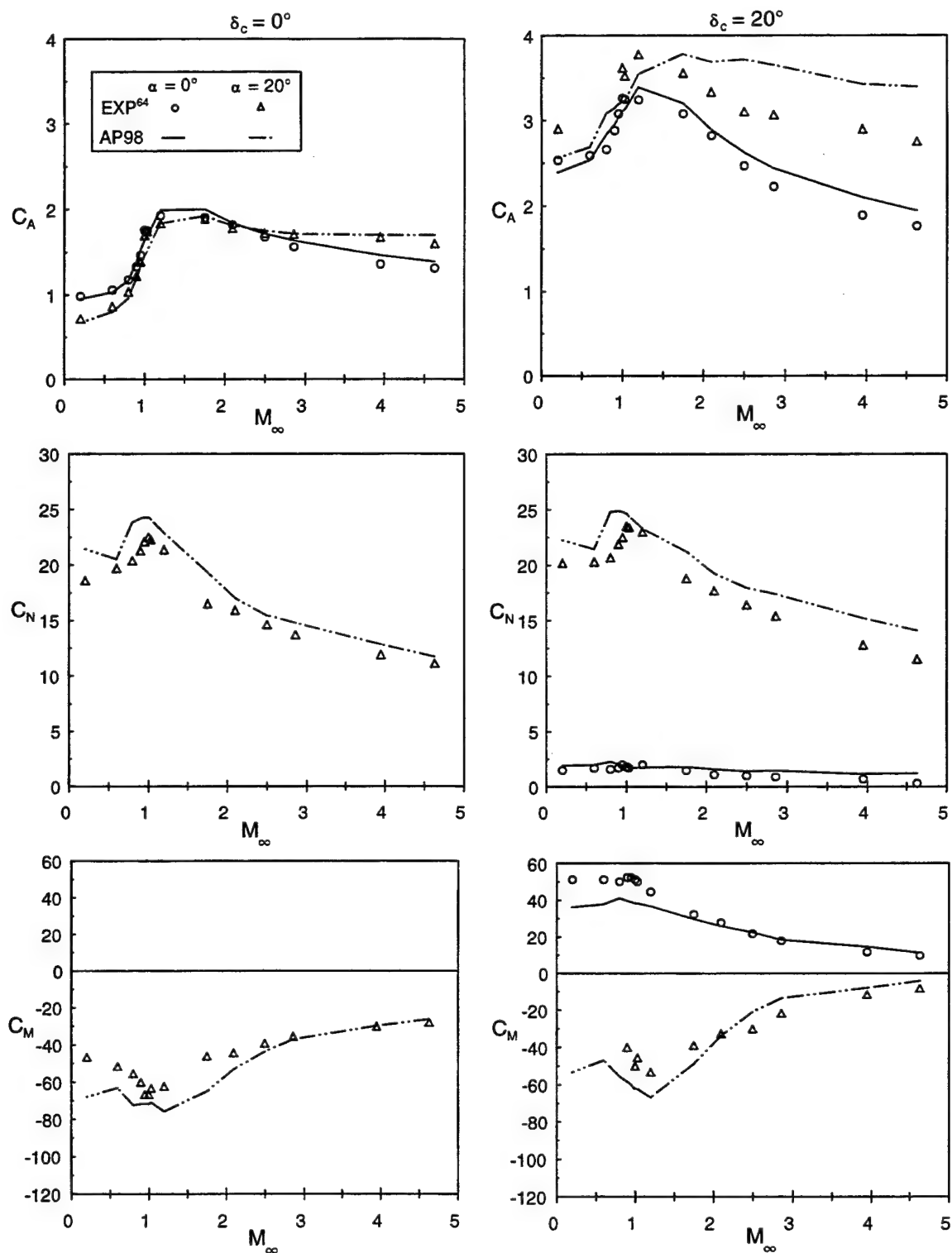
FIGURE 32C. C_A, C_N AND C_M VERSUS MACH NUMBER FOR CONFIGURATION
OF FIGURE 32A (Φ = 45 DEG)
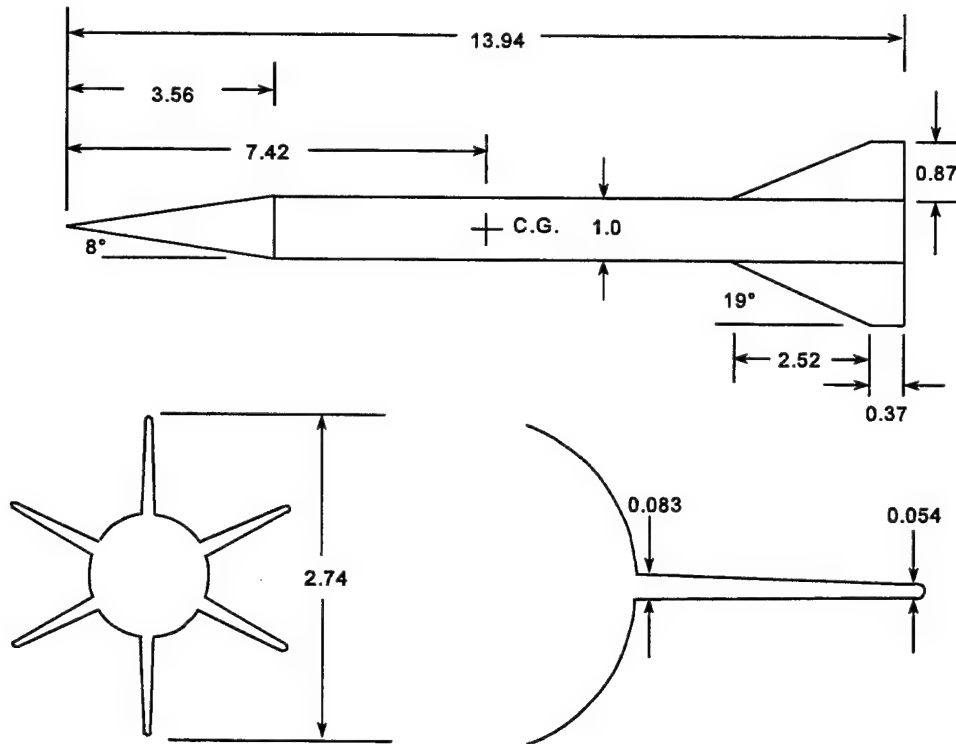
FIGURE 33A. FINNED PROJECTILE MODEL (ALL DIMENSIONS ARE IN CALIBERS, 1 CALIBER = 35.2 MM)
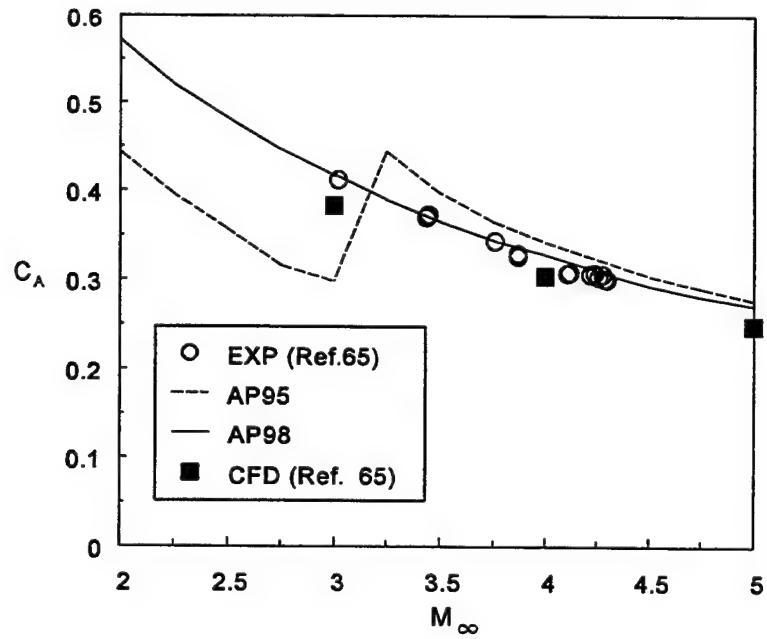
FIGURE 33B. AXIAL FORCE COMPARISONS OF THEORY TO BALLISTIC RANGE DATA FOR CONFIGURATION OF FIGURE 33A

78

The second of the six-fin configurations, and the last axisymmetric body case to be considered, is shown in Figure 34A and the details of the test and CFD analysis are given in Reference 66. This configuration is quite similar to that of Figure 33A in that the nose shape is an 8 deg half angle cone and the fin leading and trailing edges are blunt. The fins are slightly thicker than those of Figure 33A, however, and the body is 23.14 versus 13.94 calibers long as well. The diameter of the model was 27.05 mm and the same boundary option was chosen for the AP98 computations as for the previous case of Reference 65. Here, only AP98 results are shown in comparison to ballistic range and CFD results of Reference 66.

Figure 34B compares the axial force coefficient, normal force coefficient derivative and center of pressure predictions to ballistic range data and CFD results. Ballistic range data were available for $M_\infty = 3.5$ to 5.3 and CFD computations were available at $M = 5.88$, 5.0 and 4.41. AP98 results are shown for $M_\infty = 2$ to 6. Several points are worthy of note here. First of all, there is a fairly high amount of scatter in the ballistic range data for $(C_{N_\alpha})_{\alpha=0}$ and $(X_{CP})_{\alpha=0}$. It is not known why this occurs but it could be a result of AOA motion that is not accounted for in the APC or CFD computations. The AP98 and CFD axial force results compare reasonably well with the zero yaw drag results of the ballistic range tests except at lower supersonic Mach numbers. At $M = 3.5$, the ballistic range data shows a steeper increase in drag coefficient than does the AP98. It is not clear whether this is due to an underprediction of the AP98 compared to data or yaw drag not accounted for by the AP98. The previous six fin case (Figure 33 and Reference 65) had ballistic range data as low as $M = 3.0$. Excellent agreement between the AP98 and data was obtained for this configuration. Since the configuration is so similar, the only plausible explanation appears to be yaw drag in the data at the lower Mach numbers. C_{N_α} and X_{CP} values of the AP98 and CFD are in very close agreement and fall in the middle of the ballistic range data given in Figure 34B.

6.2   NONAXISYMMETRIC BODY CASES

The new nonaxisymmetric body technology developed and described in Reference 5 has been evaluated by applying it to an extensive array of aerodynamic configurations over a broad range of flight conditions. This included body alone configurations consisting of elliptical, square and triangular cross sections. The elliptical configurations considered had a/b ratios varying from 0.5 to 2.0. Square, diamond and triangular cross sections had corner roundness that varied between 0 and 0.33. Not all cases were available on all configurations, however. Freestream conditions varied from Mach numbers as low as 0.3 to as high as 14. AOA as high as 60 deg were considered.

Several wing-body cases were also considered,[5] but not nearly as much data were available as for the body alone. Configuration geometry and flight conditions were more limited as well. Only one wing-body-tail case[5] was considered as this was the only case where data was found in the literature.
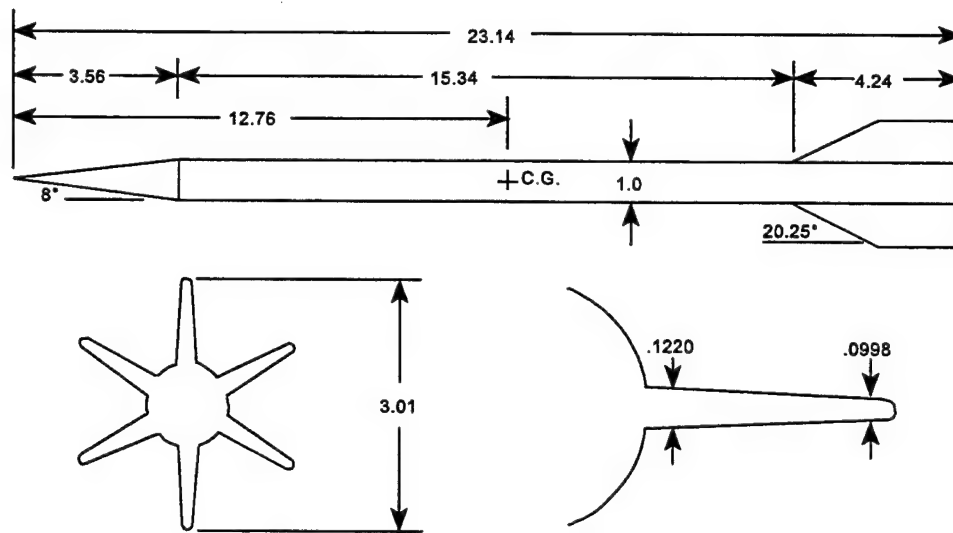
All Dimensions in Calibers (One Caliber = 27.05 mm)

FIGURE 34A. SCHEMATIC OF M829 PROJECTILE CONFIGURATION
(FROM REFERENCE 66)
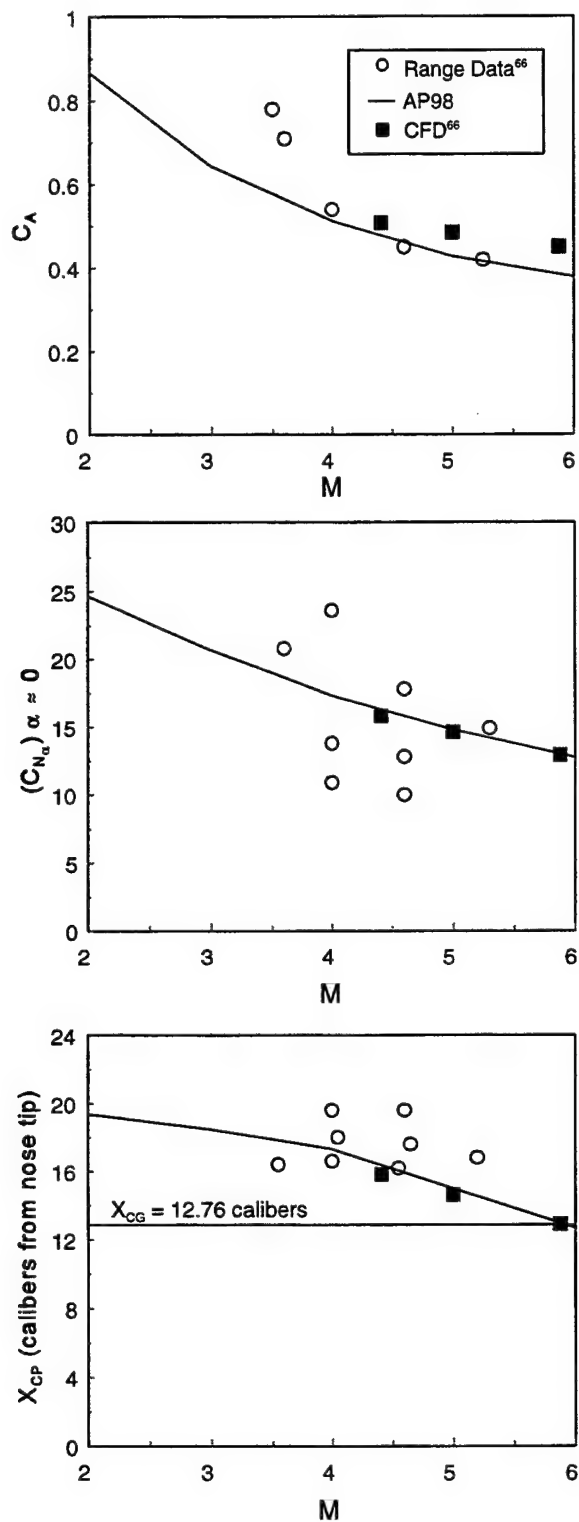
FIGURE 34B. COMPARISON OF STATIC AERODYNAMICS BETWEEN THEORY
AND EXPERIMENT FOR FIGURE 34A CONFIGURATION

Only three of the Reference 5 results will be shown here. All cases computed used an optimum value of the critical crossflow Mach number where transition from subcritical to supercritical conditions occur. This optimum value is not that critical for higher Mach number computations but is very important to accurately predict subsonic normal force. The first case considered is the configuration of Figure 35. This configuration was tested to 24 deg AOA at $M_\infty = 1.98$ and 3.88 in Reference 50. All bodies in Figure 35 have the same cross sectional area as the circle. The corner radii of the squares and triangles were very small, so a value of k = 0 was assumed in the computations. The elliptical shape 10-caliber body of Figure 35 was tested later[49] at Mach numbers 0.6 to 2.0 and to AOA 56 deg. The case shown here will thus be the elliptical 10-caliber long body tests of Reference 49, which go to 56 deg AOA, and the square and triangular tests of Reference 50, which go only to 24 deg AOA. Not all results will be shown, as the References 50 and 49 data bases were fairly extensive. Most of these results are shown in Reference 5, however.

Figures 36 through 38 give the elliptical body results for Mach numbers of 0.6, 1.2 and 2.0. Results shown are for ellipticity values of 0.5, 1.0 and 2.0 and are given in terms of normal and axial force coefficients and center of pressure. Also, the axial force coefficient does not include a base drag component. In examining the Figures 36 through 38 comparisons of theory and experiment, it is seen the theory does a fairly good job of predicting the aerodynamics on the a/b = 2.0 elliptical case at all three Mach numbers. The normal force and center of pressure predictions are quite encouraging as they are well within the average accuracy levels of ±10 percent and ±4 percent of body length respectively. The axial force prediction comparisons are not as good as desired. However, this could be due to measurement accuracy where it is difficult to get accurate axial force measurements with a sting designed for measuring normal force at high AOA. The a/b = 0.5 results are not quite as good as the a/b = 2.0 results, particularly at high AOA. This could be due to the critical value of crossflow Mach number prediction. The data appears to support supercritical flow up to AOA of 56 deg whereas the theory indicates the flow transitions to subcritical conditions around AOA 36 to 40 deg. Also the center of pressure prediction for the a/b = 0.5 case at low AOA appears to indicate a center of pressure much further toward the nose tip at M = 0.6 than the theory predicts. It is not clear what mechanism causes this. Since the nose length is 3 calibers and there is no boattail present, intuition would lead one to expect the center of pressure to lie somewhere between 1.5 and 3.0 calibers from the nose tip near $\alpha = 0$ deg.

Theoretical and experimental results for the squares and triangles of Figure 35 are given in Figures 39 and 40 respectively. Only the 10-caliber long configuration results at M = 1.98 are shown. Here the results are given in terms of lift coefficient, lift to drag ratio and center of pressure. In general, comparison of theory and experiment for the squares and diamonds is quite encouraging, although not as good as the circular cross section shapes. The triangular shaped body predictions for lift coefficient tend to be somewhat low as AOA increases. However, this is to be expected since the values for the circular cylinder results are also low. Lift to drag ratio predictions are quite good, with the peak values being reasonably well predicted. Center of pressure prediction for the triangular shape is well within the ±4 percent of body length used as a criteria for axisymmetric bodies. However, the inverted triangle center of pressure predictions slightly exceed this value.
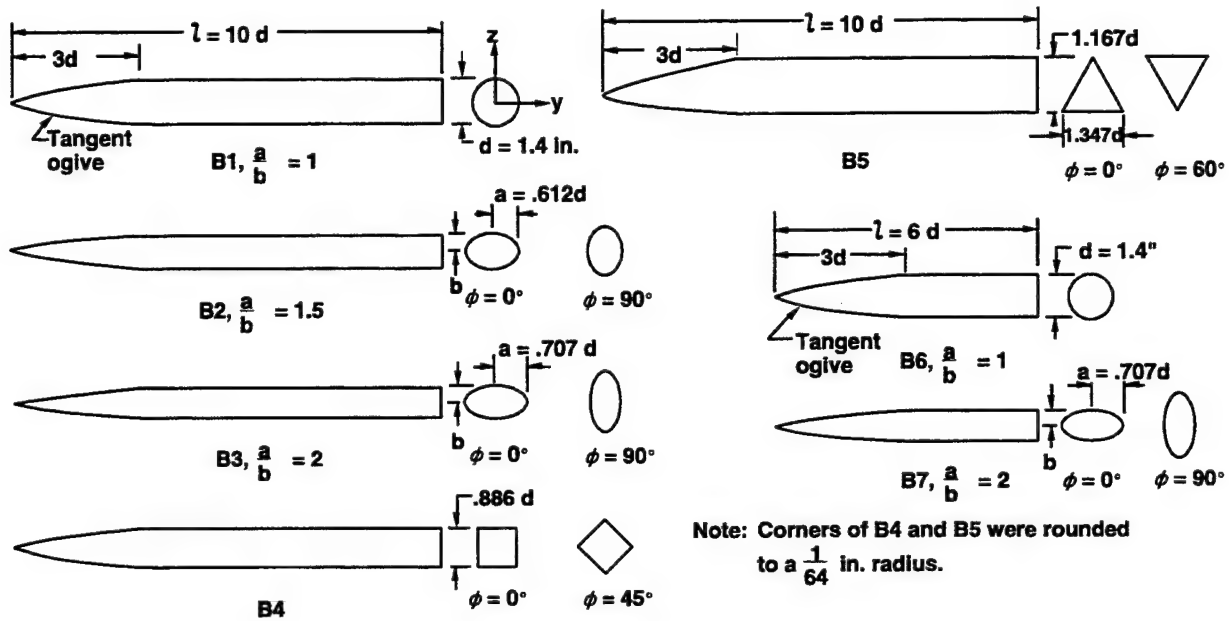
FIGURE 35. BODY ALONE CONFIGURTIONS[50] WITH ELLIPTICAL, SQUARE, DIAMOND, TRIANGULAR AND INVERTED TRIANGULAR SHAPES
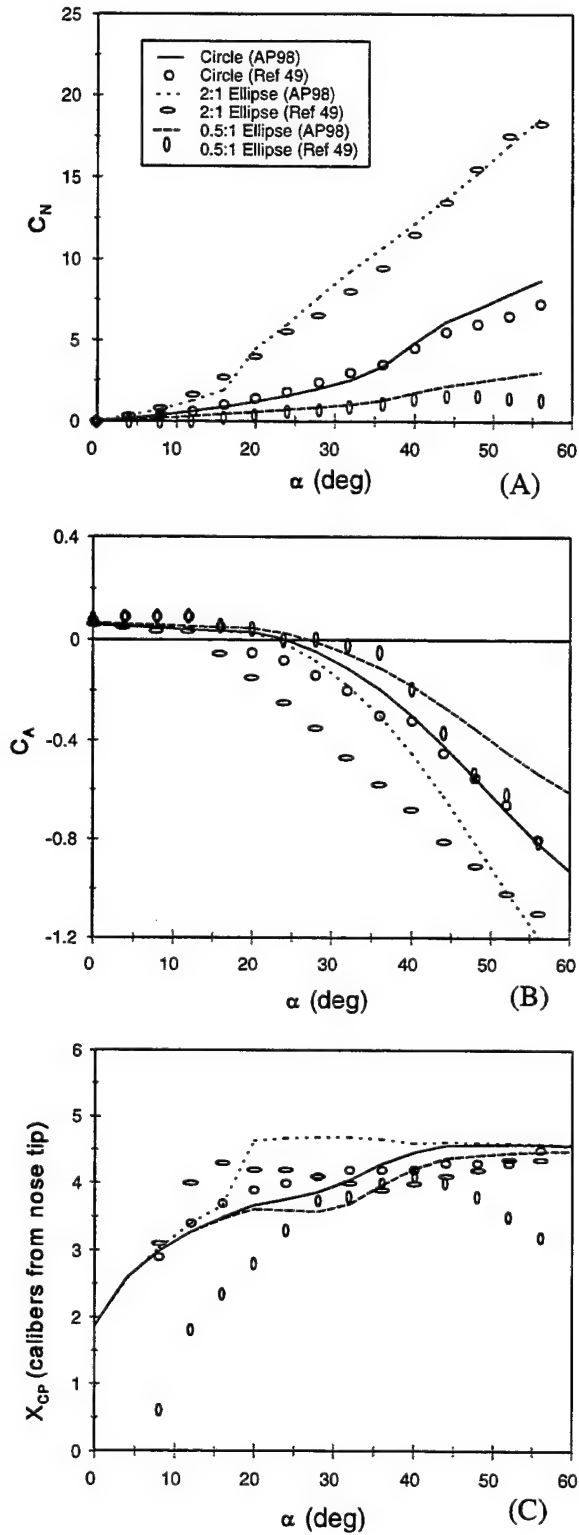
FIGURE 36. AERODYNAMIC DATA FOR 2:1 AND 0.5:1 ELLIPSES OF FIGURE 35 COMPARED
TO CIRCULAR BODY AT M = 0.6: (A) NORMAL FORCE COEFFICIENT,
(B) AXIAL FORCE COEFFICIENT, (C) CENTER OF PRESSURE
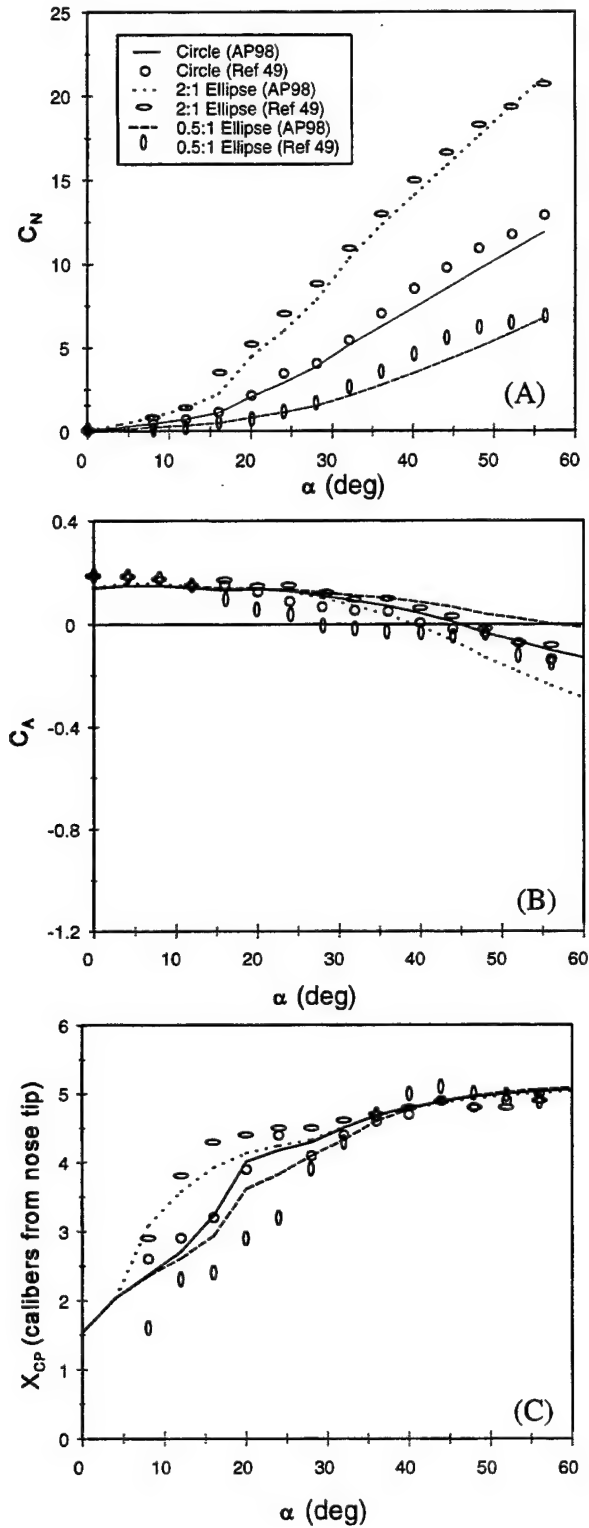
FIGURE 37. AERODYNAMIC DATA FOR 2:1 AND 0.5:1 ELLIPSES OF FIGURE 35 COMPARED
TO CIRCULAR BODY AT M = 1.2: (A) NORMAL FORCE COEFFICIENT,
(B) AXIAL FORCE COEFFICIENT, (C) CENTER OF PRESSURE
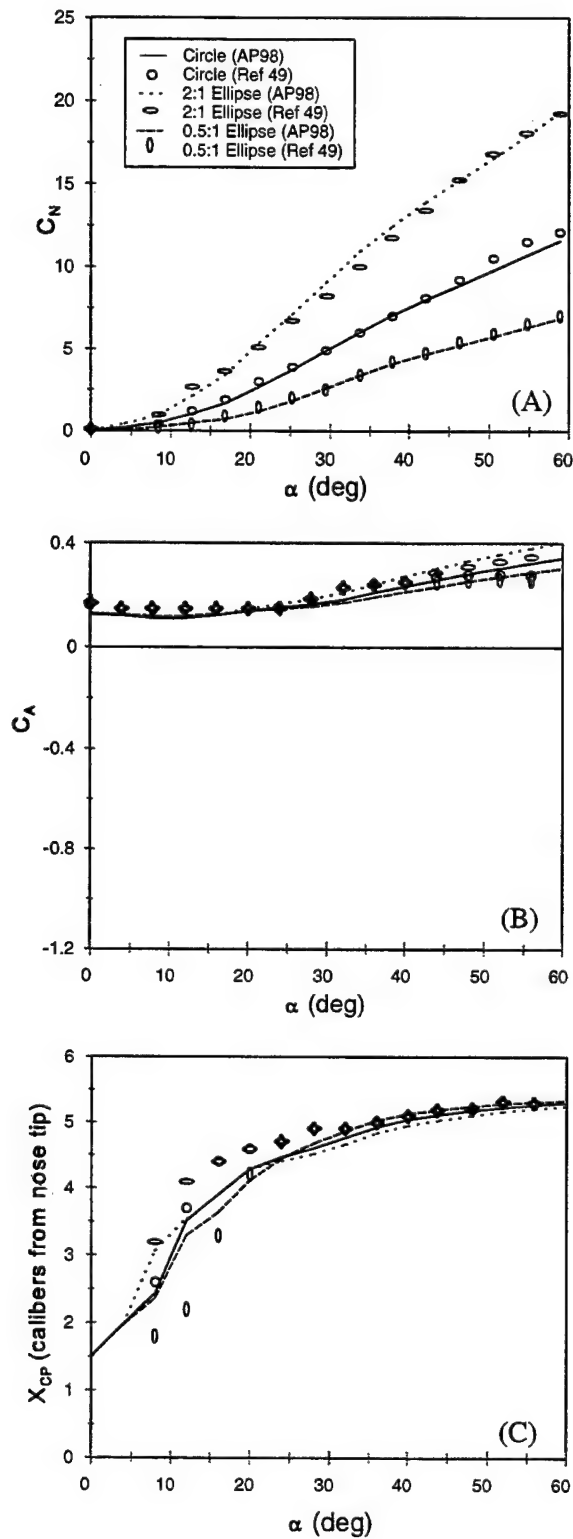
FIGURE 38. AERODYNAMIC DATA FOR 2:1 AND 0.5:1 ELLIPSES OF FIGURE 35 COMPARED
TO CIRCULAR BODY AT M = 2.0: (A) NORMAL FORCE COEFFICIENT,
(B) AXIAL FORCE COEFFICIENT, (C) CENTER OF PRESSURE
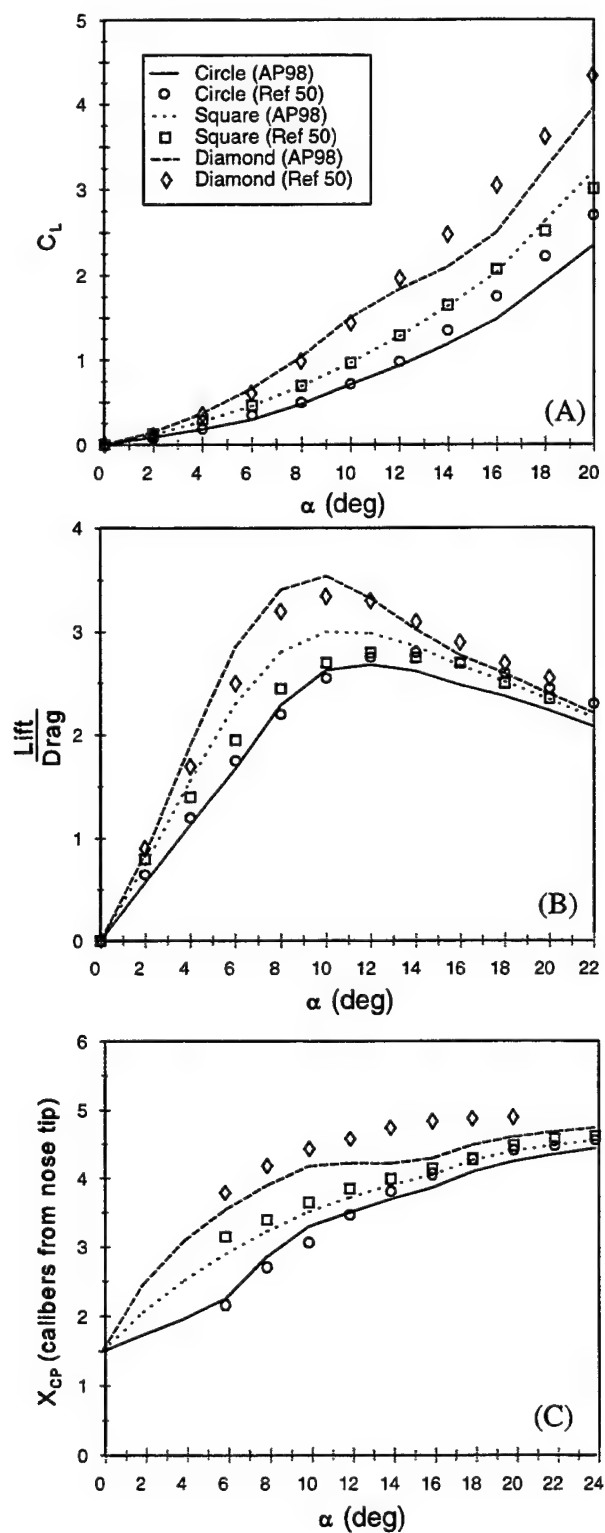
FIGURE 39. AERODYNAMIC DATA OF SQUARES (k = 0.0) AND DIAMONDS (k = 0.0)
OF FIGURE 35 COMPARED TO CIRCULAR BODY AT M = 1.98 (ℓ/d = 10):
(A) LIFT COEFFICIENT, (B) LIFT TO DRAG RATIO, (C) CENTER OF PRESSURE
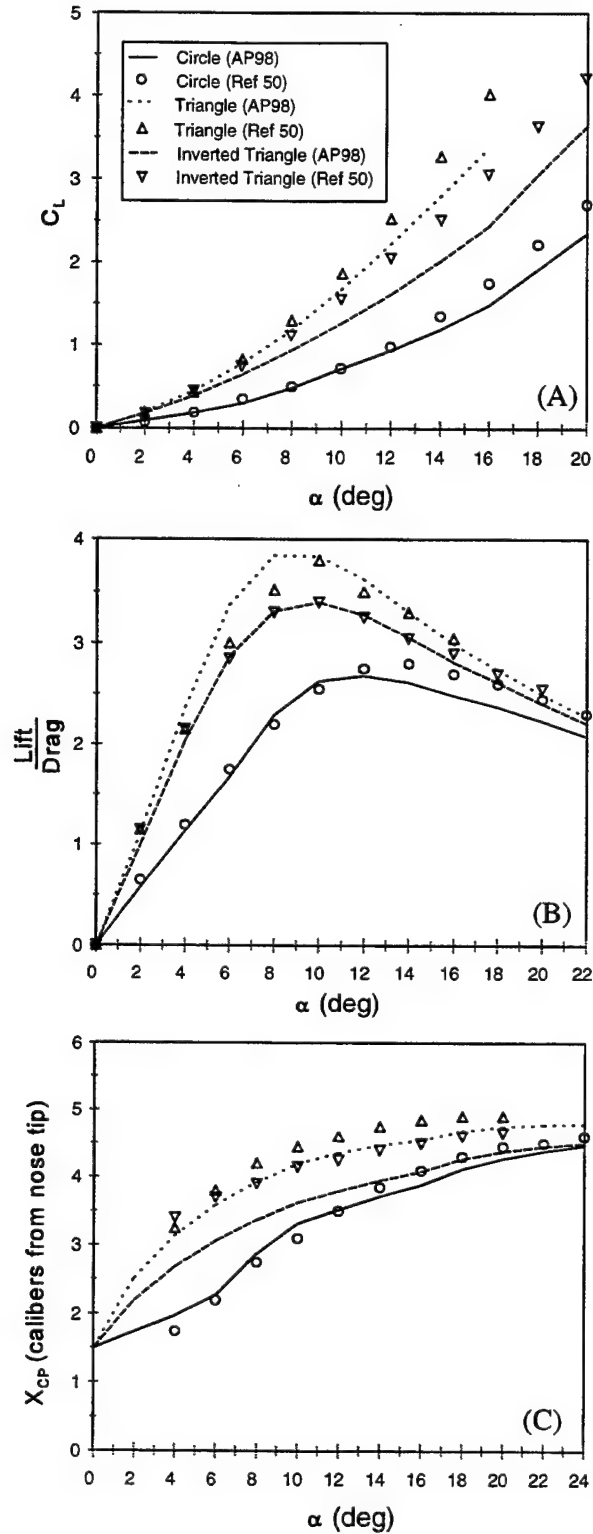
FIGURE 40. AERODYNAMIC DATA OF TRIANGLES (k = 0.0) AND INVERTED TRIANGLES (k = 0.0) OF FIGURE 35 COMPARED TO CIRCULAR BODY AT M = 1.98 (ℓ/d = 10): (A) LIFT COEFFICIENT, (B) LIFT TO DRAG RATIO, (C) CENTER OF PRESSURE

The next case considered is a 10-caliber wing-body and wing-body-tail case shown in Figure 41 (see Reference 49). The body cross section is an ellipse with an a/b = 2.0, and the nose length is 3.0 calibers. Figures 42 and 43 present the normal force and center of pressure comparisons of experiment and theory at M = 0.6 and 2.0 for the wing-body and wing-body-tail cases respectively. Data for the wing-body-tail case at M = 2.0 was only available to α = 34 deg, whereas all other cases have data to 60 deg AOA. As seen in Figures 42 and 43, theoretical predictions are quite good for center of pressure and fair to good for normal force coefficient.

The third configuration shown (see Figure 44) is a waverider configuration taken from Reference 67. Lift, drag, and pitching moment comparisons of theory and experiment at M = 14.0 to α = 25 deg are shown in Figure 45. Results are quite encouraging, even though this configuration does not quite fit the triangular shape, which has 60 deg angles in all corners. Note that these results are based on a 375 in.^{2} planform area.

7.0 SUMMARY AND FUTURE OPPORTUNITIES

In summary, new technology has been developed to allow extension of the aeroprediction code to the roll position of 45 deg (fins in "×" or cross roll orientation) in addition to the roll position of 0 deg (fins in "+" or plus roll orientation). It has also been extended to compute aerodynamics of nonaxisymmetric bodies based on an equivalent axisymmetric body. In addition, the nonlinear aerodynamic loads have been distributed over the body and lifting surfaces to provide a more useful tool for preliminary structural analysis. Finally, new technology was developed to improve the prediction of axial force at AOA.

To make the AP98 more user friendly, an improved pre- and post-processing, personal-computer interface is being developed. These new technologies have been integrated into the AP95 and will be transitioned to legitimate users as the AP98. Comparisons of the new theory have been made to both experimental data and the AP95. Comparisons of theory and experiment show the AP98 to be at least as good as the AP95 and, in general, maybe slightly better. In general, average accuracy levels of aerodynamics are ±10 percent on axial and normal force and ±4 percent of body length on center of pressure. For nonaxisymmetric body cases, accuracy can be slightly higher than these numbers, although not enough cases have been considered to make a definitive assessment. While these accuracy levels are encouraging for a semiempirical code, they could be improved upon by using computational fluid dynamics codes or additional experimental data or both to minimize assumptions.

Future opportunities are placed in two categories. These categories are defined as major technology needs and value-added technology needs. The difference between the definition of "major" and "value-added" has to do with the cost to develop the technology and integrate it into the APC. Generally, before any new technology is developed, there needs to be a request from users and sponsor support to fund the technology development.
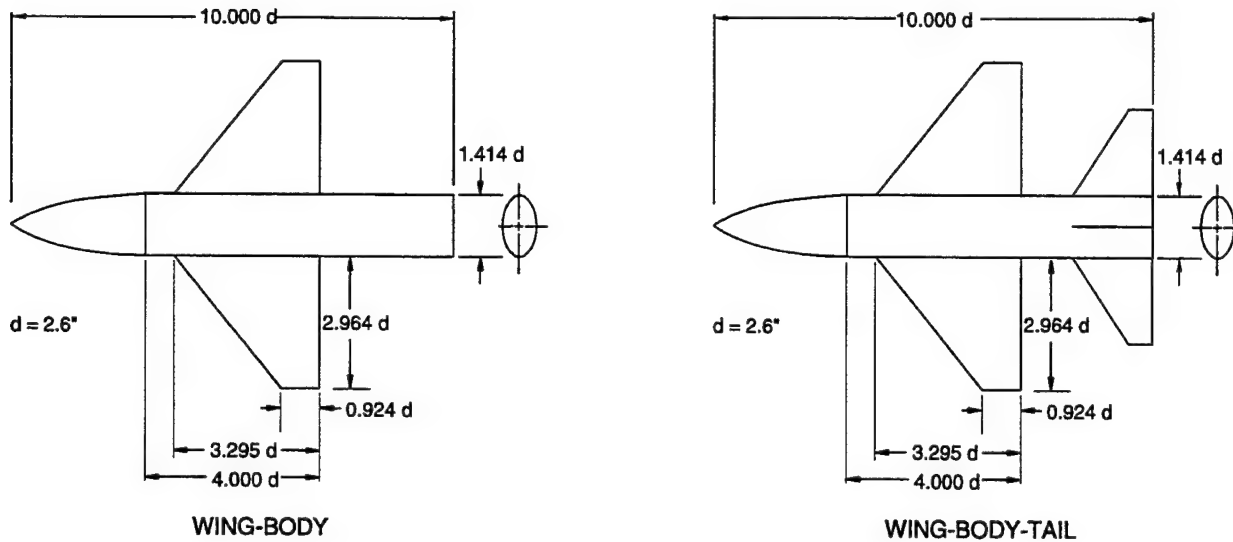
FIGURE 41. GEOMETRY OF THE WING-BODY AND WING-BODY-TAIL CONFIGURATIONS
WITH 2:1 ELLIPTICAL BODIES (FROM REFERENCE 49)
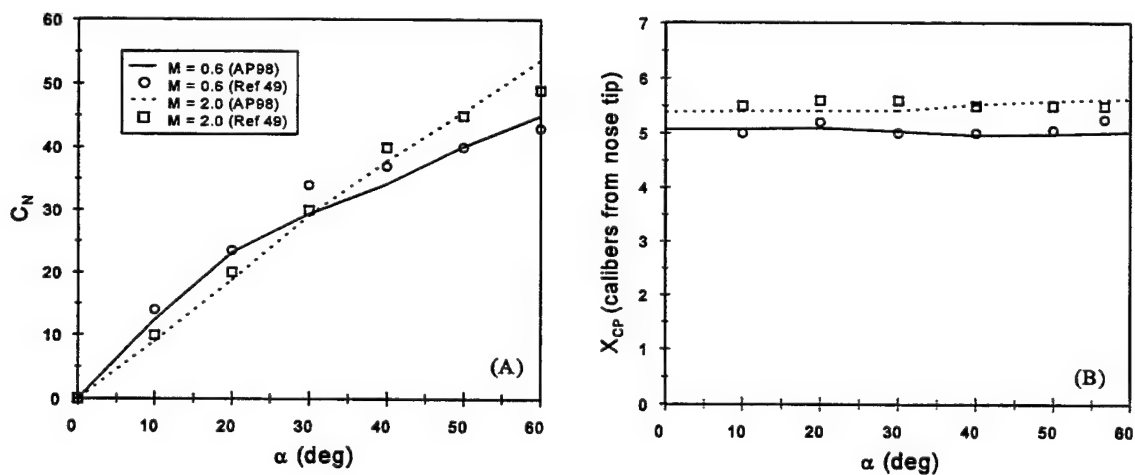
FIGURE 42. AERODYNAMIC DATA FOR THE WING-BODY CONFIGURATION OF FIGURE 41
WITH A 2:1 ELLIPTICAL CROSS SECTION BODY: (A) NORMAL FORCE COEFFICIENT,
(B) CENTER OF PRESSURE
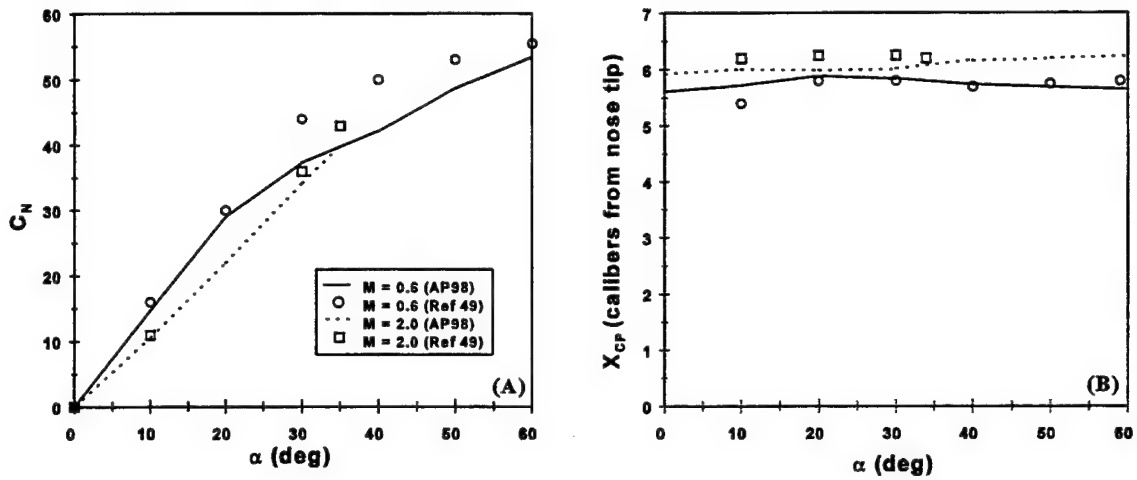
FIGURE 43. AERODYNAMIC DATA FOR THE WING-BODY-TAIL CONFIGURATION OF
FIGURE 41 WITH A 2:1 ELLIPTICAL CROSS SECTION BODY: (A) NORMAL FORCE
COEFFICIENT, (B) CENTER OF PRESSURE
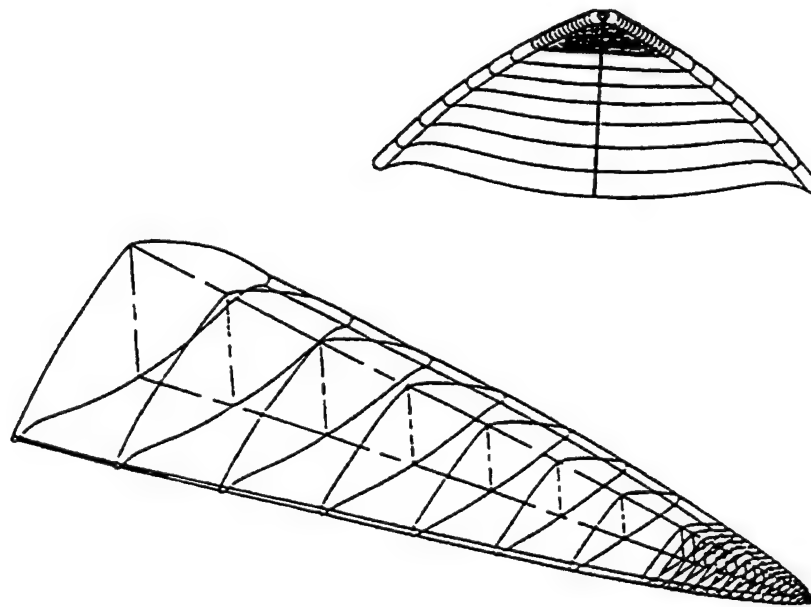
FIGURE 44. WIRE-FRAME GEOMETRY OF THE WAVERIDER (FROM REFERENCE 67)
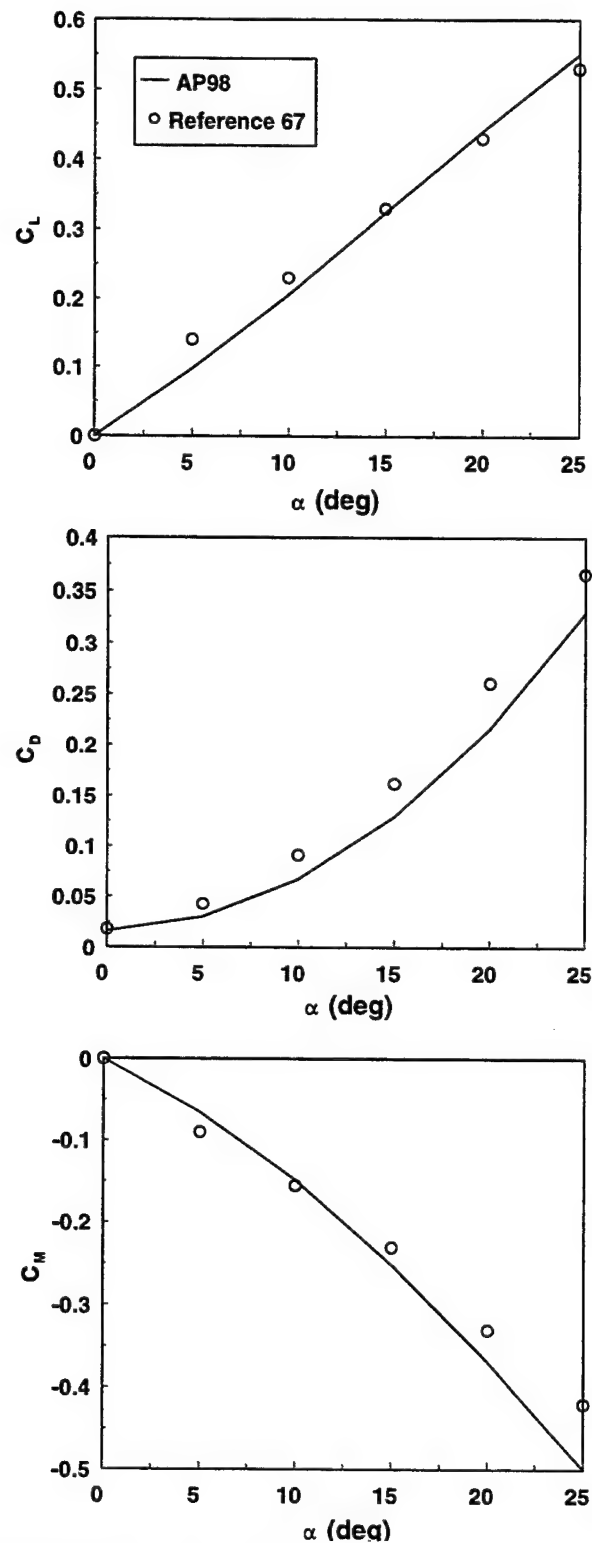
FIGURE 45. AERODYNAMIC DATA FOR THE MACH 14 WAVERIDER OF FIGURE 44: (A) LIFT
COEFFICIENT, (B) AXIAL FORCE COEFFICIENT, (C) MOMENT COEFFICIENT

The NSWCDD Aeroprediction Code has progressed to the point that it can compute planar aerodynamics with acceptable accuracy over the configuration and flight envelope of interest to most tactical weapons. The two remaining major technology needs are to account for aerodynamic effects of side jets and an accurate semiempirical code for out of plane aerodynamics. The first problem requires a good generic wind-tunnel database and this requirement is being marketed to BMDO. The latter need may be beyond the scope of a semiempirical code due to the complex out-of-pitch plane aerodynamic nonlinearities and the fact that many of these nonlinearities are within the accuracy of the data. This is particularly true for induced roll. As a result, at NSWCDD, either wind tunnel data or more accurate numerical codes have been used to predict out of plane aerodynamics. A less accurate (±25 percent) out of plane semiempirical code may be feasible, but it is not clear if this requirement is of interest and general utility.

There are several value-added technology needs which would enhance the capability of the APC significantly, while being much less costly than the two major technology needs described above. Some of these include: a) using CFD to improve the predictions outside the range of the data bases; b) using a new NASA data base for fine tuning r/s effects; c) integrating the APC with other software models to form system engineering models; d) modifying dynamic derivative calculations so flared vehicles can be handled; e) including a six-fin option into the APC; f) incorporating base bleed for projectile applications; g) including nonlinear aerodynamics into the dynamic derivatives; and h) incorporating methodology for internal shock interactions.

Over the history of the APC series (1972 to the present), significant advances have been made in semiempirical aeroprediction methods. As seen in the opportunities list, much work still remains to be done.

8.0 REFERENCES

1. Moore, F. G.; McInville, R. M.; and Hymer, T., *The 1995 Version of the NSWC Aeroprediction Code: Part I - Summary of New Theoretical Methodology*, NSWCDD/TR-94/379, Feb 1995.

2. Moore, F. G. and McInville, R. M., *Extension of the NSWCDD Aeroprediction Code to the Roll Position of 45 Degrees*, NSWCDD/TR-95/160, Dec 1995.

3. McInville, R. M.; Moore, F. G.; and Housh, C., *Nonlinear Structural Load Distribution Methodology for the Aeroprediction Code*, NSWCDD/TR-96/133, Sep 1996.

4. Moore, F. G. and Hymer, T., *An Improved Method for Predicting Axial Force at High Angle of Attack*, NSWCDD/TR-96/240, Feb 1997.

5. Moore, F. G.; McInville, R. M.; and Hymer, T., *An Improved Semiempirical Method for Calculating Aerodynamics of Missiles with Noncircular Bodies*, NSWCDD/TR-97/20, Sep 1997.

6. Moore, F. G., *Body Alone Aerodynamics of Guided and Unguided Projectiles at Subsonic, Transonic, and Supersonic Mach Numbers*, NWL TR-2976 , Nov 1972.

7. Van Dyke, M. D., "First and Second-Order Theory of Supersonic Flow Past Bodies of Revolution," *Journal of Aeronautical Sciences*, Vol. 18, No. 3, Mar 1951, pp. 161-179.

8. Tsien, H. S., "Supersonic Flow Over an Inclined Body of Revolution," *Journal of Aeronautical Sciences*, Vol. 5, No. 12, Oct 1938, pp. 480-483.

9. Lee's, L., "Hypersonic Flow," *Institution of Aeronautical Science*, preprint No. 554, 1955.

10. Eggers, A. J. and Savin, R. C., *Approximate Methods for Calculating the Flow About Nonlifting Bodies of Revolution at High Supersonic Airspeeds*, NACA TN 2579, 1951.

11. Syvertson, C. A. and Dennis, D. H., *A Second-Order Shock-Expansion Method Applicable to Bodies of Revolution Near Zero Lift*, NACA TR 1323, 1957.

12. Jackson, C. M., Jr.; Sawyer, W. C.; and Smith, R. S., *A Method for Determining Surface Pressures on Blunt Bodies of Revolution at Small Angles of Attack in Supersonic Flow*, NASA TN D-4865, Nov 1968.

REFERENCES (Continued)

13. DeJarnette, F. R.; Ford, C. P.; and Young, D. E., "A New Method for Calculating Surface Pressures on Bodies at an Angle of Attack in Supersonic Flow," AIAA paper no. 79-1552, 12th Fluid and Plasma Dynamics Conference, Williamsburg, VA, Jul 1979.

14. Moore, F. G.; Armistead, M. J.; Rowles, S. H.; and DeJarnette, F. R., *Second-Order Shock-Expansion Theory Extended to Include Real Gas Effects*, NAVSWC TR 90-683, Feb 1992.

15. Van Driest, E. R., "Turbulent Boundary Layers in Compressible Fluids," *Journal of Aeronautical Sciences*, Vol. 18, No. 3, 1951, pp. 145-160, 216.

16. Moore, F. G., *State-of-the-Art Engineering Aeroprediction Methods with Emphasis on New Semiempirical Techniques for Predicting Nonlinear Aerodynamics on Complete Missile Configurations*, NSWCDD/TR-93/551, Nov 1993.

17. Moore, F. G.; Wilcox, F.; and Hymer, T., *Improved Empirical Model for Base Drag Prediction on Missile Configurations Based on New Wind Tunnel Data*, NSWCDD/TR-92/509, Oct 1992.

18. Brazzel, C. E. and Henderson, J. H., "An Empirical Technique for Estimating Power-On Base Drag of Bodies-of-Revolution with a Single Jet Exhaust," Proceedings, Specialists Meeting Sponsored by the AGARD Fluid Dynamics Panel, held in Mulhouse, France, 5-8 Sep 1966.

19. Devan, L., *Aerodynamics of Tactical Weapons to Mach Number 8 and Angle of Attack 180°: Part I, Theory and Application*, NSWC TR 80-346, Oct 1980.

20. Park, C. and Leon, S., "Calculation of Real-Gas Effects on Blunt Body Trim Angles," AIAA paper no. 89-0685, Aerospace Sciences Meeting, Reno, NV, Jan 1989.

21. McInville, R. and Moore, F. G., *Incorporation of Boundary Layer Heating Predictive Methodology into the NAVSWC Aeroprediction Code*, NSWCDD/TR-93/29, Apr 1993.

22. Anderson, J. D., *Hypersonic and High Temperature Gasdynamics*, McGraw-Hill Book Company, 1989.

23. Beckwith, I. E. and Gallagher, J. J., *Local Heat Transfer and Recovery Temperatures on a Yawed Cylinder at Mach Numbers of 4.15 and High Reynolds Numbers*, NASA TR R-104, 1961.

24. Eckert, E. R. G., *Survey of Boundary Layer Heat Transfer at High Velocities and High Temperatures*, WADC Technical Report 59-624, Apr 1960.

REFERENCES (Continued)

25. Chadwick, W. R., External Loads Using Nonlinear Lifting Surface Theory, *Journal of Aircraft*, Vol. 11, No. 3, Mar 1974, pp. 181-188.

26. Ashley, H. and Landahl, M., *Aerodynamics of Wings and Bodies,* Addison-Wesley Publishing Company, Inc., Reading, MA, 1965, Chapter 7.

27. Moore, F. G., *Aerodynamics of Guided and Unguided Weapons: Part I - Theory and Application*, NSWCDD, Dahlgren, VA, NWL TR-3018, Dec 1973.

28. Moore, F. G. and Swanson, R. C., *Aerodynamics of Tactical Weapons to Mach Number 3 and Angle of Attack 15 Degrees: Part I - Theory and Application*, NSWCDD, Dahlgren, VA, NSWCDL TR-3584, Feb 1977.

29. Douglas Aircraft Co. Inc., USAF Stability and Control DATCOM, Revisions by Wright Patterson Air Force Base, Jul 1963, 2 Vols.

30. Pitts, W. C.; Nielsen, J. N.; and Kaatari, G. E., *Lift and Center of Pressure of Wing-Body-Tail Combinations at Subsonic, Transonic, and Supersonic Speeds*, NACA TR 1307, 1957.

31. Wardlaw, A. B. and Davis, S., *A Second-Order-Gudonov Method for Supersonic Tactical Missiles*, NSWC TR 86-506, 1986.

32. Walters, R. W.; Slack, D. C.; Cimmella, P.; Applebaum, M. P., and Frost, C., "A Users Guide to GASP," Virginia Polytechnic Institute and State University, Department of Aerospace and Ocean Engineering, Blacksburg, VA, Nov 1990.

33. Moore, F. G. and Hymer, T., *An Improved Method for Predicting Axial Force at High Angle of Attack*, NSWCDD/TR-96/240, Feb 1997.

34. Hemsch, M. J. and Nielsen, J. N., "Equivalent Angle-of-Attack Method for Estimating Nonlinear Aerodynamics of Missile Fins," *Journal of Spacecraft and Rockets (JSR)*, Vol. 20, No. 4, Jul-Aug 1983.

35. Hemsch, M. J. and Nielsen, J. N., "Extensions of Equivalent Angle-of-Attack Method for Nonlinear Flowfields," *JSR*, Vol. 22, No. 3, May-Jun 1985.

36. Stoy, S. L. and Vukelich, S. R., "Extension of Equivalent Angle of Attack Prediction Method," Paper no. 84-0311, AIAA Aerospace Sciences Meeting, 9-12 Jan 1984, Reno, NV.

37. Moore, F. G.; Hymer, T.; and Devan, L., *New Methods for Predicting Nonlinear Lift, Center of Pressure, and Pitching Moment on Missile Configuration*, NSWCDD/TR-92/217, Jul 1992.

REFERENCES (Continued)

38. NASA Langley Research Center Tri-Service Missile Data Base, transmitted from NASA/LRC Jerry M. Allen to NSWCDD, 5 Nov 1991 (formal documentation of data base in process).

39. Stallings, R. L., Jr. and Lamb, M., *Wing-Alone Aerodynamic Characteristics for High Angles of Attack at Supersonic Speeds*, NASA Technical Paper 1989, Jul 1981.

40. Baker, W. B., Jr., *Static Aerodynamic Characteristics of a Series of Generalized Slender Bodies With and Without Fins at Mach Numbers from 0.6 to 3.0 and Angles of Attack from 0 to 180 °*, AEDC-TR-75-124, Vols. I and II, May 1976, Tullahoma, TN.

41. Nielsen, J. N., *Missile Aerodynamics*, NEAR Inc., Mountain View, CA, 1988.

42. Allen, J. H. and Perkins, E. W., *Characteristics of Flow Over Inclined Bodies of Revolution*, NACA RMA 50L07, Mar 1951.

43. Nielsen, J. N.; Hemsch, M. J.; and Smith, C. A., *A Preliminary Method for Calculating the Aerodynamic Characteristics of Cruciform Missiles to High Angles of Attack Including Effects of Roll Angle and Control Deflections*, ONR-CR215-226-4F, 800 N. Quincy St., Arlington, VA 22217.

44. Moore, F. G. and McInville, R. M., *A New Method for Calculating Wing Alone Aerodynamics to Angle of Attack 180 °*, NSWCDD/TR-94/3, Mar 1994.

45. Jorgensen, L. H., *A Method for Estimating Static Aerodynamic Characteristics for Slender Bodies and Circular and Noncircular Cross Section Alone and with Lifting Surfaces at Angles of Attack from 0 ° to 90 °*, NASA TN D-7228, 1973.

46. Nelson, H. F., "Wing-Body Interference Lift for Supersonic Missiles with Elliptical Cross-Section Fuselages," *JSR* Vol. 26, No. 5, Sep-Oct 1989, pp. 322-329.

47. Est, B. E. and Nelson, H. F., "Wing-Body Carryover and Fin Center of Pressure for Missiles with Noncircular Fuselage Cross Sections," AIAA 91-2856, Atmospheric Flight Mechanics Conference, New Orleans, LA, Aug 1991.

48. Shereda, D. E.; Amidon, P. F.; Dahlem, III, V.; and Brown-Edwards, E., *Pressure Test of Three Elliptical Missile Body Configurations at Mach Numbers 1.5 to 5.0*, Wright-Patterson AFB, OH, AFWAL TM 84-236-FIMG, Dec 1984.

49. Jorgensen, L. H., *Prediction of Static Aerodynamic Characteristics for Slender Bodies Alone and with Lifting Surfaces to Very High Angles of Attack*, NASA TR R-474, Sep 1977.

REFERENCES (Continued)

50. Jorgensen, L. H., *Inclined Bodies of Various Cross Sections at Supersonic Speeds*, NASA Memo 10-3-58A, 1958.

51. Polhamus, E. C.; Geller, B. W.; and Greenwald, K. J., *Pressure and Force Characteristics of Noncircular Cylinders as Affected by Reynolds Number with a Method Included for Determining the Potential Flow About Arbitrary Shapes*, NASA TR R-46, 1959.

52. Zollars, G. J.; Yechout, T. R.; Daniel, D. C.; and Lijewski, L. E., *Experimental Aerodynamic Characteristics of Missiles with Square Cross Sections*, USAFA-TN-83-8, U.S. Air Force Academy, Colorado Springs, CO, May 1983.

53. Smith, E. H.; Hebbar, S. K.; and Platzer, M., "Aerodynamic Characteristics of a Canard Controlled Missile at High Angles of Attack," AIAA paper No. 93-0763, 31st Aerospace Sciences Meeting, Reno, NV 11-14 Jun 1993.

54. Vukelich, S. R. and Jenkins, J. E., "Missile DATCOM: Aerodynamic Prediction on Conventional Missiles Using Component Build-Up Techniques," AIAA paper 84-0388, Reno, NV, 1984.

55. Spearman, L. M., *Aerodynamic Characteristics in Pitch of a Series of Cruciform-Wing Missiles with Canard Controls at a Mach Number of 2.01*, NASA TN D839, May 1961.

56. Blair, A. B., Jr.; Allen, J. M.; and Hernandez, G., *Effect of Tail-Fin Span on Stability and Control Characteristics of a Canard Controlled Missile at Supersonic Mach Numbers*, NASA TP 2157, Jun 1983.

57. Lesieutre, D. J.; Love, J. F.; and Dillenius, M. F., *M3HAX Aerodynamic Analysis for Finned Vehicles with Axisymmetric Bodies*, NEAR TR 493-D, Feb 1996 (NEAR, Inc., 526 Clyde Ave., Mountain View, CA 94043-2212).

58. Howard, R. M. and Dunn, A., "Missile Loads at High Angles of Attack," Engineering Note in *Journal of Spacecraft and Rockets*, Vol. 28, No. 1, Jan-Feb 1991.

59. Dietz, W. E., Jr., and Altstatt, M. C., "Experimental Investigation of Support Interference on an Ogive Cylinder at High Incidence," *Journal of Spacecraft and Rockets*, Vol. 16, No. 2, Mar-Apr 1979.

60. Canning, T. N. and Nielsen, J. N., "Experimental Study of the Influence of Supports on the Aerodynamic Loads on a Ogive Cylinder at High Angles of Attack," AIAA paper 81-0007. 19th Aerospace Sciences Meeting, St. Louis, MO, 12-15 Jan 1981.

REFERENCES (Continued)

61.   Monta, W. J., *Supersonic Aerodynamic Characteristics of a Sparrow III Type Missile Model with Wing Controls and Comparison with Existing Tail-Control Results*, NASA TP 1078, Nov 1977.

62.   Robinson, R. B., *Wind Tunnel Investigation at a Mach Number of 2.01 of the Aerodynamic Characteristics in Combined Angles of Attack and Sideslip of Several Hypersonic Missile Configurations with Various Canard Controls*, NACA RM L58A21, Mar 1958.

63.   Gudmundson, S. E., and Torngren, L., *Supersonic and Transonic Wind Tunnel Tests on Slender Ogive-Cylinder Body Single and in Combination with Cruciform Wings and Tails of Different Sizes*, Technical Note FFA AU-772, Apr 1972 (The Aeronautical Research Institute of Sweden, Aeronautics Department, Stockholm, Sweden).

64.   Graves, E. B. and Fournier, R. H., *Stability and Control Characteristics at Mach Numbers from 0.2 to 4.63 of a Cruciform Air-to-Air Missile with Triangular Canard Controls and a Trapezoidal Wing*, NASA TMX 3070, Nov 1974.

65.   Guidos, B. J., "Navier-Stokes Computations of Finned Kinetic Energy Projectile Base Flow," *Journal of Spacecraft Rockets*, Vol. 34, No. 4, Jul-Aug 1997.

66.   Guidos, B. J., "Static Aerodynamics CFD Analysis for 120 MM Hypersonic KE Projectile Design," ARL-MR-84, Sep 1984 (U.S. Army Research Laboratory, Aberdeen Proving Ground, MD 21005-5066).

67.   Gillum, M. J. and Lewis, M. J., "Analysis of Experimental Results on a Mach 14 Waverider with Blunt Leading Edges," AIAA 96-0812, 34th Aerospace Sciences Meeting and Exhibit, Reno, NV, 1996.

9.0 SYMBOLS AND DEFINITIONS

AOA   Angle of Attack

APC   Aeroprediction Code

AP95, AP98   1995 and 1998 versions of the APC respectively

AR   Aspect Ratio = b^2/A_w

DOF   Degrees of freedom

LT   Linear Theory

MNT   Modified Newtonian Theory

NASA/LRC   National Aeronautics and Space Administration/Langley Research Center

NSWCDD   Naval Surface Warfare Center, Dahlgren Division

SB, SBT   Slender Body, Slender-body Theory

A_{eq} Cross-sectional area of circular cylinder equal to that of body with noncircurlar cross section

A_P Planform area of the body in the crossflow plane (ft^2)

A_{REF} Reference area (maximum cross-sectional area of body, if a body is present, or planform area of wing, if wing along)(ft^2)

A_w Planform area of wing in crossflow plane (ft^2)

a,b   Semimajor and semiminor axis, respectively, of ellipse

a' Body shape parameter (see Reference 34)

b   Wing span (not including body)(ft)

C_A Axial force coefficient

$C_{A_B}, C_{A_F}, C_{A_W}$	Base, skin-friction, and wave components, respectively, of axial force coefficient
C_{A_O}	Axial force coefficient at 0 deg AOA
C_{A_α}	Axial force coefficient term due to AOA
C_{A_δ}	Axial force coefficient term due to control deflection
C_{d_C}	Crossflow drag coefficient
C_D	Drag coefficient
Cir	Circumference of body (ft)
C_L	Lift coefficient
C_ℓ	Roll moment coefficient
C_M	Pitching moment coefficient (based on reference area and body diameter, if body present, or mean aerodynamic chord, if wing alone)
C_{M_L}	Linear component of pitching moment coefficient
$C_{M_{NL}}$	Nonlinear component of pitching moment coefficient
$(C_n/C_{n_O})_{SB}$ $(C_n/C_{n_O})_N$	Ratio of the local normal force coefficient of a body with a noncircular cross section to that with a circular cross section calculated by slender body and Newtonian theory respectively
c_n	Local normal force coefficient
C_n	Side moment coefficient
C_N	Normal force coefficient
C_{N_B}	Normal force coefficient of body alone
$C_{N_{B(V)}}$	Negative afterbody normal-force coefficient due to canard or wing-shed vortices
$C_{N_{B(W)}}, C_{N_{B(T)}}$	Normal-force coefficient on body in presence of wing or tail
C_{N_L}	Linear component of normal-force coefficient
$C_{N_{NL}}$	Nonlinear component of normal-force coefficient

$(C_{N_\alpha})_W$, $(C_{N_\alpha})_T$	Normal force coefficient slope of wing and tail respectively
$C_{N_{T(V)}}$	Negative normal-force coefficient component on tail due to wing or canard-shed vortex
C_{N_W}	Normal force coefficient of wing alone
$C_{N_{W(B)}}$, $C_{N_{F(B)}}$	Normal-force coefficient of wing or fin in presence of body
C_{N_α}	Normal-force coefficient derivative
C_P	Pressure coefficient $\left(\dfrac{p - p_\infty}{1/2 \rho_\infty V_\infty^2} \right)$
C_{P_B}	Base pressure coefficient
$(C_{P_B})_{NF,\alpha}$	Base pressure coefficient of body without fins at AOA
C_Y	Side force coefficient
c_r	Rood chord (ft)
c_t	Tip chord (ft)
cal	Caliber(s) (one body diameter)
d_B	Body diameter (ft) at base
d_{ref}	Reference body diameter (ft)
$\dfrac{dK_{W(B)}}{d\alpha}$, $\dfrac{dK_{B(W)}}{d\alpha}$	Rate at which $K_{W(B)}$ or $K_{B(W)}$ decreases
deg	Degree(s)
F, C_1, C_2, C_3	Dimensionless empirical factors used in nonlinear models of $k_{W(B)}$ and $C_{N_{T(V)}}$ to approximate effects due to high AOA or control deflection
f, h	Lateral and vertical position of wing vortex
f_W, f_T	Lateral location of wing or tail vortex (measured in feet from body center line)
i	Tail interference factor
k, k_1	Parameters used to define corner radius for squares and triangles ($k = r_n/W_M$; $k_1 = r_n/W$)

$K_{B(W)}$, $K_{B(T)}$	Ratio of additional body normal-force coefficient in presence of wing, or tail to wing, or tail alone normal-force coefficient at $\delta = 0$ deg
$k_{B(W)}$, $k_{B(T)}$	Ratio of additional body normal-force coefficient due to presence of wing or tail at a control deflection to that of wing or tail alone at $\alpha = 0$ deg
$[K_{B(W)}]_{MIN}$	Minimum value of $K_{B(W)}$ as percent of slender-body theory value
$K_{W(B)}$, $K_{T(B)}$	Ratio of normal-force coefficient of wing or tail in presence of body to that of wing or tail alone at $\delta = 0$ deg
$k_{W(B)}$, $k_{T(B)}$	Ratio of wing or tail normal-force coefficient in presence of body due to a control deflection to that of wing or tail alone at $\alpha = 0$ deg
ΔK	Nonlinear component of wing-body or body-wing interference
$[\Delta K_{W(B)}]_{\alpha=0}$ and $[\Delta K_{B(W)}]_{\alpha=0}$	Amount that the experimental values of $K_{W(B)}$ and $K_{B(W)}$ exceed slender body theory at $\alpha = 0$ deg
ℓ_{ref}	Reference length (ft)
m	Cotangent of leading edge sweep angle
M_N	Mach number normal to body $= M_\infty \sin \alpha$
M_{N_C}	Normal Mach number where flow transitions from subcritical to supercritical conditions
M_{N_o}	Value of normal Mach number to body used in Newtonian correction factor calculation
M_∞	Freestream Mach number
NF	Newtonian correction factor
NF_0	Newtonian correction factor for crossflow Mach number of zero on squares and triangles
NF_1	Newtonian correction factor for an ellipse at $\alpha \geq 20$ deg
p	Pressure (lb/ft^2)
P_ℓ, P_W	Loading factors in leeward and windward planes respectively
r	Local body radius (ft)

r_{eq}, d_{eq}	Radius and diameter, respectively, of a circular cross-section body which has same cross-sectional area as that of noncircular cross-section body
r_n	Corner radius of a rounded corner on square or triangle
R_{N_C}	Reynolds number where flow transitions from subcritical to supercritical conditions
R_{N_D}	Reynolds number based on body diameter
$R_{N_{eff}}$	An effective Reynolds number above which the flow transitions from subcritical to supercritical conditions
r_W, r_T	Radius of body at wing or tail locations
s	Wing or tail semispan plus the body radius in wing-body lift methodology
SBTSF	Slender body theory scaling factor
V_∞	Freestream velocity
V_N	Velocity normal to body
W	Length of one side of a triangle or square
W_m	Maximum diameter of a triangle or square as measured normal to the velocity vector
X_{CP}	Center of pressure (in feet or calibers from some reference point that can be specified) in x direction
$(X_{CP})_L, (X_{CP})_{NL}$	Center of pressure of linear and nonlinear terms of normal force
x,y,z	Axis system fixed with x along centerline of body
α	Angle of attack (deg)
α_C	Angle of attack where wing-body interference factor starts decreasing (deg)
α_D	Angle of attack where the wing-body interference factor reaches a minimum (deg)
α_M	Angle of attack where $K_{W(B)}$ reaches a constant value

α_W, α_T	Local angle of attack of wing or tail ($\alpha_W + \delta$ or $\alpha_T + \delta$, respectively, in degrees)
α_1, α_2	Angles of attack used in nonlinear model for $K_{B(W)}$
β	$\sqrt{M^2 - 1}$
δ	Control deflection (deg), positive leading edge up
δ_{eq}	Angle between velocity vector and tangent to body surface
δ_W, δ_T	Deflection of wing or tail surfaces (deg), positive leading edge up
η	Parameter used in viscous crossflow theory for nonlinear body normal force (in this context, it is the normal force of a circular cylinder of given length-to-diameter ratio to that of a cylinder of infinite length)
η_1	Decay constant used in second-order-shock-expansion theory
Γ	Vortex circulation, positive counterclockwise facing upstream (ft^2/sec)
Φ	Roll position of missile fins ($\Phi = 0$ deg corresponds to fins in the plus (+) orientation). $\Phi = 45$ deg corresponds to fins rolled to the cross ($\times$) orientation
λ	Taper ratio of a lifting surface $= c_t/c_r$
ϕ	Roll position of point on body with $\phi = 0$ deg being the leeward plane
θ	Local surface slope of body with respect to body axis
∞	Freestream conditions

DISTRIBUTION

	Copies		Copies
DOD ACTIVITIES (CONUS)		ATTN C KLEIN	1
		TECHNICAL LIBRARY	1
ATTN CODE 35 (ZIMET)	1	COMMANDER	
CODE 351 (SIEGEL)	1	NAVAL AIR WARFARE CENTER	
CODE 351 (CHU)	1	WEAPONS DIVISION	
CODE 332FD (LEKOUDIS)	1	521 9TH ST	
CHIEF OF NAVAL RESEARCH		POINT MUGU CA 93042-5001	
BALLSTON CENTRE TOWER ONE			
800 NORTH QUINCY ST		ATTN T C TAI	1
ARLINGTON VA 22217-5660		M J MALIA	1
		TECHNICAL LIBRARY	1
ATTN CODE 474T6OD (LOFTUS)	1	COMMANDER	
CODE 4732HOD (SMITH)	1	NSWC	
CODE 4732HOD (LAMBERT)	1	CARDEROCK DIVISION	
CODE 473COOD (PORTER)	1	WASHINGTON DC 20034	
CODE 47311OD (HOUSH)	1		
CODE 47311OD (GLEASON)	1	ATTN R M HOWARD	1
CODE 47311OD (VAN DYKEN)	1	TECHNICAL LIBRARY	1
CODE 47312OD (MACDONALD)	1	SUPERINTENDENT	
CODE 4722EOD (JETER)	1	NAVAL POSTGRADUATE SCHOOL	
TECHNICAL LIBRARY	1	1 UNIVERSITY CIRCLE	
COMMANDER		MONTEREY CA 93943-5001	
NAVAL AIR WARFARE CENTER			
WEAPONS DIVISION		ATTN HEAD WEAPONS DEPT	1
1 ADMINISTRATION CIRCLE		HEAD SCIENCE DEPT	1
CHINA LAKE CA 93555-6001		SUPERINTENDENT	
		UNITED STATES NAVAL ACADEMY	
ATTN TECHNICAL LIBRARY	1	121 BLAKE RD	
G RUDACILLE PMS 38012 7	1	ANNAPOLIS MD 21402-5000	
COMMANDER			
NAVAL SEA SYSTEMS COMMAND		ATTN DIAG DT 4T (PAUL MURAD)	2
2531 JEFFERSON DAVIS HWY		DIRECTOR	
ARLINGTON VA 22242-5160		DEFENSE INTELLIGENCE AGENCY	
		WASHINGTON DC 20301	
ATTN TECHNICAL LIBRARY	1		
COMMANDER		ATTN BRENT WAGGONER	1
NAVAL AIR SYSTEMS COMMAND		CODE 4072 BLDG 2540	
47122 LILJENCRANTZ ROAD UNIT 7		NAVAL WEAPONS SUPPORT CENTER	
PATUXENT RIVER MD 20670-5440		CRANE IN 47522-5000	

DISTRIBUTION (Continued)

	Copies
ATTN CODE 5252P (KRAUSE)	1
TECHNICAL LIBRARY	1

COMMANDER
INDIAN HEAD DIVISION
NAVAL SURFACE WARFARE CENTER
101 STRAUSS AVE
INDIAN HEAD MD 20640-5035

	Copies
ATTN TECHNICAL LIBRARY	1

COMMANDING GENERAL
MARINE CORPS COMBAT
DEVELOPMENT COMMAND
2048 SOUTH ST
QUANTICO VA 22134-5129

	Copies
ATTN E SEARS	1
L E LIJEWSKI	1
C COTTRELL	1
TECHNICAL LIBRARY	1
AFATL (ADLRA) (DLGC)	1

EGLIN AFB FL 32542-5000

	Copies
ATTN TECHNICAL LIBRARY	1

USAF ACADEMY
COLORADO SPRINGS CO 80912

	Copies
ATTN TECHNICAL LIBRARY	1

ADVANCED RESEARCH PROJECTS
   AGENCY
DEPARTMENT OF DEFENSE
WASHINGTON DC 20305

	Copies
ATTN B BLAKE (BLD 146)	1
J JENKINS (BLD 146)	1
TECHNICAL LIBRARY	1

COMMANDING OFFICER
AFSC
2210 8TH STREET
WRIGHT PATTERSON AFB OH 45433

	Copies
ATTN EDWARD JENKINS	1

NAIC TANW
HQ NAIC TANW
4115 HEBBLE CREEK ROAD SUITE 28
WPAFB OH 45433-5623

	Copies
ATTN J USSELTON	1
W B BAKER JR	1
TECHNICAL LIBRARY	1

ARNOLD ENGINEERING DEVELOPMENT
   CENTER USAF
TULLAHOMA TN 37389

	Copies
ATTN H HUDGINS	1
G FRIEDMAN	1
TECHNICAL LIBRARY	1

COMMANDING GENERAL
ARRADCOM PICATINNY ARSENAL
DOVER NJ 07801

	Copies
ATTN C H MURPHY	1
R PUHALLA JR	1
W STUREK	1
C NIETUBICZ	1
A MIKHAIL	1
P PLOSTINS	1
TECHNICAL LIBRARY	1

COMMANDING GENERAL
BALLISTIC RESEARCH LABORATORY
ABERDEEN PROVING GROUND
ABERDEEN MD 21005-5066

	Copies
ATTN CODE TNC (BLACKLEDGE)	1
RICH MATLOCK	1

DIRECTOR
INTERCEPTOR TECHNOLOGY
BALLISTIC MISSILE DEFENSE OFFICE
THE PENTAGON
WASHINGTON DC 20350

	Copies
ATTN SFAE SD ASP	1
SFAE SD HED	1

DEPUTY COMMANDER
US ARMY STRATEGIC DEFENSE COMMAND
P O BOX 1500
HUNTSVILLE AL 35807-3801

	Copies
ATTN D WASHINGTON	1
W WALKER	1
R KRETZSCHMAR	1
D FERGUSON JR	1

COMMAND GENERAL
US ARMY MISSILE COMMAND
AMSMI RD SS AT
REDSTONE ARSENAL AL 35898-5252

DISTRIBUTION (Continued)

<u>Copies</u>   <u>Copies</u>

DEFENSE TECHNICAL INFORMATION
   CENTER
8725 JOHN J KINGMAN ROAD
SUITE 0944
FORT BELVOIR VA 22060-6218   2

DIRECTOR
DEFENSE PRINTING SERVICE
BLDG 176 WASHINGTON NAVY YARD
901 M ST E
WASHINGTON DC 20374-5087   1

ATTN   CODE A76
       TECHNICAL LIBRARY   1
COMMANDING OFFICER
CSSDD NSWC
6703 W HIGHWAY 98
PANAMA CITY FL 32407-7001

ATTN   DR P WEINACHT   1
AERODYNAMICS BRANCH
PROPULSION AND FLIGHT DIV WTD
AMSRL WT PB
US ARMY RESEARCH LAB ABERDEEN
PROVING GROUND MD 21005-5066

ATTN   GREGG ABATE   1
US AIR FORCE
WRIGHT LABORATORY
WL MNAA
101 W EGLIN BLVD STE 219
EGLIN AFB FL 32542

ATTN   JOHN GRAU   1
US ARMY ARDEC
COMMANDER US ARMY ARDEC
AMSTA AR AET A BLDG 3342
PICATINNY ARSENAL NJ 07806-5000

ATTN   FRANK MACDONALD   1
NAWC CHINA LAKE
COMMANDER
CODE 473 20D
NAVAIRWARCENNSDNDIV
CHINA LAKE CA 93555

ATTN   MARK LAMBERT   1
NAWC
CODE 4732HOD
CHINA LAKE CA 93555

ATTN   MICHAEL MUSACHIO   1
DIRECTOR
OFFICE OF NAVAL INTELLIGENCE
4251 SUITLAND ROAD (ONI 2321)
WASHINGTON DC 20395

ATTN   DR ALAN NICHOLSON MSC 5B   1
DEFENSE INTELLIGENCE AGENCY
MISSILE AND SPACE INTELLIGENCE CTR
REDSTONE ARSENAL AL 35898-5500

ATTN   EDWARD HERBERT   1
US ARMY MISSILE COMMAND
AMSMI RD MG GA
BLDG 5400 ROOM 250
REDSTONE ARSENAL AL 35898

ATTN   PAUL KOLODZIEJ   1
NASA AMES RESEARCH CENTER
MS 234 1
MOFFETT FIELD CA 94035

ATTN   LCDR T HARTLINE USNR R   1
NR ONI 2109 NAVAL RESERVE UNIT
112 CRESTVIEW CIRCLE
MADISON AL 35758

ATTN   CODE 4732HOD DAVID HALL   1
PROPULSION PERFORMANCE OFFICE
NAVAL AIR WARFARE CTR WEAPONS DIV
1 ADMINISTRATIVE CIR
CHINA LAKE CA 93555-6001

ATTN   DONALD SHEREDA   1
WL FIMA BLDG 450
2645 FIFTH ST STE 30
WRIGHT PATTERSON AFB OH 45433-7936

ATTN   ROBERT VAN DYKEN 473110D   1
COMMANDER
NAWC
CHINA LAKE CA 93555

DISTRIBUTION (Continued)

	Copies		Copies

ATTN   RICK JONES
BMDO AQS
1725 JEFFERSON DAVIS HWY STE 809
ARLINGTON VA 22202
	1	ATTN D G MILLER (L 219)
		          TECHNICAL LIBRARY
		LAWRENCE LIVERMORE NATIONAL
		   LABORATORY
		EARTH SCIENCES DIVISION
			1
			1

ATTN   JEFFREY RANDORF   1
US ARMY SPACE AND STRATEGIC
    DEFENSE COMMAND
P O BOX 1500 CSSD-BC-SS
106 WYNN DRIVE
HUNTSVILLE AL 35807-3801

UNIVERSITY OF CALIFORNIA
P O BOX 808
LIVERMORE CA 94551

NON-DOD ACTIVITIES (CONUS)

ATTN   W RUTLEDGE (1635)   1
          R LAFARGE   1
          R EISLER   1
          TECHNICAL LIBRARY   1
SANDIA NATIONAL LABORATORY
P O BOX 5800
ALBUQUERQUE NM 87185-5800

ATTN   NEIL WALKER   1
NICHOLS RESEARCH CORPORATION
MS 912
P O BOX 400002
4040 S MEMORIAL PKWY
HUNTSVILLE AL 35815-1502

ATTN   WALT GUTIERREZ   1
SANDIA NATIONAL LABORATORIES
MAIL STOP 0825
P O BOX 5800
ALBUQUERQUE NM 87185-0825

THE CNA CORPORATION
P O BOX 16268
ALEXANDRIA VA 22302-0268   1

ATTN   ASSISTANT DEFENSE
          COOPERATION ATTACHE   1
EMBASSY OF SPAIN
WASHINGTON DC 20016

GIDEP OPERATIONS OFFICE
CORONA CA 91720   1

ATTN   TECHNICAL LIBRARY   1
NASA AMES RESEARCH CENTER
MOFFETT CA 94035-1099

DE/AVT
DEFENSE EQUIPMENT STAFF
BRITISH EMBASSY
3100 MASSACHUSETTS AVE NW
WASHINGTON DC 20008-3688   1

ATTN   C SCOTT   1
          D CURRY   1
NASA JOHNSON SPACE CENTER
HOUSTON TX 77058

ATTN   ASO LO IS   1
ISRAEL AIR FORCE
LIAISON OFFICER
700 ROBBINS AVE
PHILADELPHIA PA 19111

ATTN   TECHNICAL LIBRARY   1
NASA
WASHINGTON DC 20546

ATTN   W C SAWYER   1
          B HENDERSON   1
          D MILLER   1
          J ALLEN   1
          F WILCOX   1
          TECHNICAL LIBRARY   2
NASA LANGLEY RESEARCH CENTER
HAMPTON VA 23365

ATTN   GERMAN MILITARY REP US OA   1
GMR TRAFFIC AND TRANSPORTATION
    DIVISION
10 SERVICES ROAD
DULLES INTERNATIONAL AP
WASHINGTON DC 20041

DISTRIBUTION (Continued)

	Copies		Copies
ATTN PROF F R DEJARNETTE	1	ATTN E LUCERO	1
NORTH CAROLINA STATE UNIVERSITY		L TISSERAND	1
DEPT OF MECHANICAL AND		D FROSTBUTTER	1
AEROSPACE ENGINEERING		L PERINI	1
BOX 7921		TECHNICAL LIBRARY	1
RALEIGH NC 27695		APPLIED PHYSICS LABORATORY	
		JOHNS HOPKINS UNIVERSITY	
ATTN PROF J A SCHETZ	1	JOHNS HOPKINS ROAD	
VIRGINIA POLYTECHNIC AND STATE		LAUREL MD 20723-6099	
UNIVERSITY			
DEPT OF AEROSPACE ENGINEERING		ATTN B BROOKS	1
BLACKSBURG VA 24060		R STANCIL	1
		R ELKINS	1
ATTN J M WU	1	LORAL VOUGHT SYSTEMS	
C BALASUBRAMAYAN	1	P O BOX 650003	
TECHNICAL LIBRARY	1	M S EM 55	
THE UNIVERSITY OF TENNESSEE		DALLAS TX 75265-0003	
SPACE INSTITUTE			
TULLAHOMA TN 37388		ATTN PROF J D ANDERSON	1
		DEPT OF AEROSPACE ENGINEERING	
ATTN R NELSON	1	UNIVERSITY OF MARYLAND	
TECHNICAL LIBRARY	1	COLLEGE PARK MD 20742	
UNIVERSITY OF NOTRE DAME			
DEPT OF AEROSPACE AND		ATTN TECHNICAL LIBRARY	1
MECHANICAL ENGINEERING		HUGHES MISSILE SYSTEMS COMPANY	
BOX 537		P O BOX 11337 BLDG 802 MS A1	
NOTRE DAME IN 46556		OLD NOGALES HWY	
		TUCSON AZ 83734-1337	
ATTN PROF F NELSON	1		
DEPT OF MECH AND AERO ENG		ATTN M DILLENIUS	1
UNIVERSITY OF MISSOURI ROLLA		NIELSEN ENGINEERING AND	
ROLLA MO 65401		RESEARCH INC	
		526 CLYDE AVE	
ATTN DR DONALD SPRING	1	MOUNTAIN VIEW CA 95043	
AEROSPACE ENGINEERING DEPT			
AUBURN UNIVERSITY AL 36849-5338		ATTN J XERIKOS	1
		N CAMPBELL	1
ATTN ROBERT ENGLAR	1	TECHNICAL LIBRARY	1
GEORGIA TECH RESEARCH INSTITUTE		MCDONNEL DOUGLAS	
AEROSPACE SCIENCE AND		ASTRONAUTICS CO (WEST)	
TECHNOLOGY LAB		5301 BOLSA AVE	
ATLANTA GA 30332		HUNTINGTON BEACH CA 92647	

DISTRIBUTION (Continued)

	Copies		Copies
ATTN J WILLIAMS	1	ATTN DR G S SCHMIDT	1
S VUKELICH	1	LORAL DEFENSE SYSTEMS	
J FIVEL	1	1210 MASSILLON ROAD	
R GERBSCH (CODE 1111041)	1	AKRON OH 44315-0001	
TECHNICAL LIBRARY	1		
MCDONNELL DOUGLAS		ATTN W NORDGREN 721	1
ASTRONAUTICS CO (EAST)		GOULD INC OSD	
BOX 516		18901 EUCLID AVE	
ST LOUIS MO 63166-0516		CLEVELAND OH 44117	

ATTN   TECHNICAL LIBRARY 1
UNITED TECHNOLOGIES
NORDEN SYSTEMS
NORWALK CT 06856

ATTN   TECH LIBRARY 1
AEROJET ELECTRONIC SYSTEMS
P O BOX 296 III
AZUSA CA 91702

ATTN   T LUNDY 1
D ANDREWS 1
TECHNICAL LIBRARY 1
LOCKHEED MISSILES AND SPACE CO INC
P O BOX 1103
HUNTSVILLE AL 35807

ATTN   P REDING 1
G CHRUSCIEL 1
TECHNICAL LIBRARY 1
LOCKHEED MISSILES AND SPACE CO INC
P O BOX 3504
SUNNYVALE CA 94088

ATTN   W CHRISTENSON 1
D WARNER 1
ALLIANT TECHSYSTEMS INC
600 SECOND ST NE
HOPKINS MN 55343

ATTN   K C LEE 1
AEROTHERM CORP
580 CLYDE AVE
MOUNTAIN VIEW CA 94043

ATTN   TECHNICAL LIBRARY 1
B SALEMI 1
J BOUDREAU 1
RAYTHEON COMPANY
MISSILE SYSTEMS DIVISION
P O BOX 1201
TEWKSBURY MA 01876-0901

ATTN   TECH LIBRARY 1
FMC NAVAL SYSTEMS DIV
4800 E RIVER ROAD
MINNEAPOLIS MN 55421-1402

ATTN   DORIA GLADSTONE 1
BATTELLE MEMORIAL INSTITUTE
COLUMBUS DIVISION
505 KING AVE
COLUMBUS OH 43201-2693

ATTN   LLOYD PRATT 1
AEROJET TACTICAL SYSTEMS CO
P O BOX 13400
SACRAMENTO CA 95813

ATTN   JAMES SORENSON 1
VINCENT ALLEN 1
ORBITAL SCIENCES
3380 SOUTH PRICE ROAD
CHANDLER AZ 85248

ATTN   JOSEPH ANDRZEJEWSKI 1
MEVATEC CORP
1525 PERIMETER PARKWAY
SUITE 500
HUNTSVILLE AL 35806

ATTN   J FORKOIS 1
KAMAN SCIENCES CORP
1500 GARDEN OF THE GODS ROAD
P O BOX 7463
COLORADO SPRINGS CO 80933

DISTRIBUTION (Continued)

	Copies		Copies

ATTN   RON EFROMSON   1
MIT LINCOLN LABORATORY
244 WOOD STREET
LEXINGTON MA 02173-0073

ATTN   D J GIESE   1
MAIL STOP 4C 61
BOEING DEFENSE AND SPACE GROUP
P O BOX 3999
SEATTLE WA 98124-2499

ATTN   BRIAN WALKUP   1
HERCULES AEROSPACE PRODUCT CO
ALLEGHANY BALLISTIC LAB
ROCKET CENTER WV 26726

ATTN   DR T LIN   1
TRW ELECTRONICS AND DEFENSE SECTOR
BLDG 527/RM 706
P O BOX 1310
SAN BERNADINO CA 92402

ATTN   G VINCENT   1
SPARTA INC
4901 CORPORATE DR
HUNTSVILLE AL 35805

ATTN   D P FORSMO   1
      TECHNICAL LIBRARY   1
RAYTHEON COMPANY
MISSILE SYSTEMS DIVISION
HARTWELL RD
BEDFORD MA 01730-2498

ATTN   M S MILLER   1
DYNETICS INC
P O DRAWER B
HUNTSVILLE AL 35814-5050

ATTN   H A MCELROY   1
GENERAL DEFENSE CORP
P O BOX 127
RED LION PA 17356

ATTN   ENGINEERING LIBRARY   1
ARMAMENT SYSTEMS DEPT
GENERAL ELECTRIC CO
BURLINGTON VT 05401

ATTN   TECHNICAL LIBRARY   1
OAYNE AERONAUTICAL
2701 HARBOR DRIVE
SAN DIEGO CA 92138

ATTN   BRIAN EST   1
BOEING ST LOUIS
P O BOX 516
ST LOUIS MO 63166-0516

ATTN   WILLIAM FACINELLI   1
ALLIED SIGNAL
P O BOX 22200
MS 1207 3B
TEMPE AZ 85285

ATTN   DR T P SHIVANANDA   1
      TRW BMD
P O BOX 1310
SAN BERNADINO CA 92402-1313

ATTN   T R PEPITONE   1
AEROSPACE TECHNOLOGY INC
P O BOX 1809
DAHLGREN VA 22448

ATTN   ERIC MOORE   1
      MAIL STOP MER 24 1281
LOCKHEED SANDERS
P O BOX 868
NASHUA NH 03061

ATTN   DR BRIAN LANDRUM   1
      RI BLDG E33
PROPULSION RESEARCH CENTER
UNIVERSITY OF ALABAMA
HUNTSVILLE AL 35899

ATTN   BRUCE NORTON   1
      MAIL STOP BL 1
RAYTHEON
100 VANCE TANK RD
BRISTOL TN 37620

ATTN   JIM ROBERTSON   1
RESEARCH SOUTH INC
555 SPARKMAN DRIVE
SUITE 818
HUNTSVILLE AL 35816-3423

DISTRIBUTION (Continued)

	Copies		Copies

ATTN   BOB WHYTE   1
ARROW TECH ASSOCIATES INC
1233 SHELBURNE ROAD D8
SO BURLINGTON VT 05403

ATTN   JUAN AMENABAR   1
SAIC
4001 NORTH FAIRFAX DRIVE STE 800
ARLINGTON VA 22209

ATTN   TECHNICAL LIBRARY   1
TELEDYNE RYAN AERONAUTICAL
2701 HARBOR DRIVE
SAN DIEGO CA 92138

ATTN   DR KIRIT PATEL   1
SVERDRUP TECHNOLOGY INC
TEAS GROUP
BLDG 260 P O BOX 1935
EGLIN AFB FL 32542

ATTN   FRANK LANGHAM   1
MICRO CRAFT TECHNOLOGY
740 4TH ST
MS 6001
ARNOLD AFB TN 37389

ATTN   LAURA AYERS   1
DELTA RESEARCH INC
315 WYNN DRIVE
SUITE 1
HUNTSVILLE AL 35805

ATTN   BRIAN BENNETT   1
MCDONNELL DOUGLAS
MC 064 2905
P O BOX 516
ST LOUIS MO 63166-0516

ATTN   THOMAS FARISS   1
LOCKHEED SANDERS
P O BOX 868
MER24 1206
NASHUA NH 03061-0868

ATTN   COREY FROST   1
LOCKHEED MISSILES & SPACE CO INC
P O BOX 070017
6767 OLD MADISON PIKE SUITE 220
HUNTSVILLE AL 35807

ATTN   JEFFREY HUTH   1
KAMAN SCIENCES CORPORATION
2560 HUNTINGTON AVE
ALEXANDRIA VA 22303

ATTN   WILLIAM JOLLY   1
KAMAN SCIENCES
600 BLVD SOUTH SUITE 208
HUNTSVILLE AL 35802

ATTN   STEPHEN MALLETTE   1
KBM ENTERPRISES
15980 CHANEY THOMPSON RD
HUNTSVILLE AL 35803

ATTN   DONALD MOORE   1
NICHOLS RESEARCH CORPORATION
4040 SOUTH MEMORIAL PARKWAY
P O BOX 400002
MS 920C
HUNTSVILLE AL 35815-1502

ATTN   JAY NARAIN   1
LOCKHEED MISSILES & SPACE CO
P O BOX 3504
DEPT 81 10 BLDG 157 5E FAE 1
SUNNYVALE CA 94088-3504

ATTN   DAVID RESSLER   1
TRW BALLISTIC MISSILES DIV
MS 953 2420
P O BOX 1310
SAN BERNARDINO CA 92402

ATTN   MARK SWENSON   1
ALLIANT TECHSYSTEMS
MN11 262B
600 SECOND STREET NE
HOPKINS MN 55343

DISTRIBUTION (Continued)

<div style="text-align: right">Copies</div>

ATTN   JOHN SUN   1
NORTHROP GRUMMAN CORPORATION
750 LYNNMERE DRIVE
THOUSAND OAKS CA 91360

ATTN   HARRY AULTMAN   1
COLEMAN RESEARCH CORP
6820 MOQUIN DRIVE
HUNTSVILLE AL 35806

ATTN   SCOTT ALLEN   1
ALLEN AERO RESEARCH
431 E SUNNY HILLS RD
FULLERTON CA 92635

ATTN   DARRYL HALL   1
SAIC
997 OLD EAGLE SCHOOL RD
SUITE 215
WAYNE PA 19087-1803

ATTN   PETER ALEXANDER   1
MCDONNELL DOUGLAS AEROSPACE
689 DISCOVERY DRIVE
MS 11A1
HUNTSVILLE AL 35806

ATTN   SAMUEL HICKS III   1
TEXAS INSTRUMENTS
6600 CHASE OAKS BLVD
MS 8490
PLANO TX 75086

ATTN   BARRY LINDBLOM   1
ALLIANT DEFENSE ELECTRONICS
   SYSTEMS INC
P O BOX 4648
CLEARWATER FL 34618

ATTN   DR SHIN CHEN   1
THE AEROSPACE CORP
M4 967
P O BOX 92957
LOS ANGELES CA 90009

<div style="text-align: right">Copies</div>

ATTN   ROBERT ACEBAL   1
SAIC
1225 JOHNSON FERRY RD
SUITE 100
MARIETTA GA 30068

ATTN   EUGENE HART   1
SYSTEM PLANNING CORP
1000 WILSON BLVD
ARLINGTON VA 22209

ATTN   ELAINE POLHEMUS   1
ROCKWELL AUTONETICS & MISSILE
   SYSTEMS DIVISION
D611 DL23
1800 SATELLITE BLVD
DULUTH GA 30136

ATTN   MICHAEL GLENN   1
TASC
1992 LEWIS TURNER BLVD
FT WALTON BEACH FL 32547

ATTN   ROBERT ROGER   1
ADAPTIVE RESEARCH
4960 CORPORATE DRIVE
SUITE 100 A
HUNTSVILLE AL 35805-6229

ATTN   STEVEN MARTIN   1
SYSTEMS ENGINEERING GROUP INC
9841 BROKEN LAND PARKWAY
SUITE 214
COLUMBIA MD 21046-1120

ATTN   C W GIBKE   1
LOCKHEED MARTIN VOUGHT SYSTEMS
MS SP 72
P O BOX 650003
DALLAS TX 75265-0003

ATTN   CHRIS HUGHES   1
EDO GOVERNMENT SYSTEMS DIV
14 04 111TH ST
COLLEGE POINT NY 11356

DISTRIBUTION (Continued)

	Copies		Copies
ATTN DANIEL LESIEUTRE NIELSEN ENGINEERING & RES INC 526 CLYDE AVENUE MOUNTAIN VIEW CA 94043-2212	1	ATTN STEVE MULLINS SIMULATION AND ENGINEERING CO INC 8840 HWY 20 STE 200 N MADISON AL 35758	1
ATTN CARL HILL FRANCIS PRIOLO STANDARD MISSILE COMPANY LLC 1505 FARM CREDIT DRIVE SUITE 600 MCLEAN VA 22102	1 1	ATTN ROBERT BRAENDLEIU KAISER MARQUARDT 16555 SATICOY ST VAN NUYS CA 91406-1739	1
ATTN THOMAS LOPEZ COLEMAN RESEARCH CORP 990 EXPLORER BLVD HUNTSVILLE AL 35806	1	ATTN LAWRENCE FINK BOEING DEFENSE AND SPACE GROUP P O BOX 3999 MS 82-23 SEATTLE WA 98124	1
ATTN JENNIE FOX LOCKHEED MARTIN VOUGHT SYSTEMS P O BOX 650003 MS EM 55 DALLAS TX 75265-0003	1	ATTN ROY KLINE KLINE ENGINEERING CO INC 27 FREDON GREENDELL RD NEWTON NJ 07860-5213	1
ATTN JOHN BURKHALTER AUBURN UNIVERSITY 211 AEROSPACE ENGR BLDG AUBURN UNIVERSITY AL 36849	1	ATTN THOMAS KLAUSE TRW P O BOX 80810 ALBUQUERQUE NM 87198	1
ATTN DR MAX PLATZER NAVAL POSTGRADUATE SCHOOL DEPT OF AERONAUTICS & ASTRONAUTICS CODE AA PL MONTEREY CA 93943	1	ATTN DAN PLATUS THE AEROSPACE CORPORATION P O BOX 92957 LOS ANGELES CA 90009	1
ATTN MIKE DANGELO MIT LINCOLN LABORATORY 1745 JEFFERSON DAVIS HWY 1100 ARLINGTON VA 22202	1	ATTN DR REX CHAMBERLAIN TETRA RESEARCH CORPORATION 2610 SPICEWOOD TR HUNTSVILLE AL 35811-2604	1
ATTN RICHARD HAMMER JOHNS HOPKINS APPLIED PHYSICS LAB JOHNS HOPKINS ROAD LAUREL MD 20723-6099	1	ATTN DR DANNY LIU ZONA TECHNOLOGY INC 2651 W GUADALUPE RD SUITE B 228 MESA AZ 85202	1
ATTN MAURICE TUCKER BATTELLE HUNTSVILLE OPERATIONS 7501 S MEMORIAL PKWY STE 101 HUNTSVILLE AL 35802	1	ATTN PERRY PETERSEN NORTHROP GRUMMAN CORP DEPT 9B51 MAIL ZONE XA 8900 EAST WASHINGTON BLVD PICO RIVERA CA 90660-3783	1

DISTRIBUTION (Continued)

	Copies

	Copies
ATTN DR JAMES HAUSER AERO SPECTRA INC 2850 KENYON CIRCLE P O BOX 3006 BOULDER CO 80307	1
ATTN DARRELL AUSHERMAN TRW SPACE AND DEFENSE ONE SPACE PARK MAIL STATION R1-1062 REDONDO BEACH CA 90278-1071	1
ATTN JAY EBERSOHL ADVATECH PACIFIC INC 2015 PARK AVENUE SUITE 8 REDLANDS CA 92373	1
ATTN EDWARD RAWLINSON SY TECHNOLOGY INC 4900 UNIVERSITY SQUARE SUITE 8 HUNTSVILLE AL 35816	1
ATTN LAYNE COOK UNIVERSAL SPACE LINES 8620 WOLFF CT SUITE 110 WESTMINSTER CO 80030	1
ATTN PAUL WILDE ACTA INC 2790 SKYPARK DR SUITE 310 TORRANCE CA 90505-5345	1
ATTN DR MICHAEL HOLDEN CALSPAN UB RESEARCH CENTER P O BOX 400 BUFFALO NY 14225	1
ATTN RICHARD GRABOW SPACE VECTOR CORP 17330 BROOKHURST ST SUITE 150 FOUNTAIN VALLEY CA 92708	1
ATTN BRENT APPLEBY DRAPER LABORATORY 555 TECHNOLOGY SQ MS77 CAMBRIDGE MA 02139	1

	Copies
ATTN JAMES JONES SPARTA INC 1901 N FORT MYER DR SUITE 600 ARLINGTON VA 22209	1
ATTN SCOTT HOUSER PHOENIX INTEGRATION 1872 PRATT DRIVE SUITE 1835 BLACKSBURG VA 24060	1
ATTN S ROM MURTY TELEDYNE BROWN ENGINEERING MS 19 OPTICS 300 SPARKMAN DRIVE HUNTSVILLE AL 35807	1
ATTN STUART COULTER SVERDRUP TECHNOLOGY 670 2ND ST MS4001 ARNOLD AIR FORCE BASE TULLAHOMA TN 37389-4001	1
ATTN DR RICHARD HOWARD NAVAL POSTGRADUATE SCHOOL DEPT OF AERONAUTICS AND ASTRONAUTICS CODE AA HO NPS MONTEREY CA 93943	1
ATTN DR DONALD SPRING AUBURN UNIVERSITY 211 AEROSPACE ENGINEERING BLDG AUBURN UNIVERSITY AL 36849-5338	1
ATTN LT BAHMAN ZOHURI NAVAL ACADEMY WEAPONS SYSTEMS ENGINEERING DEPT 121 BLAKE ROAD ANNAPOLIS MD 21402-5000	1
ATTN J BRENT RUMINE MIT LINCOLN LABORATORY 244 WOOD STREET BUILDING S ROOM 52-327 LEXINGTON MA 02173-9185	1

DISTRIBUTION (Continued)

<u>Copies</u>　　　　　　　　　　　　　　　　　　　　　　　　<u>Copies</u>

NON-DOD ACTIVITIES (EX-CONUS)

ATTN   LOUIS CHAN   1
INSTITUTE FOR AEROSPACE
    RESEARCH
NATIONAL RESEARCH COUNSIL
MONTREAL RD
OTTAWA ONTARIO
CANADA K1A0R6

ATTN   H B ASLUND   1
SAAB MILITARY AIRCRAFT
581 88 LINKOEPING
SWEDEN

ATTN   A BOOTH   1
BRITISH AEROSPACE DEFENCE LTD
MILITARY AIRCRAFT DIVISION
WARTON AERODROME WARTON PRESTON
LANCASHIRE PR4 1AX
UNITED KINGDOM

ATTN   R CAYZAC   1
GIAT INDUSTRIES
7 ROUTE DE GUERCY
18023 BOURGES CEDEX
FRANCE

ATTN   MAJ F DE COCK   1
ECOLE ROYALE MILITAIRE
30 AV DE LA RENAISSANCE
1040 BRUXELLES
BELGIUM

ATTN   J EKEROOT   1
BOFORS MISSILES
691 80 KARLSKOGA
SWEDEN

ATTN   CH FRANSSON   1
NATIONAL DEFENCE RESEARCH
    ESTABLISHMENT
DEPT OF WEAPON SYSTEMS EFFECTS
    AND PROTECTION
KARLAVAGEN 106B
172 90 SUNDBYBERG
SWEDEN

ATTN   M HARPER BOURNE   1
DEFENCE RESEARCH AGENCY
Q134 BUILDING
RAE FARNBOROUGH
HAMPSHIRE QU14 6TD
UNITED KINGDOM

ATTN   A H HASSELROT   1
FFA
P O BOX 11021
161 11 BROMMA
SWEDEN

ATTN   B JONSSON   1
DEFENCE MATERIAL ADMINISTRATION
MISSILE TECHNOLOGY DIVISION
115 88 STOCKHOLM
SWEDEN

ATTN   P LEZEAUD   1
DASSAULT AVIATION
78 QUAI MARCEL DASSAULT
92214 SAINT CLOUD
FRANCE

ATTN   J LINDHOUT   1
N L R
ANTHONY FOKKERWEG 2
1059 CM AMSTERDAM
THE NETHERLANDS

ATTN   A MICKELLIDES   1
GEC MARCONI
DEFENCE SYSTEMS LTD
THE GROVE WARREN LANE
STANMORE MIDDLESEX
UNITED KINGDOM

ATTN   K MOELLER   1
BODENSEEWERK
    GERAETETECHNIK GMBH
POSTFACH 10 11 55
88641 UBERLINGEN
GERMANY

DISTRIBUTION (Continued)

Copies   Copies

ATTN   G MOSS   1
ROYAL MILITARY COLLEGE
AEROMECHANICAL SYSTEMS GROUP
SHRIVENHAM SWINDON
WILTS SN6 8LA
UNITED KINGDOM

ATTN   RIBADEAU DUMAS   1
MATRA DEFENSE
37 AV LOUIS BREGUET
BP 1
78146 VELIZY VILLACOUBLAY CEDEX
FRANCE

ATTN   R ROGERS   1
DEFENCE RESEARCH AGENCY
BLDG 37
TUNNEL SITE
CLAPHAM BEDS MK 41 6AE
UNITED KINGDOM

ATTN   S SMITH   1
DEFENCE RESEARCH AGENCY
Q134 BUILDING
RAE FARNBOROUGH
HAMPSHIRE QU14 6TD
UNITED KINGDOM

ATTN   J SOWA   1
SAAB MISSILES AB
581 88 LINKOPING
SWEDEN

ATTN   D SPARROW   1
HUNTING ENGINEERING LTD
REDDINGS WOOD
AMPTHILL
BEDFORDSHIRE MK452HD
UNITED KINGDOM

ATTN   P STUDER   1
DEFENCE TECHNOLOGY AND
    PROCUREMENT AGENCY
SYSTEMS ANALYSIS AND INFORMATION
SYSTEMS DIVISION
PAPIERMUEHLESTRASSE 25
3003 BERNE
SWITZERLAND

ATTN   DR R G LACAU   1
AEROSPATIALE MISSILE
DEPT E/ECN
CENTRE DES GATINES
91370 VERRIERE LE BUISSON
FRANCE

ATTN   J M CHARBONNIER   1
VON KARMAN INSTITUTE
72 CHAUSSEE DE WATERLOO
1640 RHODE SAINT GENESE
BELGIUM

ATTN   P CHAMPIGNY   1
DIRECTION DE L AERONAUTIQUE
ONERA
29 AV DE LA DIVISION LECLERC
92320 CHATILLON SOUS BAGNEUX CEDEX
FRANCE

ATTN   DR P HENNIG   1
DEUTSCHE AEROSPACE (DASA)
VAS 414
ABWEHR AND SCHUTZ
POSTFACH 801149
8000 MUENCHEN 80
GERMANY

ATTN   H G KNOCHE   1
       DR GREGORIOU   1
MESSERSCHMIDT BOLKOW BLOHM
GMBH
UNTERNEHMENSBEREICH APPARATAE
MUNCHEN 80 POSTFACH 801149 BAYERN
GERMANY

ATTN   DR S J YOON   1
AGENCY FOR DEFENSE DEVELOPMENT
AERODYNAMICS DIVISION (4-3-1)
P O BOX 35-4 YUSEONG TAEJON
KOREA

ATTN   PETER CAAP   1
       HD FLIGHT SYS DEPT
FAA AERONAUTICAL RESEARCH INST
    OF SWEDEN
BOX 11021
BROMMA SWEDEN 16111

DISTRIBUTION (Continued)

		Copies			Copies
ATTN DAVE BROWN		1	G72	(MCINVILLE)	5
WEAPON SYSTEMS DIVISION			K		1
AERONAUTICAL AND MARITIME			K40		1
RESEARCH LABORATORY			K44	(ICHNIOWSKI)	1
P O BOX 1500 SALISBURY			N		1
SOUTH AUSTRALIA 5108			T		1

INTERNAL

		Copies
B		1
B04		1
B04	(ZIEN)	1
B05	(STATON)	1
B10		1
B10	(HSIEH)	1
B51	(ARMISTEAD)	1
B60	(TECHNICAL LIBRARY)	3
C		1
D		1
G		1
G02		1
G04		5
G20		1
G205		1
G23		1
G23	(BIBEL)	1
G23	(CHADWICK)	1
G23	(COOK)	1
G23	(GRAFF)	1
G23	(HANGER)	1
G23	(HARDY)	1
G23	(HYMER)	20
G23	(OHLMEYER)	1
G23	(ROWLES)	1
G23	(WEISEL)	1
G30		1
G305		1
G32	(DAY)	1
G33	(MELTON)	1
G33	(RINALDI)	1
G50		1
G50	(SOLOMON)	1
G60		1
G70		1
G72		1
G72	(ALEXOPOULOS)	1
G72	(CHEPREN)	1
G72	(JONES)	1
G72	(ROBINSON)	1